Titre: Title:	Foundry sand reclamation by the gas-contact process
Auteur: Author:	Zhen Ning Mao
Date:	1991
Type:	Mémoire ou thèse / Dissertation or Thesis
Référence: Citation:	Mao, Z. N. (1991). Foundry sand reclamation by the gas-contact process [Mémoire de maîtrise, École Polytechnique de Montréal]. PolyPublie. https://publications.polymtl.ca/56725/

UNIVERSITE DE MONTREAL

FOUNDRY SAND RECLAMATION BY THE GAS-CONTACT PROCESS

par

Zhen Ning MAO

DEPARTEMENT DE GENIE CHIMIQUE

ECOLE POLYTECHNIQUE

MEMOIRE PRESENTE EN VUE DE L'OBTENTION

DU GRADE DE MAITRE EN SCIENCES APPLIQUEES (M.Sc.A)

(GENIE CHIMIQUE)

NOVEMBRE 1991

ISBN 0-315-72753-5

UNIVERSITE DE MONTREAL

ECOLE POLYTECHNIQUE

Ce mémoire intitulé:

FOUNDRY SAND RECLAMATION BY THE GAS-CONTACT PROCESS

présenté par: Zhen Ning MAO

en vue de l'obtention du grade de: M.Sc.A.

a été dûment accepté par le jury d'examen constitué de:

M. Pierre CARREAU, ing., Ph.D., président-rapporteur

M. Christophe GUY, ing., Ph.D., directeur de recherche

M. Jamal CHAOUKI, ing., Ph.D., co-directeur de recherche

M. Jean Guy CHOUINARD, M.Sc., M.B.A., membre (Gaz Métropolitain)

ABSTRACT

Foundry sand reclamation is undertaken in the Gas-Contact Process (GCP). This process is a concurrent downward gas-solid flow. An original aspect of this process is the continuous feed of used sand to the core of a stabilized natural gas flame produced by a counter-rotation burner, where it undergoes a high temperature incineration; the resin coating the sand particle is eliminated. The burner is fitted to the top of the vertical cylindrical furnace where the falling used sand is incinerated by a concurrent flow of hot gas. Several conclusive experiments have shown not only the good performance for foundry sand reclamation but also the polarity for various applications in divided solid thermal treatment.

The study examines the characteristics of the gas and the particle motions, and the heat and mass transfer mechanisms in the GCP. The resin combustion mechanism is also studied in detail. Based on this study, an optimum model of the GCP for the treatment of the used sand is proposed. This model can predict very satisfactorily temperature profiles of both phases in the process, and gives the trend of resin conversion, especially the exit characteristics of the treated sand. For design purposes, this model can be used to specify the furnace size and the operating conditions of the unit.

It is found that in the GCP unit:

- the solid flow is plug-flow,
- the hot gas flow is well-stirred in the burner and the entrance region of the furnace (overall length equal to 5 burner diameters), then is plug-flow in the rest of the burner,
- the heat transfer is by forced convection and radiation,
- the incineration process follows a two-step mechanisms: volatilization of part of the resin at a temperature equal to 180°C, combustion of the volatiles in the gas phase, combustion of the remaining char in the solid phase at the surface of the particle. This mechanism is heat transfer limited (volatilization), volatile diffusion limited (volatile combustion), oxygen diffusion limited (char combustion). Combustion kinetic rates are considered infinite.

SOMMAIRE

L'objectif de cette étude consiste en la modélisation des mécanismes de transfert d'énergie et de matière impliqués dans une unité gaz-contact utilisée pour la régénération de sables de fonderie. A cet effet, une unité pilote, de puissance nominale égale à 58 kW, a été utilisée. La modélisation porte sur:

- l'identification des caractéristiques de l'écoulement des gaz chauds et des particules solides, du transfert d'énergie et de matière ainsi que celles du processus d'incinération de la résine;
- la comparaison des résultats expérimentaux avec ceux prédits avec les modèles proposés;
- l'identification des limites de fonctionnement du procédé gaz-contact dans le cas de la régénération des sables de fonderie.

Le procédé gaz-contact repose sur l'écoulement descendant à co-courant d'une suspension gaz-solide. L'aspect original de ce procédé consiste en l'alimentation continue et directe du produit finement divisé au sein de la flamme issue de la combustion du gaz naturel. Ces produits sont introduits coaxialement dans un brûleur à contre-rotation utilisant l'air comprimé comme comburant. Dans ce brûleur, de section circulaire, l'air nécessaire à la combustion du gaz naturel, ce dernier

arrivant de façon radiale, est introduit par deux séries d'orifices tangentiels: ceci provoque à l'intérieur de la chambre de combustion une double rotation de l'air, dans deux sens opposés. Cette double rotation a pour effet de stabiliser la flamme sans avoir à utiliser de système mécanique. Ce brûleur est disposé sur un four, où se poursuit le traitement thermique du solide, en acier inoxydable, de diamètre intérieur égal à 0.2m et de hauteur égale à 2m. Les parois internes du four sont garnies d'une couche de réfractaire (ciment alumineux) de 80 mm d'épaisseur.

La modélisation de l'aérodynamique de l'écoulement gaz-solide repose sur l'analogie avec le transport pneumatique descendant de produits pulvérulents. La représentation théorique de l'aérodynamique de l'écoulement est régie par deux hypothèses fondamentales:

- l'écoulement du mélange gaz-solide est établi aussi bien dans le brûleur que dans le four;
- la suspension gaz-solide est considérée diluée (concentration en solide << 1%), i.e. la vitesse de glissement entre les deux phases s'identifie à la vitesse terminale de chute libre des particules solides.

La description des mécanismes d'échange d'énergie et de masse est basée sur la division du procédé gaz-contact en deux zones:

Zone I: le brûleur et l'entrée du four sont assimilés à un réacteur continu parfaitement agité.

Zone II: la partie restante du four est considérée analogue à un réacteur en écoulement piston.

Deux modèles ont été proposés pour caractériser la zone I:

- les phases gazeuse et solide sont parfaitement agitées;
- la phase gazeuse est parfaitement agitée alors que la phase solide est en écoulement piston.

Quant à l'analyse du processus d'incinération de la résine enrobant le sable, deux résistances au transfert de masse et d'énergie ont été considérées:

- diffusion des produits volatils vers la phase gazeuse;
- diffusion de l'oxygène vers la surface du grain de sable.

La quantité de produits volatils et le coefficient stoechiométrique relatif à l'oxygène ont été considérés comme des paramètres d'ajustement des modèles proposés.

L'étude paramétrique systématique du comportement d'une unité gaz-contact montre que:

- les profils de température des phases gazeuse et solide sont affectés par le débit d'alimentation en solide, le taux d'aération et la puissance au brûleur;
- le degré d'avancement de l'incinération de la résine dépend

principalement du taux d'aération au brûleur, autrement dit de la concentration d'oxygène qui diffuse vers la surface du grain de sable.

Par ailleurs, la comparaison des résultats théoriques avec les mesures expérimentales montre que l'approche théorique proposée permet de prédire de façon raisonnable les échanges d'énergie et de matière impliqués dans le procédé gaz-contact. De cette comparaison, il ressort que la phase gazeuse est parfaitement agitée dans la zone I alors qu'elle devient en écoulement piston dans la zone II. En revanche, la phase solide est en écoulement piston aussi bien dans la zone I que II. En outre, le processus d'incinération est limité par la diffusion des produits volatils vers la phase gazeuse et ce pour des températures inférieures ou égales à 180°C. An delà de cette température, le processus est contrôlé par la diffusion d'oxygène vers la surface du grain de sable. Lorsque le diamètre des particules est égal à celui du grain de sable propre, l'élimination de la résine est terminée.

Enfin, les conséquences essentielles de notre recherche sont:

- *d'un point de vue industriel*, la possibilité de prédire la longueur du four nécessaire à la régénération des sables de fonderie;

- *d'un point de vue fondamental*, l'approche théorique proposée apporte une meilleure compréhension du mécanisme d'incinération de la résine enrobant les sables de fonderie.

ACKNOWLEDGEMENTS

The author would like to express his sincere gratefulness to his supervisor Prof. Christophe Guy and co-supervisor Prof. Jamal Chaouki for their constant supervision, support and advice at every stage of this research, and full financial aid provided during the period of his research program.

The author also wishes to express his sincere thanks to Prof. Pierre Carreau for his constant encouragment and providing the opportunity to study here.

The author would like to express his special thanks to Dr. Marzouk Benali for his design of the unit, his constant help and discussions.

The author also appreciates Mr. Jean Guy Chouinard and Gaz Metropolitain for their support of this project.

The author also acknowledges all of the technical staff of the department of chemical engineering for their skillful aid during the construction of the experimental set-up, and his friend Mr J.Y. Cheng for his sincere help.

Finally, the author would like to express his heartfelt thankfulness to his wife, Xia, for her constant source of support, encouragment and pressure each at the right moment, and to their family.

TABLE OF CONTENTS

LIST OF FIGURES

LIST OF TABLES

NOMENCLATURE

A_p	cross sectional area	(m^2)
A_r	refractory surface	(m^2)
A_T	total area of the load and refractory	(m^2)
Bi	Biot number	(-)
b	constant	(-)
C_D	drag coefficient	(-)
C_p	calorific capacity	(J/kg.$^\circ$C)
c	constant	(-)
d_L	droplet diameter	(m)
d_p	mean diameter of particle	(m)
D_f	internal diameter of furnace	(m)
dz	a elemental length of furnace	(m)
E	activation energy	(J/mole)
G_o	evaporation flux	($kg/m^2.s$)
(GP)	the total-exchange area for radiative heat transfer	(m^2)
g	gravitational acceleration	(m^2/s)
h	convective heat transfer coefficient	($w/m^2.K$)
h_c	free convection coefficient	($w/m^2.K$)
H_c	heat of combustion of resin	(J/kg)
H_p	resin decomposition latent heat	(J/kg)
H_{H2O}	water evaporation latent heat	(J/kg)
K	specific rate constant of incineration reaction	(-)

L	length	(m)
L_m	equivalent length of radiation	(m)
$\dot{m}_f$	mass burning rate	(kg/s)
Δm	mass change of the resin	(kg)
M	molecular weight	(g)
Nu	Nusselt number	(-)
n_p	number of particles per unit volume of gas	(m^{-3})
P	pressure	(atm)
PCI	low heating value of natural gas	(MJ/Nm^3)
PCS	higher heating value of natural gas	(MJ/Nm^3)
Pe	Peclet number	(-)
Pr	Prandtl number	(-)
$Q_{g\,p}$	net radiant heat exchange	(J)
R	universal gas constant	(J/mole.K)
Re	Reynolds number	(-)
Re_p	particle Reynolds number	(-)
r_L	radius of fuel droplet	(m)
s	stoichiometric ratio	(-)
T_g	gas temperature	(K)
T_p	particle temperature	(K)
T_{H2O}	water temperature	(K)
t	time	(s)
t_r	relaxation time of the external temperature	(s)
t_e	the characteristic heating time of the particles	(s)

U_{mf}	minimum fluidization velocity	(m/s)
U_p	terminal velocity of particle	(m/s)
U_{sl}	average slip velocity	(m/s)
V_f	gas velocity	(m/s)
V_p	particle velocity	(m/s)
V_t	terminal velocity of particle	(m/s)
W_f	volumetric flowrate of fumes	(m^3/s)
W_p	volumetric flowrate of particles	(m^3/s)
X_{vap}	mass fraction of resin vapor	(-)
X_o	mass fraction of oxygen	(-)
ϵ	voidage of solid-gas flow	(-)

Greek letters

α_g	gray-gas absorptivity	(-)
β	diffusion coefficient	(m^2/s)
γ_{gp}	gray-gas absorptivity	(-)
ε	void fraction	(-)
ε_g	gas emissivity	(-)
λ	thermal conductivity	(W/m.K)
μ	dynamic viscosity	(Pa.s)
ρ	density	(kg/m^3)
σ	Stefan Boltzmann constant	($W/m^2.K^4$)

τ	residence time	(s)
$\sum \upsilon$	value of the atomic diffusion volumes	(m^3)
φ	mixing convection parameter	(-)
ϕ	inter-pretation	(-)
κ	mass concentration of the matter	(%)
ψ_{vol}	diffusion coefficient of the volatile	(m^2/s)
ψ_{ox}	diffusion coefficient of the oxygen	(m^2/s)

Subscripts

b	burner
f	furnace
g	gas
gas	flue gas
gp	from gas to particle
H2O	water
init	initial position
mf	minimum fluidization
out	final position
o	initial condition
ox	oxygen
p	particle
r	resin

s	solid
s+r	solid and resin
vol	volatile
w-in	inside surface of the wall of the furnace
w-out	outside surface of the wall of the furnace
∞	infinity

CHAPTER 1. INTRODUCTION

1.1 CONTEXT AND MOTIVATION

As a result of tighter environmental restrictions and escalating transportation and dumping fees, most industries are concerned with the treatment of solid wastes and sludges. Waste treatment, for the purpose of reusing it or destroying it, can be undertaken by many available techniques. Among them, incineration is a major solution for the disposal of many industrial solid wastes and sludges. This method has been used since the early 1900s, it shows several potential advantages over other processes:

—— maximum volume reduction;

—— detoxification;

—— energy recovery.

As heat is released during the process, it can be used for various heat transfer applications and the noncombustible residue can be recyled or used for different purposes.

If the heating value of the solid wastes and sludges is low or the required incineration temperature is high, hot air or

burners are needed. Fluidized bed, rotating kilns, moving beds, cyclone-cascades and raining particle heat exchangers are among the incineration systems based on heat transfer from high temperature fumes or gas to solids by direct contact. The selection of one of these systems is usually based on several parameters and criteria such as operating conditions (gas and solid flowrates), low pressure drop, high thermal efficiency, stability and flexibility of operation, easy integration in the overall industrial unit and low investment and operating costs [Benali, 1989].

Recently, Gaz de France [Gaurier, 1987] has proposed a new system, called the Gas-Contact Process (GCP), which is a novel heat treatment technique for divided solid wastes or sludges. An original aspect of this process is the continuous injection of the solid wastes or sludges directly into the core of the flame of a counter-rotation natural gas burner where they undergo a high temperature incineration, thus benefiting from the "gas-contact" action. The burner is fitted at the top of a vertical cylindrical furnace where incineration of the falling particles is completed concurrently with the hot gas. A schematic of a typical Gas-Contact unit is shown in Figure (1-1).

The "counter-rotation" burner was developed by Gaz de

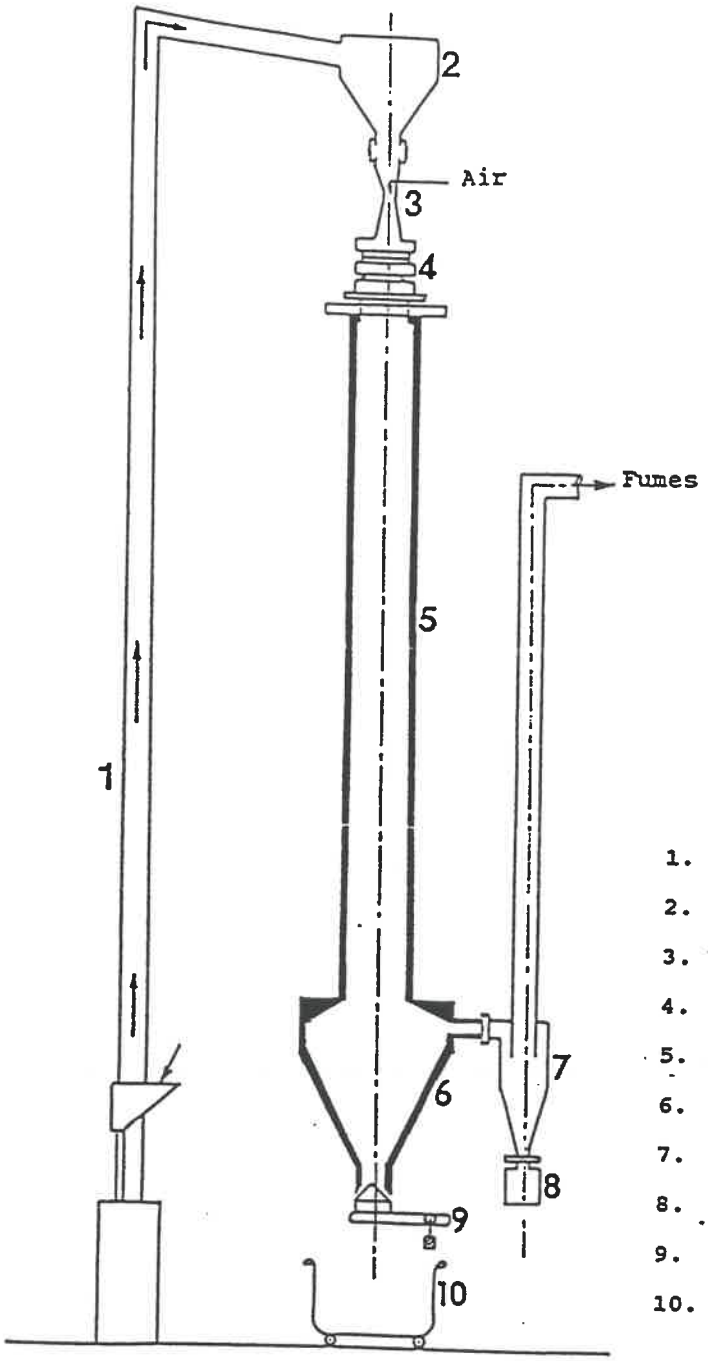

1. Solid waste elevator
2. Solid waste hopper
3. Injector
4. Burner
5. Furnace
6. Expansion chamber
7. Cyclone
8. Collector
9. Conical Valve
10. Treated solid container

Figure (1-1) Schematic view of the Gas-Contact unit

France (Figure (1-2)). It has a combustion chamber with fluid injection ports as follows:

—— one row of radial gas ports;

—— two rows of tangential air ports. The rotational directions imparted by these two rows are opposite. They create a high degree of turbulence, favoring quick air and gas mixing.

This configuration results in intense combustion and a short stable flame while maintaining the burner's centerline free from mechanical parts.

The overall dimensions of this burner can be determined by means of graphs depending on the desired output. Power may vary between 20 and 11000 kW for air and gas supply pressures less than or equal to 2 kPa. The aeration rate may vary between 1.05 (30% excess air) and 15 (1400% excess air).

For its applications in the GCP, the rear of the burner features an axial port and is fitted with a device for ejecting the product to be processed (Figure (1-2)). The product is thus injected in the flame where it is caught in the turbulence created by the counter rotation effect. Therefore, each grain of the product is subjected to an intense heat transfer, known as

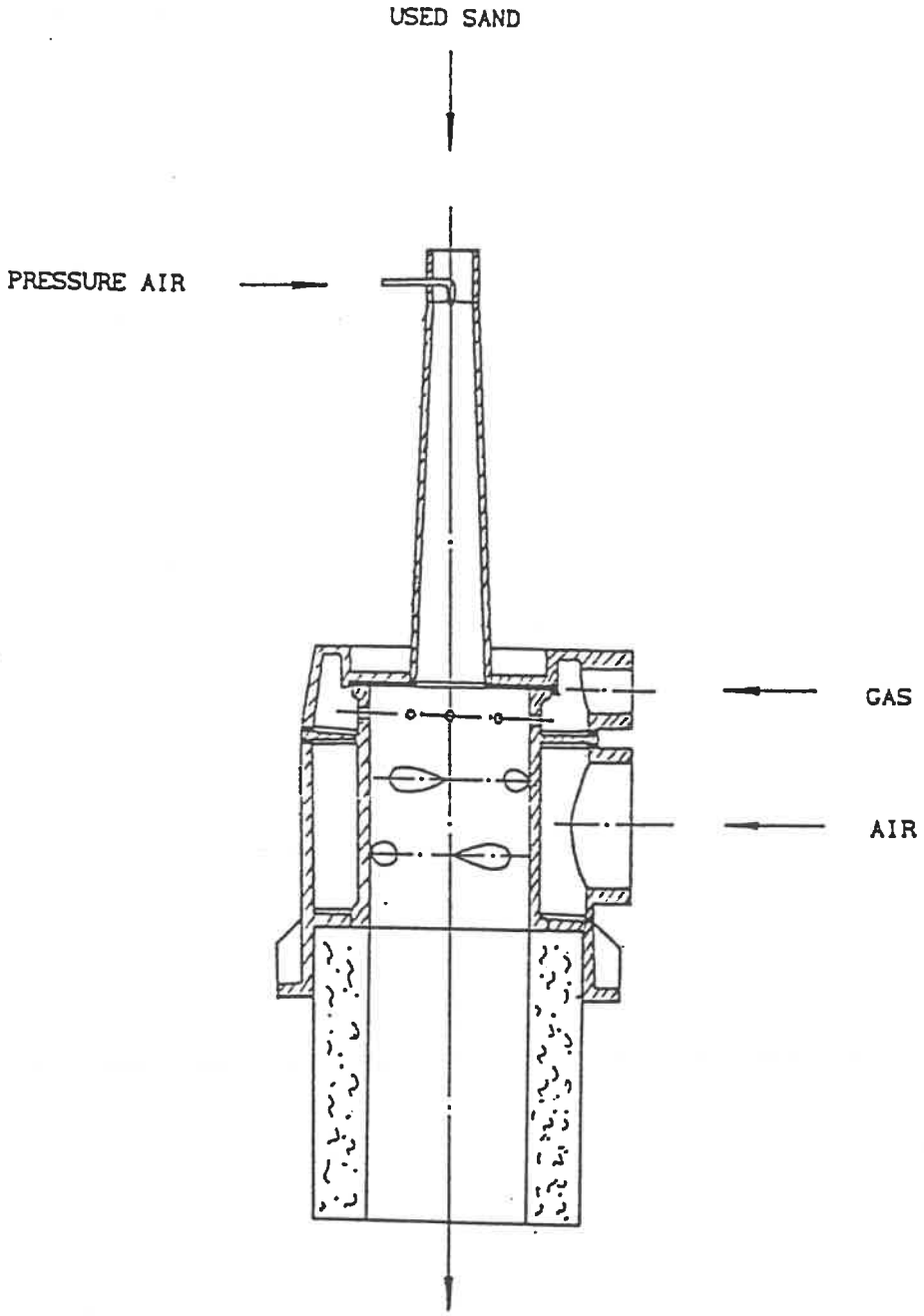

Figure (1-2): The "counter-rotation" burner

the Gas-Contact action.

The burner must be mounted in a furnace in order to reach the minimum product treatment time. Various types of furnaces have been studied by Gaz de France to be used selectively. For waste treatment applications, two types of furnaces have been used:

—— a horizontal or inclined unit used for incineration applications. A cyclone may be added at the chamber end to recover unburned matter or ashes;

—— an upright unit, followed by a decelerating chamber and a dust-removing cyclone in the case where waste may be reused. The recovered portion of the product is collected at the bottom of the decelerating chamber (Figure (1-1)).

An evaluation of the Gas-Contact action has been carried out during prototype tests by Gaz de France [1986]. As an example, a method of eliminating impurities under the action of heat was studied. The comparative results obtained under the same conditions are given in Figure (1-3). For the same operation temperature, GCP reduces the impurity content by approximately 40%. With an equal residual content, the Gas-Contact action could mean a decrease in the required temperature, resulting in energy saving.

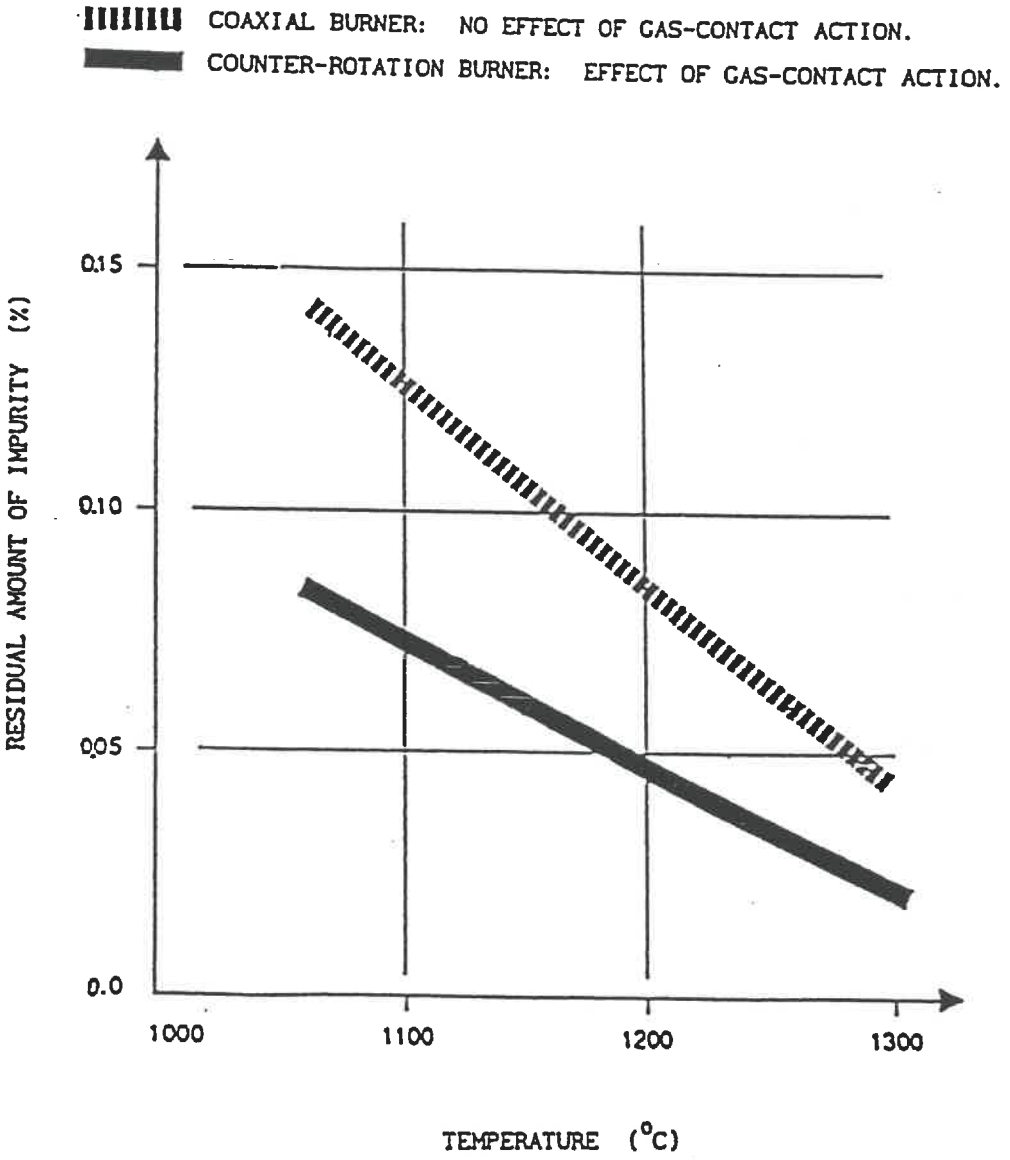

Figure (1-3): Effect of Gas-contact Action

[Caurier L. 1989]

In the last two years, The Gas-Contact Process has attracted considerable attention because of its compactness, its good thermal efficiency and its ability to operate at high temperatures ($600^{0}C$-$1200^{0}C$). Several conclusive experiments have been carried out by Gaz de France on a pilot scale unit [Gaurier, 1987] for various applications, such as:

—— regeneration of foundry sand;

—— gypsum dehydration;

—— dust decyanidation in manganese production;

—— incineration of electrical insulation waste products;

—— incineration of paint and cataphoresis sludges;

—— cleansing of metal shavings (de-oiling).

These tests show that GCP presents many advantages for the treatment of solid wastes or sludges:

—— the versatility of counter-rotation burners enables to do the design of units adapted to each problem confronted;

—— the Gas-Contact Process favors size reduction of the wastes by burning or eliminating part of them;

—— the continuous passage of the product to be treated avoid equipment clogging during shutdowns, facilitates maintenance and reduces restart time;

—— the short product residence time in the equipment during the process means high output;

—— the absence of moving parts reduces maintenance.

The economic aspect can be examined from the application of foundry sand reclamation [Gaurier, 1987]. The upright type unit with an expansion chamber was equipped with a cooling stage based upon the "Air-contact" principle. For an annual treatment of 1500 ton/year, the savings would equal the cost of the investment in 1.2 years at constant monetary values.

So GCP offers a simple, easy-to-use, flexible and low cost method of treating solid wastes or sludges.

While the Gas-Contact Process holds great promises for the treatment of divided solid wastes and sludges, it is still in the prototype stage. Design criteria are not yet available. Research work should intend to examine the mechanism of energy exchange, mass exchange involved in the direct contact of solid particles with the hot gas, and propose appropriate models based on transfer equations as well as phase change and incineration kinetics to predict the temperature profiles of both the hot gas and the solid, as well as the particle composition and size, through the burner and the furnace. Recently, some essential models of incineration of foundry sand have been proposed [Benali et al.(a), 1991]. We will complete and develop these models and assess their validity through appropriate experiments.

1.2 OBJECTIVES

The objective of this project is the modeling of the behaviour and the performance of a gas-contact unit used for foundry sand reclamation. It is part of a longer term study which aim is the development of design criteria of gas-contact units for different applications. A 58kW unit with a vertical cylindrical furnace is investigated in this study. The modeling requires:

- identification of the characteristics of the gas and the particles motions, the heat and mass transfers, the incineration kinetics and development of appropriate models;
- comparison of the experimental data with the predicted values of the temperature profiles of both combustion gas and the particle, and of the resin content of the particles.
- identification of the range of operating parameters leading to good thermal treatment conditions and short residence time of the particles in the process for different particle characteristics.

The originality of this study is threefold:

- accurate experimental data on the axial temperature profiles of both gas and solid and on the solid composition profiles are collected for the first time. A specific experimental

method for the measurement of solid temperature is especially designed and used.

—— it is the first conclusive attempt at modeling the mass and energy exchange in a GCP. The proposed model that will be presented in the following chapters provides more detailed understanding on the functioning and on the performance of the GCP.

—— the model can be used for design purposes and to determine the optimum operating conditions of GCP installations.

1.3. ORGANIZATION OF THE THESIS

The successive chapters of this thesis are:

—— review of the incineration methods applied to foundry sand reclamation;

—— review of related literature of two phases flow, heat and mass transfer, droplet and particle combustion processes;

—— process modeling;

—— description of the experimental set up and methodology;

—— experimental results and discussions;

—— conclusions.

CHAPTER 2. REVIEW OF THE THERMAL METHODS OF FOUNDRY SAND RECLAMATION

2.1 INTRODUCTION

The reclamation of used sand in the foundry industry is a matter concerning not only the environment but also the economic performance of the industry. Modern, advanced foundry management is well aware of today's environmental requirements and subsequent laws and regulations enforced in connection with effective sand reclamation for used foundry sand. In addition it is no longer justifiable to throw away the still useable raw material sand, considering the cost of new sand and subsequent disposal. Many technologies for foundry sand reclamation have been developed. They can be classified into two categories: mechanical and thermal recovery methods. The mechanical recovery methods are based on the attrition of the binder from the sand. It is effective for clayey sand and mineral binder. And the thermal recovery methods are more effective in eliminating organic resins, in which all the residual resins are burnt away. Because of this advantage, although the costs are more expensive than mechanical methods, the thermal recovery methods have many competitive and developmental opportunities. Furthermore, the use of natural

gas as fuel for new-type units recently affords additional economy and efficiency. In thermal recovery methods, the direct contact between the hot combustion gas and the used sands is usually selected.

This chapter is confined to a review of popular types of thermal reclamation units in recent years. After describing the principle of each type unit, their main features are compared. However, in practice, there are also other important factors which have to be taken into account, such as the stability of the process, the flexibility of operation, the size of unit and the ease of integration of the unit in the existing process. The discussion in this chapter will concern some of these factors.

2.2 THERMAL RECLAMATION OF FOUNDRY SAND

The more popular types of thermal reclamation units of foundry sand can be classified as fluidized beds, rotary kilns and combustion chamber. The GCP is a new process for foundry sand reclamation, no installation has been operated in the industry till now.

Fluidized beds

Fluidized beds are the most popular units. Under usual operating conditions, a fluidized bed (Figure (2-1)A) consists of a gas-solid emulsion with the presence of bubbles. The typical operating superficial gas velocities vary, depending on solid particles, between 0.1 and 5 m/s [Meunier and Large, 1981]. In order to obtain a counter-current effect and to improve the efficiency, multicell or multistage configurations could be used (Figure (2-1)B and C). Their advantages are a uniform temperature and a high heat transfer rate between gases and particles. The high flowrate of hot air necessary for sand fluidization ask for a high capacity costly air compressor. Moreover, thermal losses due to the outlet of the hot gases are important. However, the high pressure drop of the gas phase and the high gas flowrate increase the operating cost. Moreover multi-type configuration of fluidized beds makes the design and the maintenance work more difficult, especially for high temperature conditions.

Figure (2-2) shows one kind of fluidized bed unit used for foundry sand reclamation, made by Gudgeon Brothers limited (Canada). The feature of this unit is a two stage fluidized bed. The other special type is shown in Figure (2-3). It

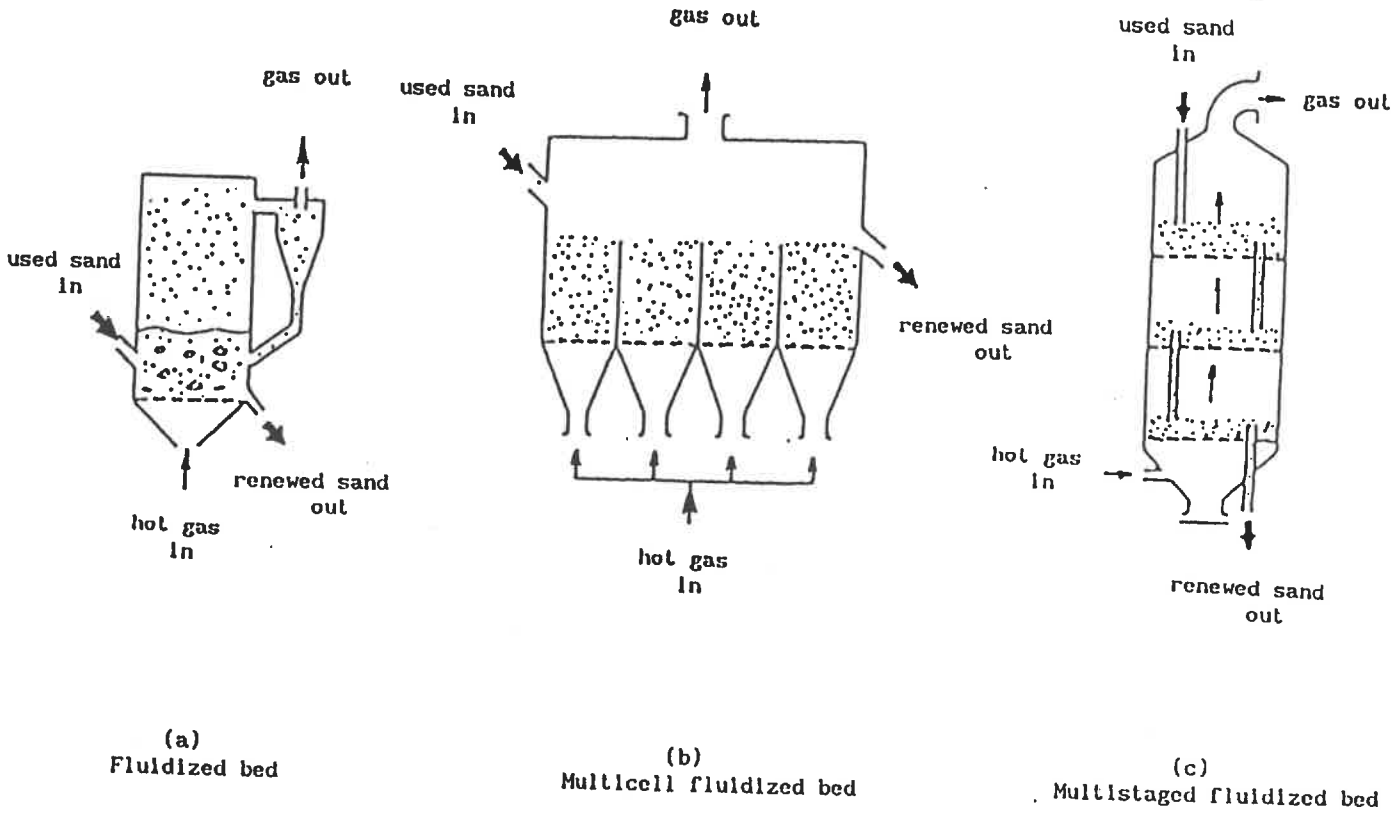

Figure (2-1): Schematic view of fluidized beds applied to foundry sand reclamation

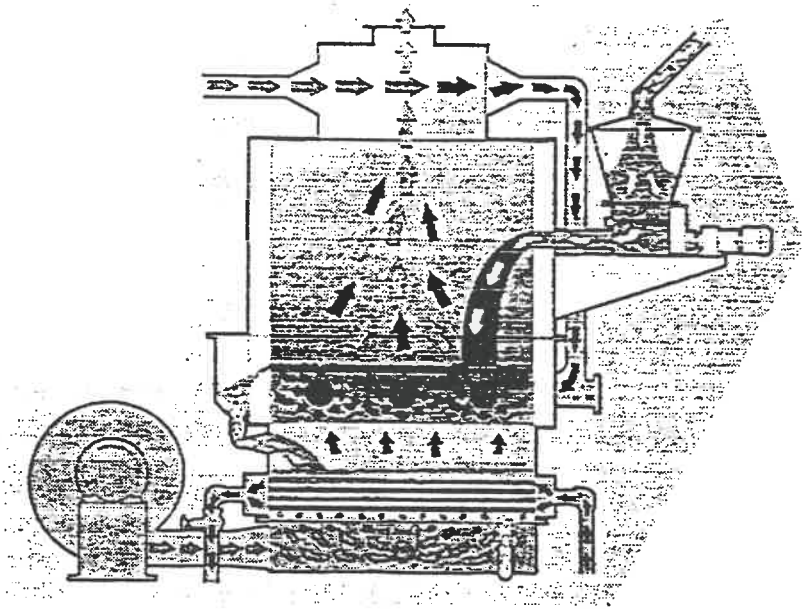

Foundry Sand

Preheated air
- to fluidize air in cacining bed
- from heat exchanger to gas burner

Dust and Fines to Dust Collector

Ambient temperature used to fluidize the stacked beds and used to combustion air

Water from cooling tower or chiller to heat exchanger pipes in the colling bed

Figure (2-2) Flow chart of Gudgeon Brothers' thermal foundry sand reclaimer

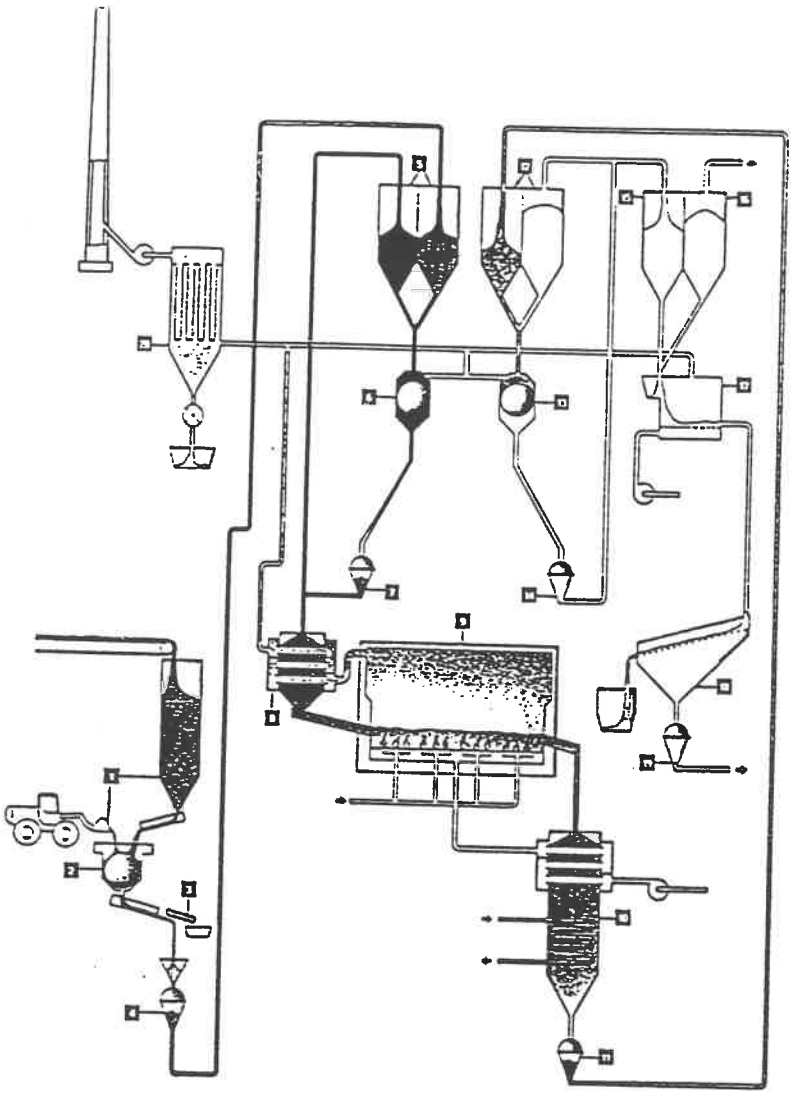

1 Used sand charging / used sand bin
2 Dryer / lump sand breaker
3 Magnetic separator
4 Pneumatic conveyor
5 Intermediate bin
6 Centrifugal cleaner (mechanical precleaning)
7 Pneumatic conveyor
8 Sand preheater
9 Fluidized bed furnace
10 Cooler (air, water cooling)
11 Pneumatic conveyor
12 Intermediate bin
13 Centrifugal cleaner (mechnical aftercleaning)
14 Pneumatic conveyor
15 Reclaim bin
16 New sand bin
17 Fluidized bed separator
18 Oscillating screen
19 Pneumatic conveyor to user
20 Filter unit

Figure (2-3): Three-stage treatment system of foundry used sand reclamation.

(KGT company, GERMANY)

is designed by KGT company (Germany). The principle is mechanical precleaning, fluidized bed and mechanical aftercleaning. It is three stage treatment.

Rotary kiln

It is made of a long inclined rotating cylindrical shell (Figure (2-4)), in which gases and solid flow co- or counter-currently. The solid moves along the unit due to gravity and rotation effects. Usually, longitudinal or spiral-shape flights are welded to the internal wall of the kiln to help distribute the solids. The design of such a kiln is sophisticated because of the complex nature of heat transfer mechanisms involved (conduction, convection and radiation). The thermal efficiency of a rotary kiln increases with its length, and hence often leads to very large equipment.

Figure (2-5) shows a rotary kiln used for foundry sand reclamation.

Combustion chamber

The principle of the combustion chamber is similar to the incinerator. The F.A.T. company (Germany) shows one kind of combustion chamber unit for foundry sand reclamation (see Figure (2-6)).

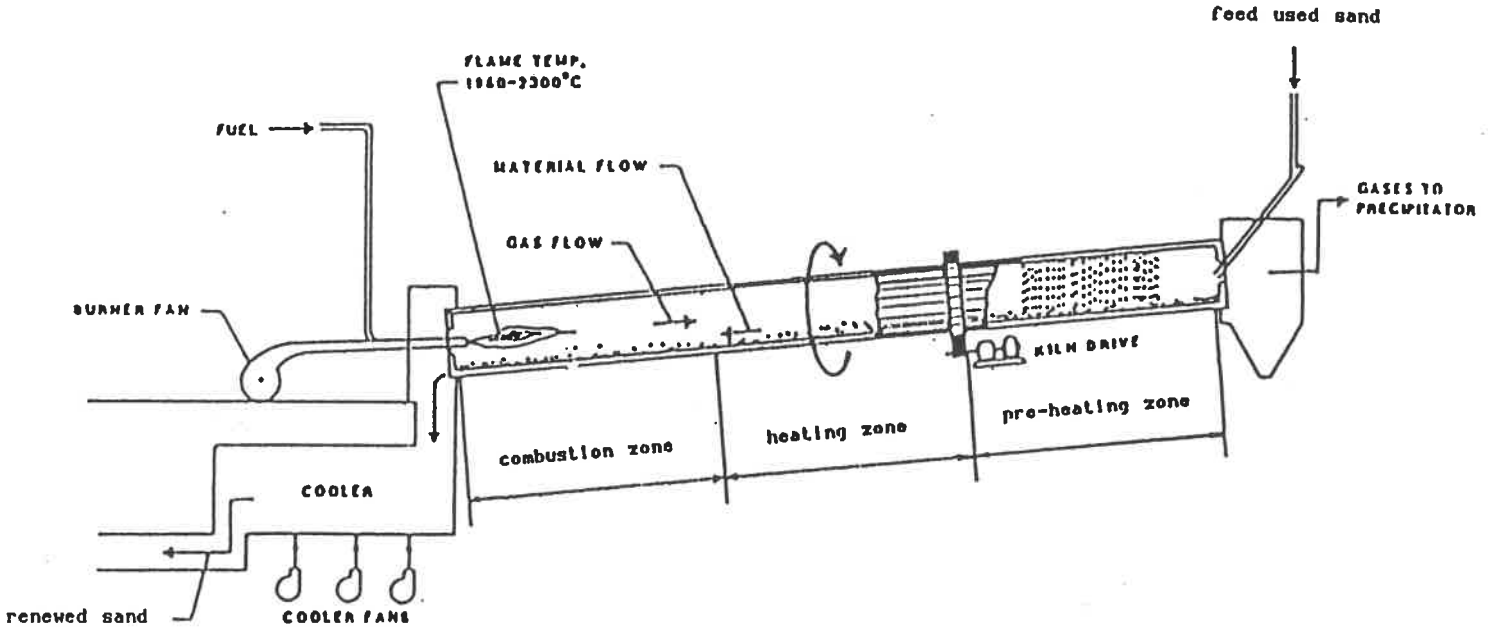

Figure (2-4): Schematic view of rotary kiln applied to foundry used sand reclamation

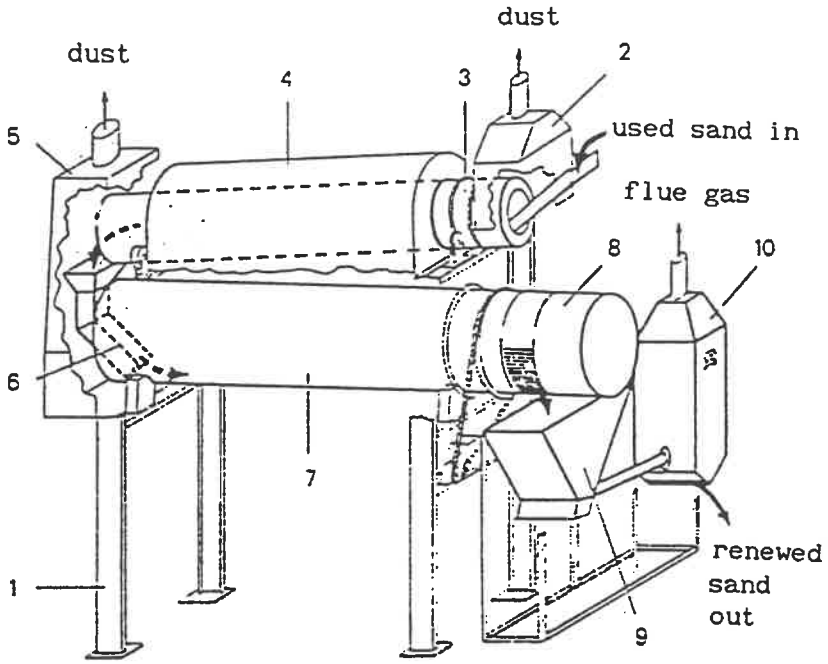

1. steel structure
2. roof for dust exhaust
3. rotary kiln
4. insulation
5. cover for flue gas and dust exhaust.
6. slip way of sand
7. cooling cylinder
8. sieve
9. sand scrubber
10. separator

Figure (2-5): Rotary kiln applied to foundry used sand reclamation

(F.D.C. company, SWITZERLAND)

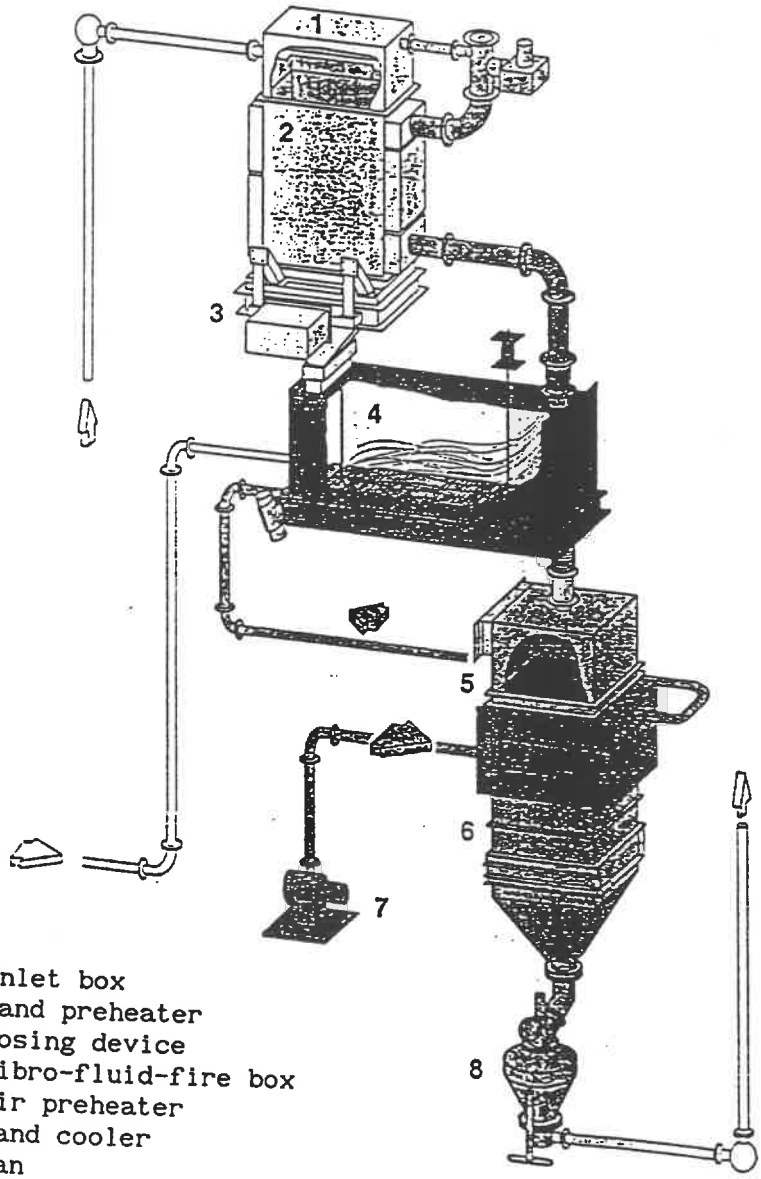

1. inlet box
2. sand preheater
3. dosing device
4. vibro-fluid-fire box
5. air preheater
6. sand cooler
7. fan
8. pneumatic conveyor

Figure (2-6): Combustion chamber type unit applied to foundry used sand reclamation

The combustion chamber is called "vibro-fluid-fire box". The LOREK company (SWITZERLAND) show a multistage configuration unit. In Figure (2-7), every stage can be considered a combustion chamber.

Gas-contact process

As introduced in Chapter 1, the "counter-rotation" burner shows a high heat transfer rate between the two phases. It is operated at a lower solid density. The pressure drop of the gas is much lower than in a fluidized bed, and it can operate under a high temperature (800°C-1400°C). Much less air is used than in a fluidized bed which reduces heat losses. However, the GCP does not allow for long solid residence time.

2.3 COMPARISON OF THERMAL METHODS OF FOUNDRY SAND RECLAMATION

Table (2-1) summarizes the main factors of the different types of thermal methods of foundry sand reclamation.

Table (2-1) shows that the GCP system has lower cost than others, and that the consumption of gas is also lower.

1. steel structure
2. discharge stage
3. combustion stage
4. preheating stage
5. feeding stage
6. chimney
7. heat exchanger
8. feeding hopper
9. burner
10. grate
11. aperture plate
12. discharge

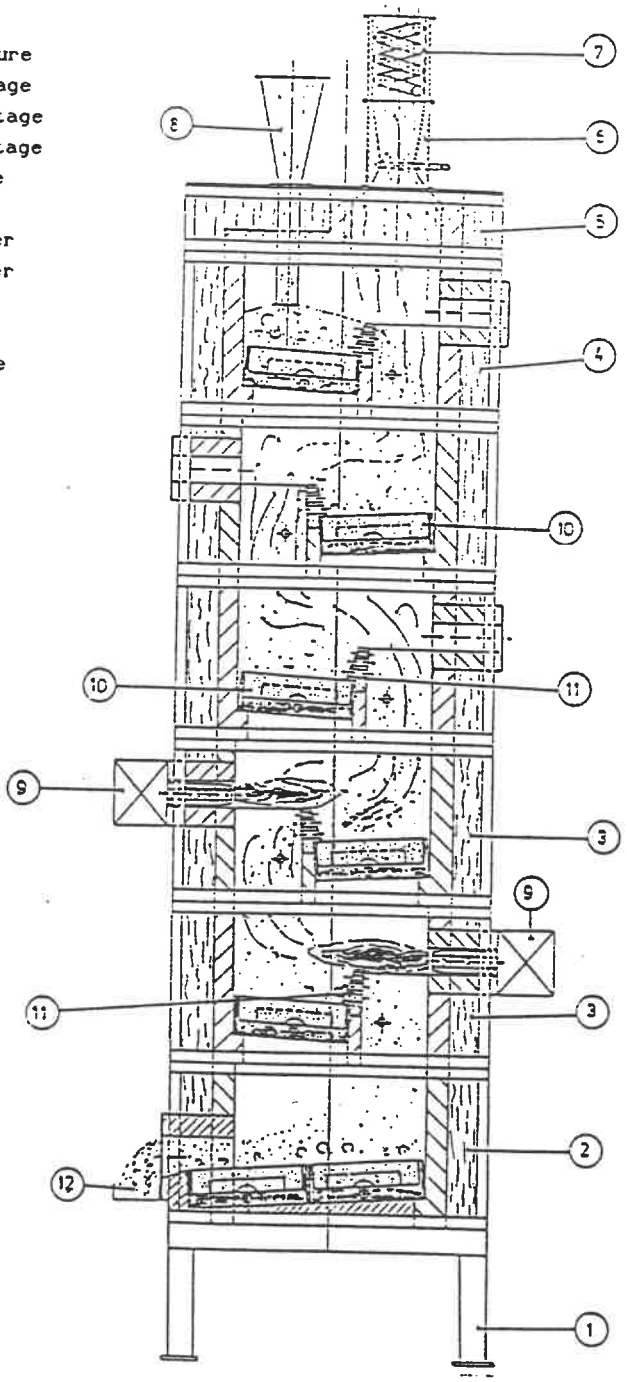

Figure (2-7): Multistage combustion chamber unit applied foundry used sand reclamation

Table (2-1): Comparison of thermal methods of foundry used-sand reclamation. *

	Gas contact	Fluidized beds	Rotary kiln	Combustion chamber
Compactness	++	+	-	+
Gas consumption	+	++	+	-
Air consumption	++	--	+	+
Thermal loss	-	--	-	-
Contact time	-	++	++	+
Temperature	++	+	-	++
Capacity	+	++	++	+
Quality of Product	++	++	+	-
Operation cost	++	-	--	+
Investment cost	++	-	--	+

* excellent : ++
good : +
average : -
bad : --

CHAPTER 3. LITERATURE REVIEW

3.1 INTRODUCTION

The principle of the GCP has been presented in the first chapter. The treatment of foundry sand by the GCP is a thermal process, which concerns the heat transfer rate between the gas and particles, residence time of both phases in the unit, and incineration of the resin that is coating the sand. The heat transfer rate depends not only on the particle size and solid loading but also on the gas temperature and local velocities. Therefore, this chapter presents a literature review on the regimes of gas-solid flow and some relevent results on the gas and particle velocity distribution first. Then, the heat transfer between the gas and the particles (including convection and radiation) is reviewed. Some studies on fuel droplet combustion and solid fuel particle combustion which are relevant to the incineration of resin coated sand are also discussed. The aim of this chapter is to summarize published materials on the subject in a manner useful to the modeling of the GCP.

3.2 GAS-SOLID VERTICAL FLOW REGIMES

Particulate solids can be transported up or down a vertical pipe. Such a pipe, with solids traveling downwards cocurrently or countercurrently to a fluid, is referred to as a standpipe. A pipe in which solids are lifted upwards by a fluid is known as a riser. Standpipe and riser together form whole types of gas-solids vertical flow. The GCP is concerned with the flow of particles down a standpipe. Therefore, the downflow regimes are paid special attention in this review section.

When the flow of a fluid upwards through a packed bed of granular solids is gradually increased, the solids remain stationary, as a packed bed initially, until the minimum fluidization velocity (U_{mf}) is reached. And the voidage at this condition is defined as ϵ_{mf}. The average slip velocity (U_{sl}), defined as the average fluid velocity minus the average solid velocity, is given by U_{mf}/ϵ_{mf} at minimum fluidization since the average solid velocity in this case is zero. At $U_{sl} < (U_{mf}/\epsilon_{mf})$, the bed of particles is in the packed state. While at $U_{sl} \geq (U_{mf}/\epsilon_{mf})$, the particles are fluidized [Cheremisinoff, 1984].

Many publications have shown that at a given slip velocity, the behavior of a fluidized bed is similar to that of a vertical flow of the same fluid-particle system. Thus, in a standpipe or a riser, when $U_{sl} \geq (U_{mf}/\epsilon_{mf})$, the particles in the standpipe/riser will be fluidized. Similarly, the voidage in the vertical flowing system will be the same as that in the stationary fluidized bed at the same slip velocity. This analogy forms the backbone of the analysis of solids flow in vertical standpipes and risers [Cheremisinoff, 1984].

Taking all velocities as positive in the upwards direction, the average slip velocity in the standpipe (or riser) is given by:

$$U_{sl} = V_f - V_p \qquad (3\text{-}1a)$$

$$= U_f/\epsilon - U_p/(1-\epsilon) \qquad (3\text{-}1b)$$

For downflow of solids in a standpipe, U_{sl} can be positive or negative. In a riser, U_{sl} is generally positive. From the analogy between a fluidized bed and a flowing system, the two general flow regimes are given by Leung and Jones [1984]:

1. *Fluidized solid flow,* in which particles are in suspension:

$$U_{sl} \geq (U_{mf}/\epsilon_{mf}) \qquad \text{and} \qquad \epsilon \geq \epsilon_{mf}$$

2. *Nonfluidized solid flow,* in which particles move en bloc with little relative motion:

$$U_{sl} < (U_{mf}/\epsilon_{mf}) \qquad \text{and} \qquad \epsilon < \epsilon_{mf}$$

Nonfluidized flow has been referred to as moving-bed flow, packed-bed flow and slip-stick flow. There are further subdivisions within the nonfluidized regime. But in this thesis, the interest is further subdivisions within the fluidized regime.

Within the fluidized mode in standpipe, Leung and Jones [1980] suggested the following criterion for demarcation:

1. *Type I fluidized solid flow* defined by:

$$\left(\partial U_f/\partial \epsilon \right)_{U_p} < 0 \qquad \text{and} \qquad U_{sl} \geq (U_{mf}/\epsilon_{mf})$$

2. *Type II fluidized solid flow* defined by:

$$\left(\partial U_f/\partial \epsilon \right)_{U_p} > 0 \qquad \text{and} \qquad U_{sl} \geq (U_{mf}/\epsilon_{mf})$$

Staub [1980] proposed the terms " dilute " and " dense " to describe systems in which $(\partial U_f/\partial \epsilon)_{U_p}$ is less than or greater than zero. It means the "*Type I*" can be said "*dilute fluidized solid flow*", and the "*Type II*" can be said "*dense fluidized solid flow*".

Typical pressure profiles for different flow patterns in standpipe flow are given in Figure (3-1). Figure(3-1a) shows the

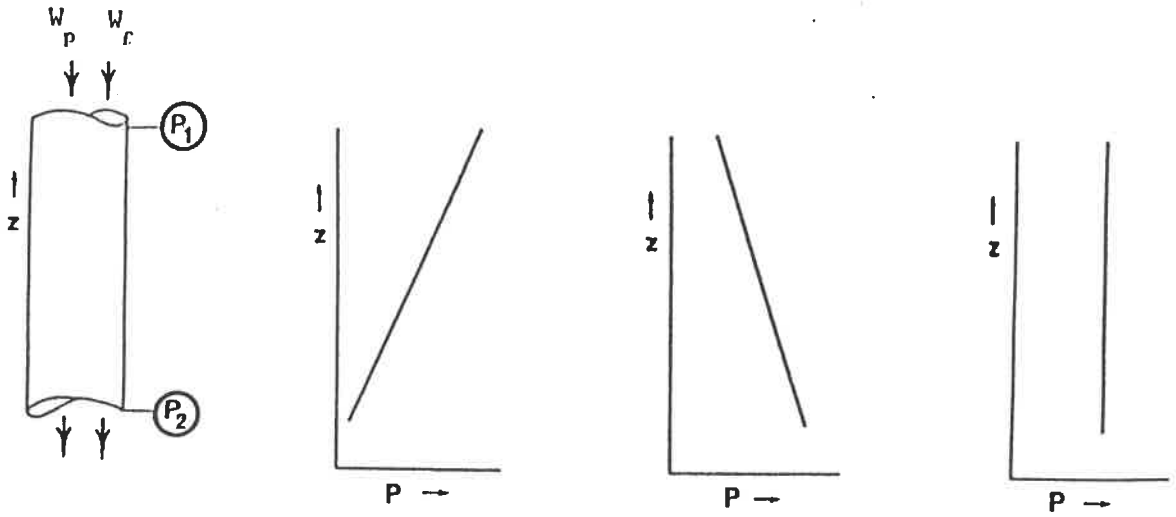

(a) Nonfluidized flow

(b) dense fluidized flow

(c) dilute fluidized flow

Figure (3-1): Pressure profile for different types of flow

[Leung and Jones, 1978]

unique pressure profile for nonfluidized flow with a negative slip velocity. The pressure profile depicted in Figure (3-1b) can refer to dense fluidized solid flow with a positive pressure gradient. The pressure profile in Figure (3-1c) may represent dilute fluidized solid flow with little change in pressure along the tube [Leung and Jones, 1980]. In some published materials, the dilute fluidized solid downflow in standpipe are considered as a part of pneumatic transport.

Quantitative demarcation between "dilute" and "dense" fluidized flow is possible. Because for a given fluid-solid system, there is a unique relationship between slip velocity and voidage. This relationship can be obtained experimentally by measuring the fluidization characteristics of the system. If the published correlations are not available, roughly, the critical factor for determining the "dilute" and "dense" fluidized solid flow is the mass ratio of solid to gas. For dense fluidized flow, the mass ratio is in the hundreds. Dilute fluidized flow have a mass ratio in the tens or less. The dividing line if often taken at eighty. In alternate language, the dividing is at a voidage of about 0.1 [Kunii and Levenspeil, 1969; Geldart and Rhodes, 1986].

For the reclamation of foundry sands in GCP unit (for example: 58kW burner, 100kg/h used-sand feeding), the mass ratio of particles to gas is about 1-2% (solid hold-up 10^{-2}- 10^{-3} in in volume), so this system closely relates to the dilute fluidized solid flow.

3.3 PARTICLE DYNAMICS AND DILUTE FLUIDIZED SOLID FLOW

In the previous section, the slip velocity was used to describe the analogy between fluidized solid flow regime and nonfluidized solid flow regime. From the definition of slip velocity (equation (3-1)), it relates to the gas and the solid velocities. As the motion of solids in flowing fluid streams is a complex hydrodynamic phenomenon, the review of particle dynamics needs to be presented. Furthermore, for considering dilute fluidized solid flow regime in GCP, we also need to refer to the published work concerning this field.

The general equation of motion is based on treatments of particle dynamics by Bassel, Boussinesq, and Ossen and it is essentially an application of Newton's second law [Soo,1967]:

$$\underbrace{\left\{\frac{\pi d_p^3 \rho_p}{6}\right\}\frac{dV_p}{dt}}_{A} = \underbrace{\left\{\frac{\pi d_p^3 \rho_p}{6}\right\}\left\{\frac{3 C_D \rho_f}{4 d_p \rho_p}\right\}|V_f - V_p|(V_f - V_p)}_{B}$$

$$\underbrace{-\left\{\frac{\pi d_p^3}{6}\right\}\frac{\partial p}{\partial x}}_{C}$$

$$\underbrace{+\frac{1}{2}\left\{\frac{\pi d_p^3}{6}\right\}\rho_f \frac{d(V_f - V_p)}{dt}}_{D}$$

$$\underbrace{+\left\{\frac{3 d_p^2}{2}\right\}(\pi \rho_f \mu_f)^{1/2}\int_{to}^{t}\frac{(dV_f/dt') - (dV_p/dt')}{\sqrt{t - t'}}\,dt'}_{E} + \underbrace{Fe}_{F} \qquad (3\text{-}2)$$

The lettered terms can be given a physical interpretation:

-A = mass*acceleration of the particle, which is present only in unsteady flow situations representing the force necessary to accelerate the particle.

-B = drag force containing a drag coefficient that is a function of Reynolds number.

-C = the force from the pressure gradient in the fluid surrounding the particle.

-D = the force due to the acceleration of the apparent mass of the particle relative to the fluid.

-E = Basset force, which is the force due to the deviation of the flow pattern around the particle from steady-state

conditions; this depends on the previous motion of the particle and fluid.

-𝔽 = external force.

Various investigators have solved Equation (3-2) assuming different terms to be zero.

Boothroyd [1971] has made several observations on the order of magnitude of certain terms in Eq. (3-2) for gas-solid systems. For large values of ρ_p/ρ_f, which is common in gas-solid systems except possibly for very high pressure flow systems, the term ℂ, 𝔻, and 𝔼 are small compared to 𝔸 and 𝔹. Of course, at steady state, term 𝔸 is zero, leaving only 𝔹 and 𝔽 of importance. The drag coefficient (C_D) is highly dependent on the fluid regimes whether laminar or turbulent. For the laminar regime (Rep<2), Stokes [1851] solved the fluid dynamics equations for flow past a sphere, determining the drag coefficient by:

$$C_D = \frac{24\ \mu_f}{D_p\ |V_f - V_p|\ \rho_f} \qquad (3\text{-}3)$$

Figure (3-2) shows the behavior of the drag coefficient as a function of the Reynolds number for spherical particles. The

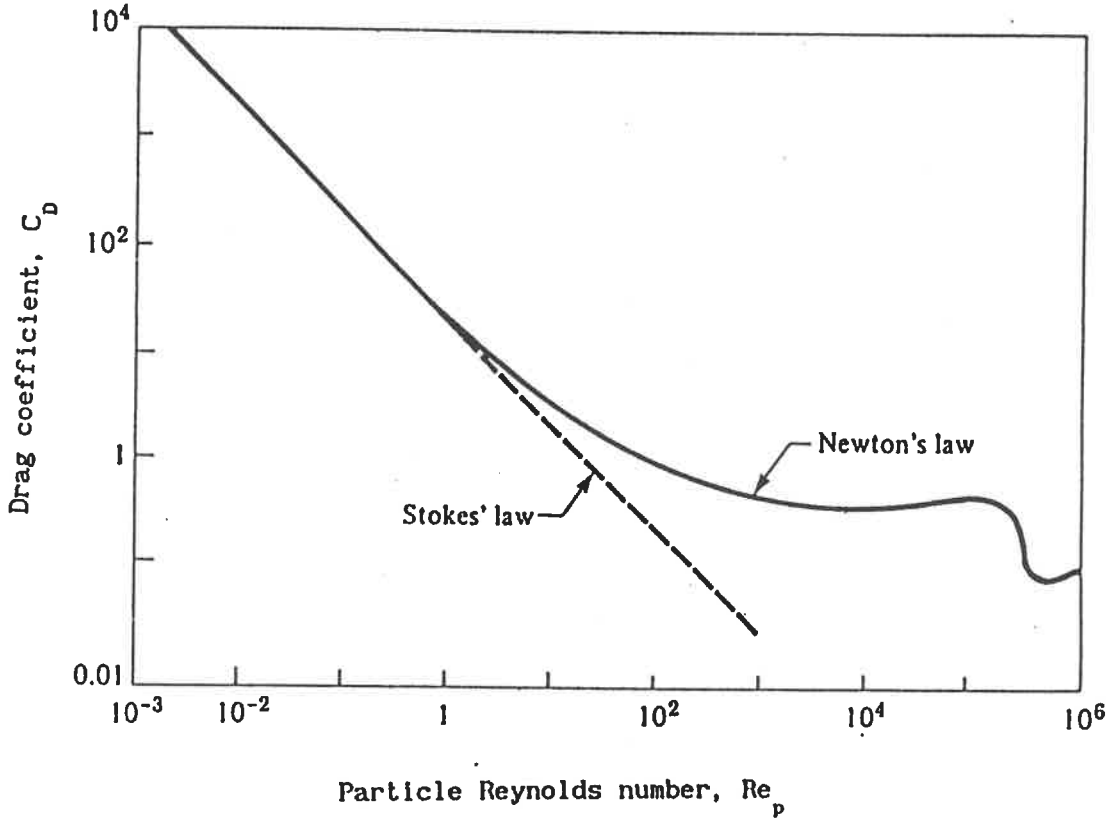

Figure (3-2): Drag coefficient of a sphere as a function of Reynolds number [Boothroyd, 1971]

Stockes and Newton ranges are designated [Bothroyd, 1971]:

$$C_D = \frac{18.5}{Re_p^{0.6}} \qquad \text{if } 0.4 < Re_p < 500$$

and

$$C_D = 0.44 \qquad \text{if } 500 < Re_p < 200,000$$

Clift and Gauvin [1970] have closely investigated the motion of particles in turbulent gas flow. The turbulence intensity of the gas stream may drastically affect the drag coefficient of the particle. These investigators define a critical Reynolds number Re_c as the point where the drag coefficient cuts the 0.3 value (see Fig. (3-3)). Experimental value of drag coefficients in this region show that it depends on the turbulence intensity, as shown in Figure (3-3).

For dilute fluidized solid flow, when the particles flow is fully developed, the particles approach a slip velocity which is nearly equal to the terminal velocity of the particle, it means A=0, and B=F [Matsumoto, 1984].

Tsuji et al. [1983] measured the air and solid-particle velocities in an upward vertical pipe by the use of a laser-Doppler velocimeter (LDV). The range of particle diameter is

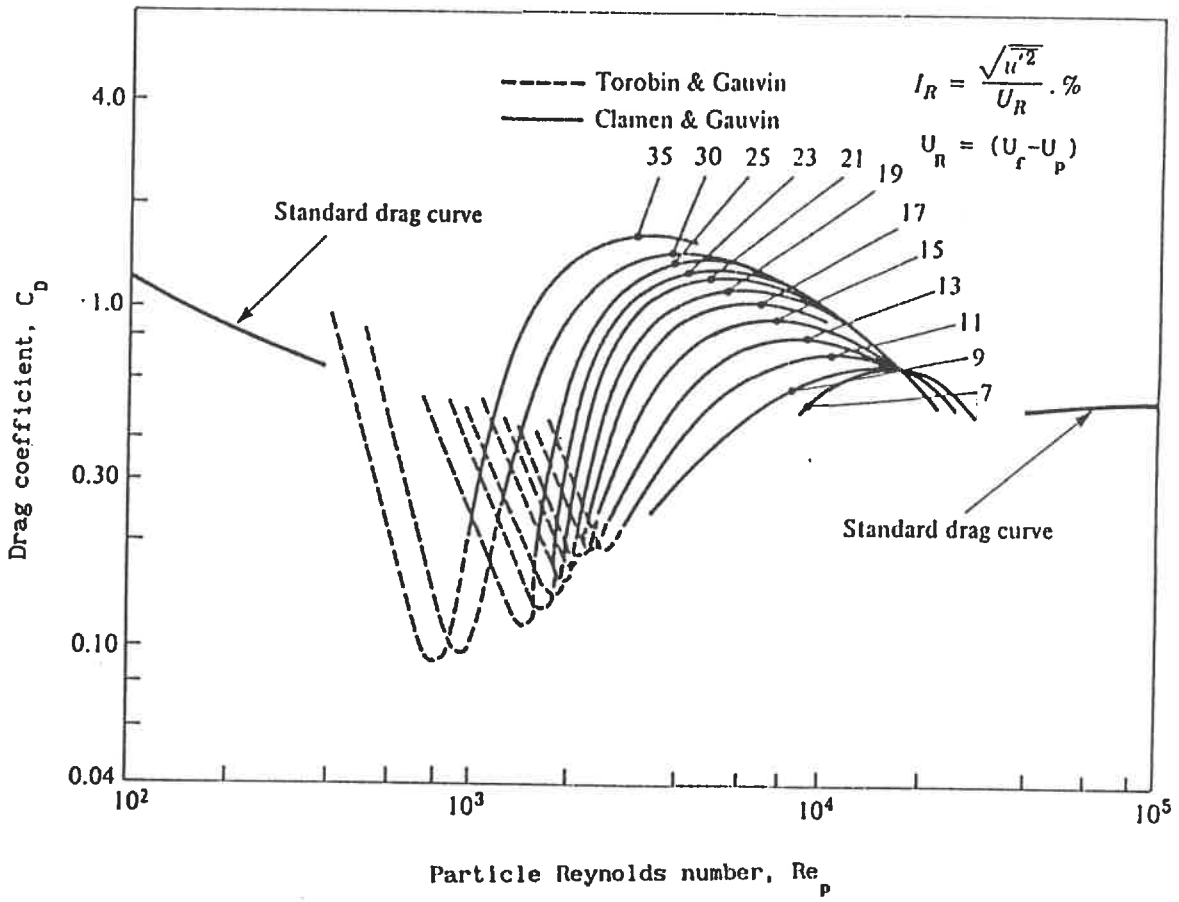

Figure (3-3): Effect of relative intensity of turbulence I_R on the drag coefficients of spheres in the supercritical regime [Clift and Gauvin, 1970]

from 3mm to 200μm, and mass flow ratio is the same (around $3.0*10^2$kg/h). The particle velocity reaches a constant value at a section located at hundreds of "mm" from the beginning of flow.

Shigeru [1983], in a mathematical analysis of pneumatic drying of grains, indicated that the solid accelerates in a short distance, and reaches an almost constant velocity at a low mass flow rate. The distance is in the range of the millimetre for the downward flow and diameter of the particles around 1 – 4 mm.

In the GCP, gas-solid flow is a dilute solid phase mixture in a downward flow. The solid particles can be considered as a well distributed dispersion and reaching a constant velocity (terminal velocity) immediately [Benali et al., 1991a].

3.4 HEAT TRANSFER IN GAS-SOLID FLOW

The GCP is a process in which hot gas contacts directly with the particles. Usually we consider this kind of heat transfer has high efficiency. Grace [1986] proposed a calculation of gas-particle heat transfer in an upward pneumatic

transport. Two representative sizes of particles were taken (50μm and 500μm), the conditions of the calculation were: 8 m/s superficial gas velocity, 1123K gas temperature, and atmospheric pressure. Terminal velocities and gas-particle heat transfer coefficients had been estimated from the relationship of Clift et al [1980] for widely separated spherical particles. The minimum residence time was approximated by assuming a slip velocity equal to the terminal settling velocity, ignoring particle acceleration and clustering. The results show that: with d_p=500 μm, about two seconds are required for the temperature difference between the particles and the surrounding gas to be reduced by 99%. For 50μm particles, the heat-up time is much shorter. These conclusions are reached without considering radiation and "turbulence" effects which would further reduce the heat-up time.

The heat transfer mechanisms occurring in the GCP may be described as follows:

- Gas-particle heat transfer;
- Particle-particle heat transfer;
- Particle-walls heat transfer;
- Gas-walls heat transfer.

Assuming that the solid phase is sufficiently dilute, the heat transfer between colliding particles and the heat transfer due

to wall collision can be ignored [Benali et al., 1991b]. For the heat transfer between the gas and the wall, Grace [1986] pointed out that it may be estimated using correlations for gas alone flowing through the column at the same superficial gas velocity and with the same physical properties. Any errors caused by this procedure will usually be small when the flow is in the dilute solid phase. Furthermore, the heat transfer forms are convection and radiation. It is reasonable to divide the overall heat transfer coefficient into two parts — convective and radiative coefficient.

3.4.1 HEAT TRANSFER TO THE PARTICLES BY CONVECTION

Knowledge of convection heat transfer coefficient of a single spherical particles, moving in a fluid, is important for the analysis of the GCP. Usually, this coefficient is calculated from the well-known experimental correlation of Ranz and Marshall [1952];

$$Nu = h_c D_p/\lambda_f = 2.0+(0.5/0.9)Re^{1/2}Pr^{1/3} \qquad (3\text{-}4)$$

The correlation (3-4) results from experiments which were carried out under steady-state conditions, i.e. when the surface temperature of the particle, Tp, was maintained constant and the temperature field around the particle was established. Therefore,

the use of Equation (3-4) is equivalent to the assumption that heat transfer to the particles is a quasi-steady-state process, i.e.:

$$t_r \ll t_e \qquad (3\text{-}5)$$

where "t_r" is the relaxation time of the external temperature field and "t_e" is the characteristic heating time of the particles. The value of "t_e" is a function of the Biot number of the particle ($Bi=h_c D_p/\lambda_p$). The value of "t_r" is a function of the gas Peclet number and the physical properties of the gas.

Grober [1961] gave "t_e" a classical solution for the unsteady heat conduction in a sphere. In the limiting case of thermal Biot number (hL/λ), one obtains:

$$t_e = 0.056\ d_p^2 / \alpha_p \qquad (3\text{-}6)$$

while for $Bi \ll 1$:

$$t_e = 2\ d_p^2 / (3\ \alpha_p Bi) \qquad (3\text{-}7)$$

Clift [1978] and Abramzon [1976] gave "t_r" a theoretical solution. In the simple case of Pe=0 (perfectly mixed), we obtain:

$$t_r = 100\ d_p^2 / \alpha_f \qquad (3\text{-}8)$$

at large Peclet number:

$$t_r = d_p^2 / (\alpha_f\ Pe^{2/3}) \qquad (3\text{-}9)$$

As it can be seen from the expression given above for "t_e" and

"t_r", the condition (3-5) is not satisfied if the gas Peclet number are moderate (Pe < 10-100) and the physical properties of the particles and gas are similar ($\alpha_f = \alpha_p$; $\lambda_f = \lambda_p$).

Abramson [1976] analyzed theoretically to explain this phenomenon (Pe < 10-100). Some experimental data on the direct contact heat transfer from the particle moving freely in spray-columns show anomalously low values of Nusselt number in comparison with those predicted by Eq.(3-5). A "film model" had been proposed, the asymptotical values of Nu_{obs} was given.

For the heat transfer to many particles by convection, an exact analysis of this problem is exceedingly difficult, if not impossible. That is because of the complex hydrodynamics involved. One way is the direct measurement of heat transfer coefficients coupled with correlations on the basis of dimension-less groups. Most of the theoretical analysis are based on single particle Equation (3-4) in the flow system and consider the effects between particles.

No published results for gas-particle direct contact heat transfer have been found concerning a flow regime identical to the GCP. Equation (3-4) appears to be the best correlation for the estimation of the convection heat transfer coefficient.

3.4.2 HEAT TRANSFER TO CLOUDS OF PARTICLES BY RADIATION

According to many studies [Flamant and Meniganlt, 1988; Vorteyer, 1978, 1979; Tien and Drolen, 1987; Reiss, 1988], thermal radiation becomes an important mode of heat transfer in fluidized beds at temperature above 750°C. Treatment of solid wastes by the GCP operates at high temperature (i.e. more than 600°C for reclamation of foundry sand). In this case, thermal radiation becomes significant. The gas and particles can absorb, emit and scatter radiation. In radiative heat transfer calculations, the accuracy of the predictions depends not only on the representation of the radiative transfer model, but also on the radiative and thermophysical properties of the medium used.

(a) Model for the radiation properties of gases:

The properties of gases can be obtained only through the understanding of the molecular structure of the gaseous species. Because molecular emission and absorption take place in discrete wavelengths, gas radiative properties are not continuous over the wavelength spectrum but are concentrated in "lines" [Viskanta, 1990]. In modeling gas properties, these lines are considered to make "narrow" or "wide" bands of spectrum.

A detailed discussion of the narrow-band models to predict radiation properties of gases was given by Ludwig et al. [1973] and in review articles by Tien [1978] and Edwards [1976]. Narrow-band models generally require an extensive library of input data, and the calculations cannot be performed with reasonable computational effect. As long as the concentration distributions of gaseous species are not accurately known, the high resolution and accuracy obtained for the spectral radiative properties from this model are not warranted.

Since radiation emission/absorption by gases is not continuous but is in spectral bands, experimental data for most common gases of interest in combustion systems have been correlated using wide-band models [Tien, 1978; Edwards, 1976], the significance of these semi-empirical methods is that they offer improved accuracy, and they enable extrapolation of gas emissivities to high temperature and pressure conditions that are not favorable for accurate experimentation.

When the very accurate determination of the temperature and heat flux distributions are not required or warranted, radiative heat transfer can be facilitated using total emissivity /absorptivity mean-beam-length model [Hottel, 1967]. For example, mixtures of carbon dioxide and water vapor, the predominant products of natural gas combustion, can be treated

on the Hottel's charts [Siegel, 1985], i.e., $\varepsilon_g = f(T_g, P_g L_m, P_g/P)$. Scaling rules can be used in Edwards's charts [1984] to extend the range of applicability of the total emissivity and absorptivity of combustion gases. In order to use the charts in computer models, curve-fitted correlations are desirable. For example, for carbon dioxide-water vapor mixtures, a simple correlation for the gas emissivity is given by [Taylor and Foster, 1974]:

$$\varepsilon_g = \sum_{i=1}^{4} (b_{1,i} + b_{2,i} T_g) \, [1-\exp(-6\, k_{g,i} P_{co2} L)] \qquad (3\text{-}10)$$

where L is the equivalent length of radiation given by four times the ratio of the volume of the furnace to its peripheral surface:

$$L = \pi D_f L_f / (2 L_f + \pi D_f) \qquad (3\text{-}11)$$

The values of the coefficients $b_{1,i}$, $b_{2,i}$ and $k_{g,i}$ are given in Table (3-1):

Table (3-1) : Value of coefficients $b_{j,i}$ in Eq.(3-10)

i	$b_{1,i}$	$b_{2,i}$	$b_{3,i}$
1	0.364	4.73×10^{-5}	0
2	0.266	7.19×10^{-5}	0.69
3	0.252	-7.41×10^{-5}	7.40
4	0.118	-4.52×10^{-5}	80.0

* Taylor and Foster [1974]

(b) Radiation properties of particles:

Although particle radiation is continuous over the wavelength spectrum, radiative properties of particles can be determined if the shape, size, concentration and emissivity of different kinds of particles in the medium are known.

When a beam of radiation is incident upon a suspension of particles, some of it is transmitted, some absorbed and some scattered. Figure (3-4) illustrates what happens when radiation is incident upon a black particle suspended in a transmitting medium. For the spherical particle, the low concentration of suspension particles (loading ratio < 1%), the absorbing cross-sectional area is given [Gray et al.,1976]:

$$A_p = n_p \pi d_p^2/4 \qquad (m^2/m^3) \qquad (3\text{-}12)$$

where "n_p" is the number of particles per unit volume of gas, and "d_p" is the average diameter of the particle expressed in μm.

(c) Engineering model of radiative transfer:

The radiation properties depend on the position , local temperature and composition. In order to solve the radiative transfer problem, simplifying assumptions are to be introduced. Since it is not possible to develop a general solution method for the radiative transfer equation, different models have been developed over the years. For the

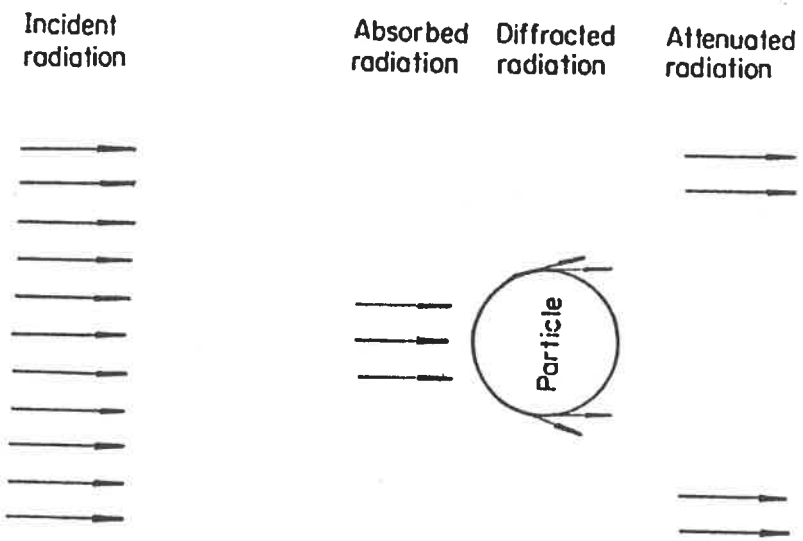

Figure (3-4): Attenuation of radiation by a particle

GCP, according to the nature of the physical system modeled, the radiation characteristics of the medium, the level of detail and degree of accuracy required, and the availabity of computer resources, the mean beam length-emissivity model can be adopted for modeling radiative transfer. Since it is not the object of this thesis to discuss all the models of radiative transfer, the reader is refered to the recent reviews of Smoot et al.[1985] and Viskanta [1987].

Consider the radiation exchange in a gray wall enclosure, i.e., in furnace chamber, the radiation incident on a load surface (particles) usually comes both directly and indirectly from the gas and refractory walls, hence by refraction and / or reradiation through the gas to the load at temperature T_p. If the refractory surface is radiatively adiabatic (usually a good approximation since the difference between convection from gas to refractory and conduction outwards through the refractory wall is smaller compared to irradiation on the refractory), it is possible to show that the net radiant heat exchange between the gas and the load by the combined mechanisms is given by [Hottel, 1967]:

$$Q_{g\ p} = (GP)\ \sigma\ (\ T_g^4 - T_p^4\ ) \qquad (3\text{-}13)$$

where (GP), having the dimension of an area, is called the total-exchange area for radiative heat transfer between gas and load surface A_p, in the presence of refractory surface A_r. The value $(GP)/(A_p+A_r)$ is a dimensionless quantity, which, from the definition of emissivity, can be identified as an average emissivity evaluated at the same beam length, denoted by L_m. Therefore, this approach is called the mean beam length emissivity model [Viskanta, 1989]. Depending on how sophisticated a model has been set up to describe the very complex processes of radiative heat transfer, the expression for (GP) takes one of the virial forms [Hottel, 1974]. For example, for a mixture of a gray plus clear gas with a gray load emissivity ε_p, the total exchange area (GP) is given by [Hottel, 1974]:

$$(GP) = A_T \left[\frac{1}{(c\,\varepsilon_p)} + \frac{1}{\varepsilon_{gp}} - \frac{1}{\gamma_{gp}} + \frac{(1/\gamma_{gp}) - 1}{c\,\varepsilon_g + (1-c)\varepsilon_r}\right]^{-1} \qquad (3\text{-}14)$$

where A_T $(=A_p+A_r)$ = total area of the load (A_p) and refractory (A_r).

c $(=A_p/A_T)$ = cold fraction.

ε_g ε_p and ε_r = emissivity of the gas load and refractory, respectively.

ε_{gp} and γ_{gp} = equivalent gray-gas emissivity and gray gas absorptivity, respectively.

The mean beam length-emissivity model is zero-order approximation for radiative transfer; it is simple and allows for the possibility of including detailed band information for infrared radiating gas.

Solving the model of radiative transfer asks to determine the gas and particle radiative properties for a given temperature, pressure and concentration. Therefore, before evaluating the properties of a given system, it is necessary to determine the local temperature, pressure and concentration distributions in the medium. Hence, the governing equations of energy, combustion and radiative transfer, as well as model equations for the radiative properties, need to be solved simultaneously.

3.5 PARTICLES COMBUSTION

Treatment of divided solids or sludges by the GCP usually involves a particle combustion process. For foundry sand reclamation, the coating resin is burned sequently during the process. Then clean sand is obtained. In this process, the particle diameter will change and energy will be released.

Particles combustion can be classified into liquid

particles combustion (i.e. fuel droplets) and solid particles combustion (i.e. coal). Generally droplet combustion process is found to be physically controlled (diffusion limitation). Solid particles combustion process is sometimes a physically controlled process too, but chemical kinetics factors often play an additional part. However, the aspect of the combustion models of the two kinds of particle is very similar. Indeed, the solid particle combustion can be regarded in some respects as a special case of a burning droplet [Spalding, 1979]. So the droplet combustion model is considered as our modeling fundament.

3.5.1 **DROPLET COMBUSTION**

The commonly considered case of droplet combustion in a surrounding oxidizing atmosphere is droplet heating, droplet vaporization, and since oxidant and vapour are initially separated, vapour and oxidant burning in a diffusion flame surrounding the droplet. Most of the published theoretical studies on droplet combustion have taken the classical spherico-symmetric diffusion controlled model [Spalding, 1979; Williams, 1983]. They are illustrated in Figure (3-5). The droplets have been considered spherico-symmetric, quasi-steady, single-component, surfactant-free, isolated. However, this

model is only applicable to diluted spray system [Williams, 1973].

Generally, research on droplet combustion has been devoted to studies of the combustion of a stationary isolated single droplet, because of the belief that it is fundamental to the whole understanding of droplets combustion. The major objective of these assumptions is the prediction of the burning rate of the droplet. It has been demonstrated many times experimentally, as shown in Figure (3-6), that under burning conditions, the square of the droplet diameter is a function of burning time (d^2-law), being related by a proportionality constant K, which has been named the burning-rate coefficient or evaporation constant. The form is [Ayyaswamy, 1989]:

$$d(d_L)^2/dt = (-2m_F)/\pi\rho_L r_L = K \qquad (3\text{-}15)$$

where m_F is mass burning rate, ρ_L is the density of the droplet at the appropriate temperature, r_L is the droplet radius and d_L is the droplet diameter.

According to the d^2-law, Spalding [1979] took the assumptions of stationary isolated droplet, infinitely fast chemical reaction rate, spherico-symmetric diffusion controlled

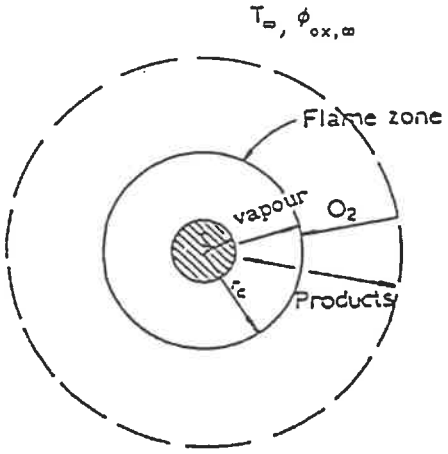

Figure (3-5): Typical model of droplet burning [Williams, 1973]

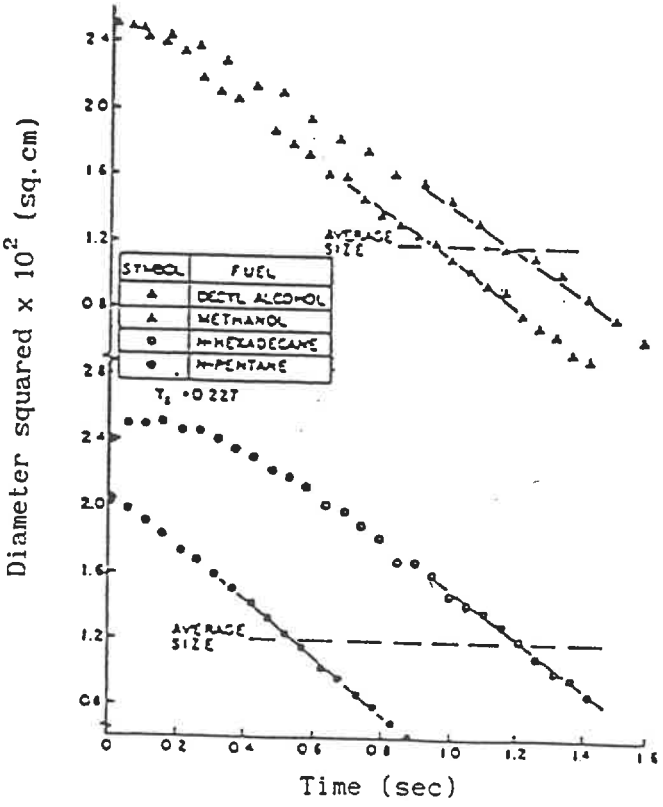

Figure (3-6): Typical plot of d^2 against time for stationary droplets burning in flame gases. [Faeth and Lazar, 1971]

model, and got the basic burning rate equation:

$$\frac{G_o d_{po}}{2 \rho_\phi \beta_\phi} = \ln \left[1 + \frac{(\phi_0 - \phi_\infty)}{- \rho_\phi \beta_\phi (d\phi/dr)_o / G_o}\right] \qquad (3\text{-}16)$$

where, G_o is the evaporation rate on the surface of the droplet, ϕ is a conserved property, usually takes "C_{vap}-C_{ox}/ss". (C-mass fraction, s- stoichimetric ratio). β is the diffusion coefficient. By interpretation of ϕ in the various possible ways, useful results are obtained. For example, it is possible to obtain the result for solid particle combustion (see next section).

The previous analysis is based only on a stationary droplet. In real combustion devices, the heating, vaporization, combustion processes of the droplet are all strongly influenced by forced convection. Forced convection effects result in enhanced heat and mass transfer rates in the region surrounding the droplet due to the thining of the gas film layer. Fernandez-Pello [1986] gave more information about this case.

3.5.2 SOLID-FUEL PARTICLE COMBUSTION

We consider the coal-particle combustion. Although coal has a volatile component, consisting of hydrocarbon gases which are released when the temperature of coal is raised, this volatilisation is very different from the vaporisation of a droplet. Hydrocarbon gases are released from coal as a consequence of a chemical reaction, not a simple phase change. The release of the gases may indeed be exothermic rather than endothermic, as is vaporisation. Moreover, there is no distinct temperature at which vapour release occurs, but the rate of release increases with the temperature. The substance which remains after the volatilisation process still contains much more carbon. It is indeed what is known as "coke". It consists of pure carbon. So the carbon-oxygen reaction on the particles is the main reaction of coal-particle combustion. The combustion of solid carbon is often influenced kinetically [Smoot, 1979]. Spalding [1979] used Equation (3-16) to get the coal particle burning rate equation. As ϕ_o , the mass fraction of carbon, is negligible small, therefore $\phi_\infty = -\phi_{ox,\infty}/s$, and equation (3-16) becomes:

$$\frac{G_o\, d_{po}}{2\, \rho_{ox}\, \beta_{ox}} = \ln\left[1 + \frac{(\phi_{ox,o} - \phi_{ox,\infty})}{-\rho_{ox}\beta_{ox}(d\phi_{ox}/dr)_o/G_o}\right] \qquad (3\text{-}17)$$

Then considering the influence of chemical kinetics, the value of $\phi_{ox,o}$ (the oxygen concentration at particle surface) can be written as follows [Spalding, 1979]:

$$\frac{\phi_{ox,o}}{\phi_{ox,\infty}} = [1 + (s + \phi_{ox,o}) \frac{K\ p\ d_{po}}{2\ \rho_{ox}\beta_{ox}} \exp\left(\frac{-E}{RT}\right)]^{-1} \qquad (3\text{-}18)$$

When the particle diameter d_p is very small (<30μm), the second term in the square bracket is also small. The ratio $\phi_{ox,o}/\phi_{ox}$ must be close to unity. The process is kinetically controlled. If d_p is not too small and the surface temperature is high, the second term in the bracket of Equation (3-18) becomes prominent, the consequence is that $\phi_{ox,o}/\phi_{ox,\infty}$ tends to zero. It amounts to writing that the oxygen diffusing to the surface is used by the carbon as soon as it arrives. In this case, the combustion process is controlled by oxygen diffusing. So the solid-particle combustion is controlled physically or kinetically depending on the specific conditions.

3.5.3 RESIN-COATED SAND COMBUSTION

Organic resin contains such products as phenol, formaldehyde, furfural alcohol, urea, amines or acid compound [Kane, 1968; Ham et al., 1987]. When the resin is heated to

a high temperature (300-500°C), decomposition happens first [Fenimore and Martin , 1972]. Volatile matter and carbon can be produced. So,the resin-coated sand combustion process is more similar to the coal-particle combustion process. Because the particle diameter is around 300μm, and the surface temperature is high enough, it is considered that the resin-coated sand combustion process is controlled by oxygen diffusion to the particle surface.

3.6 MODELING OF THE TWO-PHASE FLOW SYSTEM

For the rigorous solution of flow, energy, mass and chemical reaction equations in two-phase flow system, extensive computations are required. However, usually there is a lack of physical input data, especially of the gas and the particle properties in two-phase flow system, because the constitutive equations of these properties changing with time and position in the system are very complex. So one has to rely on calculation methods based on simplifying assumptions. These assumptions lead up to different models of two-phase flow system. Two essential models, well-stirred model and plug-flow model, are presented in this section. The most complex models are constituted by these two essential models [Ishii, 1981].

3.6.1 WELL-STIRRED MODEL

This model is based on the assumption that mixing in the system is so effective that the gas and particles properties (i.e. temperature and concentration) are uniform throughout the system volume. The model was discussed in detail by Hottel [1967, 1974]. This model is considered to be a zero-dimensional model, uniform but different properties of gas and particles in the system can be taken. Hottel [1974] compared the experimental data with the model predictions. The results showed that the stirred-vessel heat transfer model can be successfully applied to those systems in which there is no appreciable axial drop of the mean gas temperature. This condition is roughly met in combustion chambers fired with high-velocity burners and furnaces where the flame length is approximately equal to the furnace length. Under these conditions, a maximum error of ±20% can be expected in calculating the absorbed heat flow to the load being heated.

3.6.2 PLUG-FLOW MODEL

Plug-flow model assumes that the gas and the particles properties and characteristics (i.e. temperature, density) vary along the direction of flow, but are uniform across any cross

section. The model was discussed in detail by Frisch [1982]. As an application of this one-dimensional model, a conservation balance on a short elemental length of gas in the system and each elemental region being assumed well-stirred is written. The results show that as the number of elemental regions in the system increases, the accuracy of the model for predicting physical properties distributions of gas and particle (i.e. temperature) increases.

For the Gas-Contact Process, at the beginning of the process, we can choose a well-stirred model to calculate the temperature profile of both gas and particle because of the intensive turbulence and mixing created by the burner. In the following zone, the plug-flow model can be used.

3.7 CONCLUSION

Although studies on gas and particle mixing flow, contact heat transfer from the surface of gas and particle mixing flow and fuel-particle combustion are abundant, published literature on particle flow charateristics in two-phase flow, heat transfer between the cloud of particles and gas at high temperature, and resin decomposion and combustion kinetics are scarce. All the existing studies on this topic require the

determination of at least one empirical parameter to estimate the velocities of gas and particles, the heat transfer coefficient and the burning rate of the particles. Effects of particle size, quantity of resin and high temperature conditions should be especially investigated.

CHAPTER 4. THEORETICAL APPROACH

4.1 INTRODUCTION

Detailed modeling is known as solving numerically the governing conservation equations of mass, momentum and energy of the real process. Solving these equations requires input data such as transport coefficients, chemical reactions that can occur, boundary conditions and so on. For reclamation of foundry sand by the GCP, it relates to the characteristics of the two phase flow, the heat transfer between the gas and the particles, even the refractory, and the resin combustion that coats the sand particle. The rigorous theoretical analysis and determination of these characteristics is difficult. Some of them do not have a mature theory or experimental results, especially for resin combustion process. However, for the numerical simulation, main control steps are taken as limitative conditions to derive the models.

The purpose of this chapter is to assume some control process through the theoretical analysis, and advance some models for the Gas-Contact Process. These models will be tested through the experiments in the next step. Then a computational model can be used as an engineering design tool.

4.2 THEORETICAL ANALYSIS

First, the gas and the particles flow regime is considered. As indicated in chapter 3, the used sand in the GCP is in low solid concentration (solid hold-up 10^{-2}–10^{-3}, density: 10^{-3} g/cm^3) and small diameter (d_p=300μm). The aerodynamics characteristics of the GCP is the same as low bulk density mixture flow. Pneumatic transport characteristics can be taken to simulate this two phase movement in the system. The particle flow is assumed fully developed, and the particle approaches a slip velocity, which is nearly equal to the terminal velocity of the particle. Furthermore, the process is considered to be divided in two regions. First region includes the burner and part of the furnace. The gas phase is considered in high degree turbulence due to the counter-rotation and high temperature effects. In the second region the turbulence of the gas phase will decline gradually. Based on these characteristics, three possible models for flow regime can be advanced:

(I) Plug flow model for both the gas and the solid phases in the whole process (Figure (4-1b)).

(II) Well-stirred model for both the two phases in the first region, and plug flow in the second region (Figure (4-1a)).

(III) Well-stirred model for the gas phase and plug-flow for the solid particle in the first region, then plug flow model for the two phases in the second region (Figure (4-1c)).

Different flow regime models will have different heat transfer characteristics between the two phases.

Second, consider the resin eliminating process. Resin combustion rate depends on temperature of solid particle, oxygen concentration, and combustion mechanism. The solid temperature depends on the heat transfer rate between the two phases. If resin combustion rate is assumed infinite and there is enough oxygen, only the heat transfer rate is a limiting step. It is called heat transfer limitation model.

The heat transfer rate is determined by heat transfer coefficients and temperatures of two phases. The heat transfer coefficients (including convection and radiation) are determined by the behaviour of gas and particle flow, the physical properties of the gas and the particles (even the refractory), the geometrical shape and the size of the system and particles.

Normally the organic resin contains such products as phenol, formaldehyde, furfural alcohol, urea, amines or acid compounds

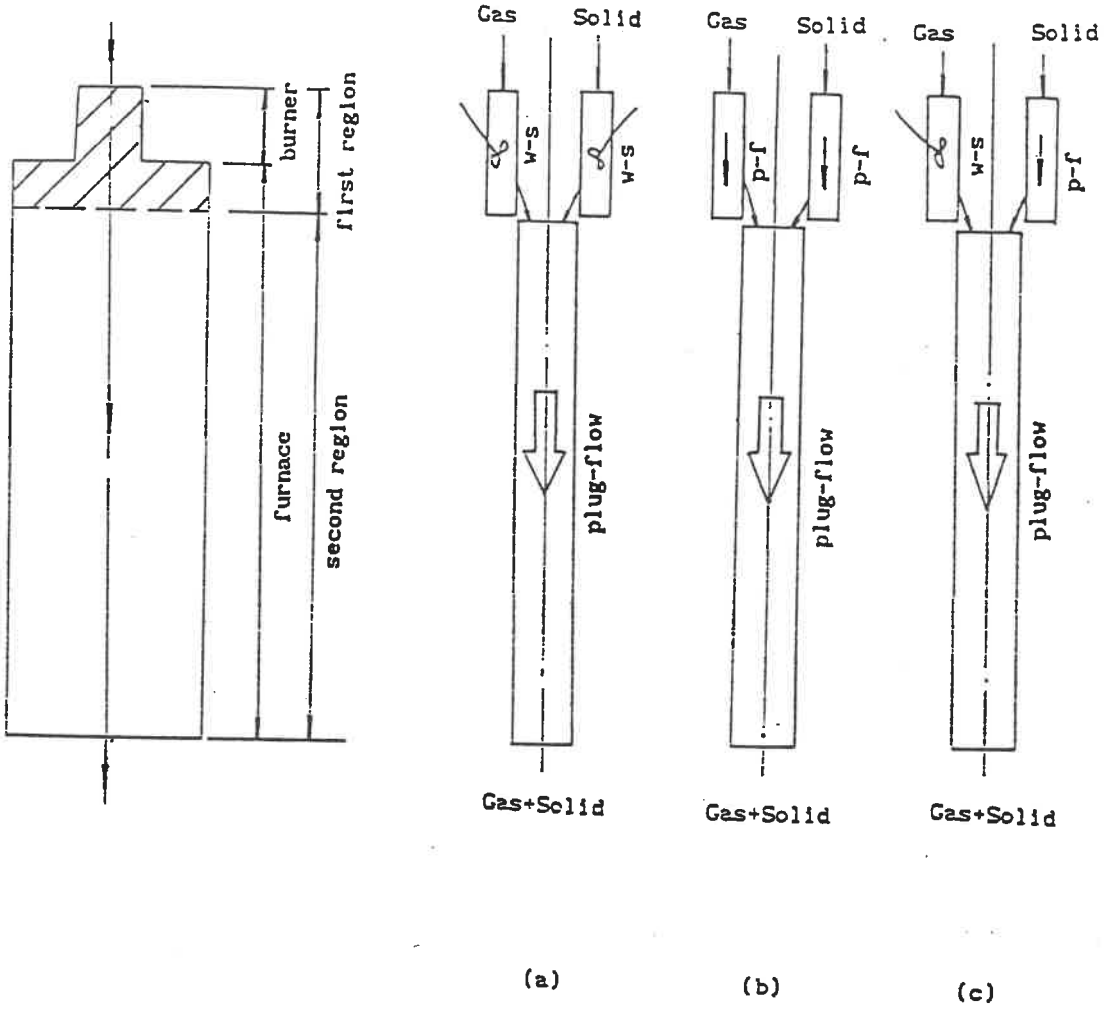

Figure (4-1) Flow regimes for different models

[Kane, 1968]. Thus the resin combustion process is a complex process. No publication concerning the detailed analysis of the resin combustion process has been found. Some possible processes for simulating the resin combustion need be assumed.

In foundry sand, the resin quantity is very small (about 1% - 2% mass radio), resin phase change process can be ignored. So resin will be decomposed first. Because the organic resin is a high-molecule compound, in general, these molecules are too large for vaporization to occur without decomposition of the molecules. Thus, a high-molecular resin must be decomposed to smaller molecules in order to volatilize [Wall, 1972]. Resin decomposition probably produces the volatile and the char that stays on the particle surface.

Two decomposing products lead to two types of resin combustion models. The first one is called the volatile diffusion combustion model. The assumption is that the volatile combustion process is similar to a liquid fuel droplet combustion in hot gas (figure (4-2)). That is the resin decomposes first, and then the volatiles diffuse into the atmosphere of the gas. The combustion occurs around the particle. The second one is called the char combustion model. The assumption is that the char combustion process is similar to

a solid fuel particle combustion in hot gas. That means that the oxygen diffuses from the atomsphere to the particle, and the char burns on the particle surface.

For the volatile diffusion-combustion model, the chemical reaction between the volatile and oxygen is assumed instantaneous as for fuel droplet combustion. The flame is in a very narrow region around the particle. The resin combustion rate depends on the volatile diffusion rate and the oxygen concentration in the gas. The heat radiation from the flame to the particle is ignored. It is assumed that all the combustion heat is absorbed by the gas.

For the char combustion model, the reaction is also assumed instantaneous as for coal combustion for particles larger than 30 μm (see 3-5-2). Because the combustion occurs on the particle surface, the oxygen diffusion rate is the limiting step of the resin combustion process. All the combustion heat is assumed absorbed by the particle.

The surface concentration of the volatile on the particle is one of the main parameters for the determination of the volatile diffusion rate. This value is determined by the resin decomposition rate, particle temperature, and pressure around

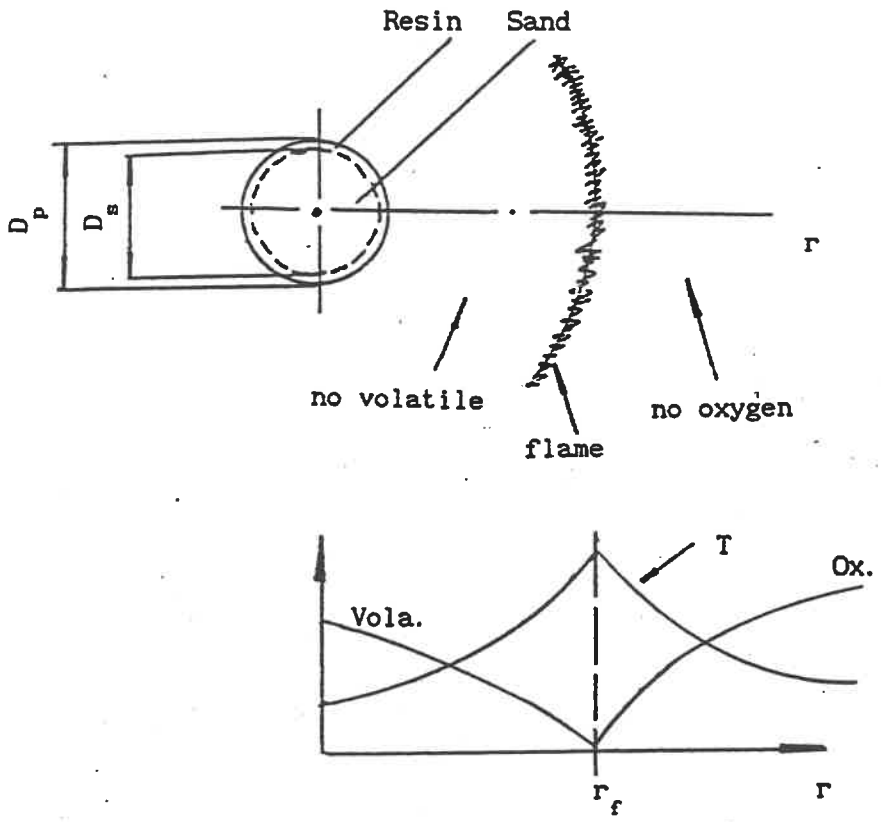

Figure (4-2) Volatile diffusion-combustion model

the particle. If the pressure is considered constant and the decomposition rate is infinite, the concentration of volatile only depends on the particle temperature.

Therefore, four possible models for resin combustion process can be advanced:

(1) Heat transfer rate is the only limiting step of the process.

(2) Heat transfer rate and volatile diffusion rate are both limiting steps of the process. And resin combustion is considered to be a one hundred percent volatile combustion.

(3) Heat transfer rate and oxygen diffusion rate are both limiting steps of the process. And resin combustion is considered as char combustion due to ignoring the lower volatile ratio.

(4) Heat transfer rate and volatile/oxygen diffusion rates are limiting steps of the process. And resin combustion is considered as volatile and char two-step combustion.

By combination of the flow regime models and resin combustion models, there are twelve possible models that need to be verified by experiment. These models are divided in two categories:

- Only the heat transfer rate is a limiting step for the used sand reclamation process. Resin combustion is instantaneous. The

different flow models of the two phases are considered.

- Both the heat transfer rate and the resin combustion process are limiting steps. The different flow models of the two phases are also considered.

Before giving the mathematical equations for these models, respectively, another characteristic that need to be mentioned is the temperature distribution in the particle. There are three types of temperature profiles in the particle:

– First case: for a large particle diameter and thick layer of resin coating, the temperature is assumed non-uniform in the particle and resin layer:

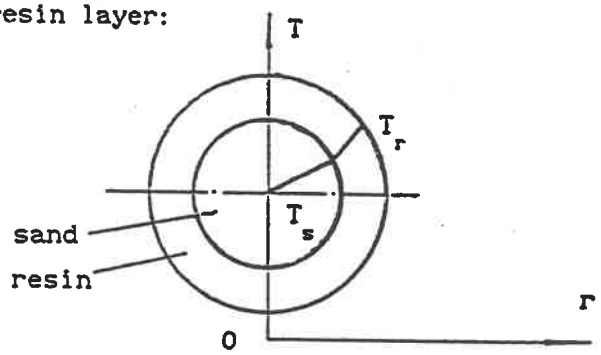

- Second case: for a large particle diameter and thin layer of resin coating, the particle temperature is assumed non-uniform, and the resin temperature is uniform:

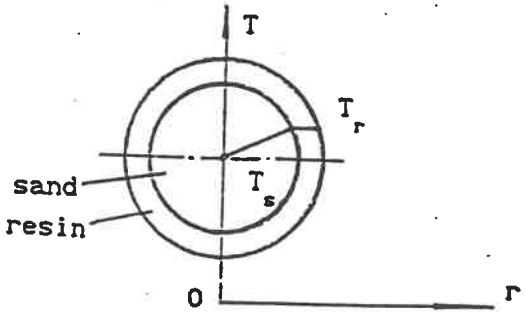

- Third case: both the particle diameter and the resin layer are small and thin. The temperature in the two parts is assumed uniform and the same:

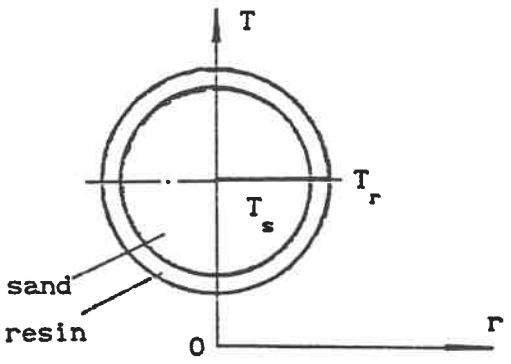

For used foundry sand, the particle diameter is in the order of a tenth of a millimetre (10^{-4}m), and the layer of resin coating is about 0.5% to 2% of the sand diameter. Therefore, the temperature profile is of the third type. The temperature is uniform and the same in the particle and in the resin layer.

The theoretical analysis for differentiating between "thin system" and "thick system" is the Biot number [Weast et al., 1985]. The Biot number reports the rate of internal thermal resistance (conduction) with outside thermal resistance (convection):

$$Bi = h\, d_p/\lambda.$$

"h" is the convective heat transfer coefficient to the surface,

"d_p" is the size of the particle,

"λ" is the thermal conductivity of the particle.

The critical distinction of the Biot number for determining the thin or thick system is [Weast et al, 1985]:

- thin system: Bi < 0.1
- thick system: Bi > 0.1

For foundry sand used here, the Nusselt number is approximately equal to one, the thermal conductivity of sand is near 0.6 W/m K, and the diameter of particle is about $3*10^{-4}$m. The Biot number is in the order of 10^{-2}. So the assumption of a thin system is justified. In the models developed here, a uniform temperature inside the sand particle is considered.

4.3 HEAT TRANSFER RATE LIMITATION MODELS

In this case, the resin combustion rate is determined by the ratio of heat transfer flux from the gas to the particle with the resin volatilization latent heat. Heat transfered from the gas is used first to decompose the resin, and second, if any remains, to heat the sand particle. While in the gas phase, the resin burns instantaneously and the combustion heat is released to the gas phase.

4.3.1 WELL-STIRRED FLOW IN THE TWO PHASES AND HEAT TRANSFER RATE LIMITATION MODEL

This model is based on the assumption that mixing in the region is so effective that the gas and the particle temperature and concentrations of the two phase are uniform throughout the volume of the region. The model is considered to be a zero-dimensional model, at the same time, we can take uniform but different properties of the gas and the particles in the system. So the mean temperature of the gas [T_{g-out}] and the particles [T_{p-out}] are considered, respectively. The heat transfer includes forced convection and radiation between the gas and the particle, even the refractory. T_{g-out} and T_{p-out} are not function of the position in this region. They are function of the residence time τ_g and τ_p, respectively.

For the mean residence time of the gas, we take an average gas volume flowrate [W_g, m^3/s] at the gas temperature in the whole region [T_{g-out}]; the gas residence time (τ_g) is:

$$\tau_g = (1/4)\pi(D_b^2 \ L_b + D_f^2 \ L_{f1} \ )/W_g \qquad (4-1)$$

Here, "D_b" and "D_f" are inside diameters of the burner and the furnace, respectively. "L_b" is the length of the burner. "L_{f1}" is the length of the well-stirred region in the furnace.

When the particle flow is fully developed, the particles approach a slip velocity which is nearly equal to the terminal velocity of the particles. So the relative velocity between the two phases equals the terminal velocity:

$$| V_g - V_p | = V_t \qquad (4\text{-}2)$$

and the terminal velocity (V_t) of the particle is given by Kunii [1969];

$$V_t = [(4gd_p(\rho_p-\rho_g))/3\rho_g C_d]^{1/2} \qquad (4\text{-}3)$$

where C_d is an experimentally determined drag coefficient. For spherical particles, the drag coefficient is given by Kunii [1969]:

$$C_d = 24/Re_p \qquad \text{for } Re_p < 0.4 \qquad (4\text{-}4)$$

$$C_d = 18.5/Re_p^{0.6} \qquad \text{for } 0.4 < Re_p < 500 \qquad (4\text{-}5)$$

$$C_d = 0.44 \qquad \text{for } 500 < Re_p < 200{,}000 \qquad (4\text{-}6)$$

Taking the gas velocity (V_g) at $T_{g\text{-}out}$, the particle velocity is:

$$V_p = V_t + V_g \qquad (4\text{-}7)$$

Then the mean residence time of the particles is written as:

$$\tau_p = (L_b + L_{f1})/V_p \qquad (4\text{-}8)$$

The other assumptions for the conservation equations of the well-stirred model are summed up below:

- The physical properties of each phase are independent of the position and time, such as specific heat (C_p), conductivity, and so on. It is assumed that they can be taken at an average temperature of each phase in the whole region [$T_{g\text{-}out}$, $T_{p\text{-}out}$].
- The resin-coated sand particle is considered as a spherical particle. The particle temperature is uniform [Bi<0.1].
- The distance between the particles is much larger than the particle diameter.
- The heat transfer is by forced convection and radiation (mixture of a gray and clean gas with a particle emissivity).
- In the well-stirred region, the heat loss to the surrounding is neglected.
- The temperature of the refractory is uniform.

The stirred vessel model is a zero-dimensional model. It yields only the total heat transfer rate to the load (particles) without providing information on the local heat flux distribution to the load. The resin elimination process is similar to the high temperature drying process: preheating of

the particles up to the temperature where volatization starts, volatilization at constant particle temperature, heating of particle when all the resin is eliminated. The only difference is that the resin undergoes a combustion reaction while in the gas phase.

For the heating of particles, the energy conservation equation on the particles can be written as :

$$\dot{m}_p \tau_p C_{pp} (T_{p\text{-out}} - T_{p\text{-init}})$$

$$= [(GP)\ \sigma_R (T^4_{g\text{-out}} - T^4_{p\text{-out}}) + h\ (T_{g\text{-out}} - T_{pout})\ A_p]\tau_p \qquad (4\text{-}9)$$

and the energy conservation equation on the system can be written as:

$$\dot{m}_g\ \tau_g\ C_{pg}\ (T_{g\text{-init}} - T_{g\text{-out}}) = \dot{m}_p\ \tau_p\ C_{pp}\ (T_{p\text{-out}} - T_{p\text{-init}}) \qquad (4\text{-}10)$$

where $T_{g\text{-init}}$ is the natural gas combustion temperature. $T_{p\text{-init}}$ is the initial solid temperature. h is forced convection heat transfer coefficient between the gas and the particles. As discussed in Chapter 3 (Equations (3-5) and (3-6)), since the thermal conductivity of particle is near 0.6 W/(m K), the thermal conductivity of the gas is around 10^{+2}- 10^{+3} W/(m K)

[Weast et al. 1982], the particle diameter is about $3*10^{-4}$m, and the Biot number is in the order of 10^{-2}, then "t_e" is in the order of 10^{-6} s, and "t_r" is in the order of 10^{-8}-10^{-9} s. Thus $t_r << t_e$. Equation (3-3) can be used for calculating h:

$$h = (2+0.6Re^{1/2}Pr^{1/3})\lambda_g/d_p \qquad (4\text{-}11)$$

the Prandtl number (Pr) is:

$$Pr = C_{pg}\,\mu_g / \lambda_g \qquad (4\text{-}12)$$

the particle Reynolds number (Re_p) is:

$$Re_p = \rho_g\, d_p\, (V_g - V_p)/\mu_g \qquad (4\text{-}13)$$

and from discussion above, the "$|V_g - V_p|$" is equal to the particle terminal velocity (V_t).

Back to Equation (4-9), $(GP)_R$, as discussed in Chapter 3, is called the total-exchange area for radiative heat transfer between the gas and the particle surface (A_p) in the presence of a refractory surface (A_r). The value $(GP)_R/(A_p+A_r)$ is a dimensionless quantity, which from the definition of the emissivity can be identified as an average emissivity evaluated at the same beam length, denoted by "L_m". That is why it is called the mean beam length emissivity model [Viskanta, 1987]. For a mixture of a gray and clear gas with a gray particle emissivity (ε_p), $(GP)_R$ is given by Hottel [1974]:

$$(GP)_R = A_T \left[1/(C\varepsilon_p)+1/\varepsilon_g-1/\alpha_g+\frac{1/\alpha_g - 1}{C\varepsilon_p+(1-C)\varepsilon_r}\right]^{-1} \qquad (4\text{-}14)$$

where A_T $(=A_p+A_r)$: total area of the particles (A_p) and the the refractory (A_r).

C $(=A_p/A_T)$: cold fraction.

ε_p and ε_r: emissivity of particles and the refractory, respectively.

ε_g and α_g: equivalent gray-gas emissivity and gray-gas absorptivity, respectively.

The area of the refractory is expressed as:

$$A_r=\pi D_b L_b+\pi D_f L_{f1} \qquad (4\text{-}15)$$

The area of the particles is expressed as:

$$A_p=(\dot{m}_p \tau_p/\rho_p)\ (1/((1/6)\pi d_p^3))\ (\pi d_p^2/4) \qquad (4\text{-}16a)$$

By simplify equation (4-16a), we have:

$$A_p= 1.5(\dot{m}_p \tau_p)/(\rho_p d_p) \qquad (4\text{-}16)$$

The cold fraction varies around 0.80 to 0.95 in the GCP.

The total gray-gas emissivity (ε_g), of the hot gas (CO_2-H_2O mixture), is given by "one-clear gas and three-gray gas model" proposed by Taylor and Foster [1974]:

$$\varepsilon_g = \sum_{i=1}^{4} (b_{1,i}+b_{2,i}T_g)[1-\exp(-6K_{g,i}P_{CO2}L_m)] \qquad (4\text{-}17)$$

"L_m" is the equivalent length of radiation given by four times the ratio of the volume of the furnace to its peripheral surface. Here we simplify the equation, only considering the furnace diameter:

$$L_m = \pi D_{furnace} L_{furnace+burner} / (2L_{furnace+burner} + \pi D_{furnace}) \qquad (4\text{-}18)$$

"P_{CO2}" is the partial pressure of carbon dioxide which is usually taken as 0.1 bar for the natural gas combustion [Gray et al, 1976]. The values of coefficients $b_{1,i}$, $b_{2,i}$ and $K_{g,i}$ are given in Table (3-1).

"ε_r" is the emissivity of the refractory wall which is given in the appropriate temperature range by Geiger and Poirier [1973]:

$\varepsilon_r = 0.32-0.61$ for T=535-1565°C

"ε_p" is the emissivity of the sand which is given by Weast and Astle [1983]:

$$\varepsilon_p = 0.80 \qquad \text{for } T = 1000^{\circ}C$$

For the gray-gas , we can take: $\varepsilon_g = \alpha_g$ [Bird, 1960]. Now $(GP)_R$ can be solved. In equation (4-9), "σ" is the Stefan-Boltzman constant.

When the particle temperature is equal to or higher than the starting volatilization temperature (between 150°C to 300°C), the resin evaporates and burns instantaneously when in the gas phase. The energy conservation equations of both the particles and the system are changed, they can be shown as:

$$\dot{m}_P \tau_P C_{PP} (T_{p\text{-}out} - T_{p\text{-}init})$$

$$= [(GP)\sigma_R (T^4_{g\text{-}out} - T^4_{P\text{-}out}) + h(T_{g\text{-}out} - T_{P\text{-}out}) A_P] \tau_p - m_{resin} H_P \qquad (4\text{-}19)$$

$$\dot{m}_g C_{Pg} \tau_g (T_{g\text{-}init} - T_{g\_out}) = \dot{m}_P \tau_P C_{PP} (T_{P\text{-}out} - T_{p\text{-}init}) + m_{resin} H_P - m_{resin} H_C \qquad (4\text{-}20)$$

where: "H_P" is the resin decomposition latent heat (kJ/kg),

"H_C" is the resin combustion heat (kJ/kg),

"m_{resin}" is the quantity of burned resin (kg).

Simultaneous resolution of Equations of (4-19) and (4-20) gives the temperature and resin content profiles of both phases in the GCP unit.

4.3.2 PLUG-FLOW IN THE TWO PHASES AND HEAT TRANSFER RATE LIMITATION MODEL.

Plug-flow in the two phases means that the velocities of the gas and the particles is downwards and with no radial dependency. The plug-flow model assumes that the gas and the particles properties (i.e. temperature) varies along the gas path, but is uniform across any cross section of the furnace. A conservation balance is set up on a short elemental length of gas path (dz), each elemental region can be assumed as a well-stirred region. Heat loss from the wall of the furnace is considered. All other assumptions for the conservation equations are the same as in the well-stirred model.

A short elemental length of gas path (dz) is taken, in this elemental region, the mean residence time of each phase can be shown as:

$$\tau_g = dz/V_g \qquad (4\text{-}21)$$

$$\tau_p = dz/V_p \qquad (4\text{-}22)$$

where "V_g" and "V_P" are the same as in the well-stirred model.

For heating particles, the energy conservation equation on the particles is:

$$\dot{m}_P dz/V_P \; C_{PP} dT_P = [(GP)_R \sigma(T_g^4 - T_P^4) + h(T_g - T_P)A_P] dz/V_P \qquad (4\text{-}23a)$$

Simplifying equation (4-23a), we have:

$$\dot{m}_P C_{PP} dT_P = (GP)_R \sigma(T_g^4 - T_P^4) + h(T_g - T_P)A_P \qquad (4\text{-}23)$$

where "h" is the same as in Equation (4-11), and in Equation (4-14), "A_p" can be written as:

$$A_T = A_P + A_r = 1.5(m_p/(\rho_p d_p))(dz/V_P) + \pi D_f dZ = A_T' dz \qquad (4\text{-}24)$$

So $(GP)_R$ is shown as:

$$(GP)_R = A_T' \; dz \; [1/(c\varepsilon_P) + 1/\varepsilon_g + 1/\alpha_g + \frac{(1/\alpha_g) - 1}{c\varepsilon_p + (1-c)\varepsilon_r}]^{-1} \qquad (4\text{-}25)$$

Equation (4-25) is rewritten as:

$$(GP)_R = (GP)_R' dz \qquad (4\text{-}26)$$

Then Equation (4-23) can be rewritten as:

$$\dot{m}_P C_{PP} dT_P = [(GP)_R' \sigma(T_g^4 - T_P^4) + h(T_g - T_P)1.5m_P/(\rho_P d_P V_P)] dz \qquad (4\text{-}27)$$

Equation (4-27) shows that the particles temperature (T_p) is a function of "dz".

The energy conservation equation on the system can be written as:

$$\dot{m}_g(dz/V_g)C_{pg}dT_g = \dot{m}_p(dz/V_p)C_{pp}dT_p + Q_W(dz/V_g) \qquad (4\text{-}28)$$

then we have:

$$\dot{m}_g C_{Pg} dT_g = \dot{m}_P C_{PP} V_g/V_p \, dT_P + Q_W \qquad (4\text{-}29)$$

"Q_W" is the heat loss from the wall (kJ/s). It is given as follows [Bird et al. 1960]:

$$Q_W=[(1/(D_f h_{in})+\ln(D_{f,out}/D_f)/(2\lambda_W)+1/(D_{f,out}h_{out})]^{-1}\pi dz(T_g-T_{amb}) \qquad (4\text{-}30)$$

in which the heat transfer coefficients h_{in} and h_{out}, respectively due to the forced convection inside the furnace and the free convection outside the furnace, are also given by Bird et al. [1960]:

$$h_{in}=0.026Re^{0.8}Pr^{0.4}\lambda_g/D_f \qquad (4\text{-}31)$$

$$h_{out}=0.59(GrPr)^{1/4}\lambda_g/dz \qquad (4\text{-}32)$$

In which "Gr" is the Grashof number $[Gr=\rho_g^2 g\beta dz^3(T_w-T_{amb})/\mu_g^2]$, and "$T_w$" is the temperature of the outside surface of the wall.

When the particle temperature is equal to the starting volatilization temperature, the resin vaporizes and, when in the gas phase, reacts instantaneously. The energy conservation equations of the particles and the system are changed as:

$$\dot{m}_p C_{pp} dT_p =$$

$$[(GP)'_R \sigma(T_g^4-T_p^4)+h(T_g-T_p)1.5\dot{m}_p/(\rho_p d_p V_p)]dz - m_{resin} H_p V_p/dz \qquad (4\text{-}33)$$

$$(\dot{m}_g/V_g)C_{pg} dT_g=(\dot{m}_p/V_p)C_{pp} dT_p+Q_W/V_g+m_{resin} H_p/dz-m_{resin} H_c/dz \qquad (4\text{-}34)$$

and "H_P" and "H_c" have the same definition as in the well-stirred model.

Simultaneous resolution of Equations (4-33) and (4-34) gives temperature and resin content axial profiles.

4.3.3 WELL-STIRRED FLOW IN THE GAS PHASE, PLUG-FLOW IN THE SOLID PHASE AND HEAT TRANSFER RATE LIMITATION MODEL

This model considers that the gas phase is well-stirred and its temperature is uniform in the whole region, and that the solid temperature is a function of the axial position in the region (plug-flow). All the assumptions and definitions are the same as in the last two models. The energy conservation equation on the particles is:

$$\dot{m}_P C_{PP} dT_P = [(GP)_R' \sigma (T_{g\text{-}out}^4 - T_P^4) + h(T_{g\text{-}out} - T_P) 1.5\dot{m}_P / (\rho_P d_P V_P)] dz \qquad (4\text{-}35)$$

Equation (4-35) is the same as Equation (4-27), but the gas temperature is taken as $T_{g\text{-}out}$ that is a uniform temperature in the whole region.

The energy conservation equation on the system is:

$$\dot{m}_g C_{Pg} \tau_g (T_{g\text{-}init} - T_{g\_out})$$

$$= \int_o^L [(GP_R)' \sigma (T_{g\text{-}out}^4 - T_P^4) + h(T_{g\text{-}out} - T_P) 1.5\dot{m}_P / (\rho_P d_P V_P)] \tau_p dz \qquad (4\text{-}36)$$

When the temperature of the particles reaches the resin starting volatilization temperature, the energy conservation equations of the two phases are changed as:

$$\dot{m}_P C_{PP} dT_P = [(GP)_R' \sigma(T^4_{g\text{-}out} - T^4_P) + h(T_{g\text{-}out} - T_P) 1.5\dot{m}_P/(\rho_P d_P V_P)]dz - m_{resin} H_p V_p/dz \quad (4\text{-}37)$$

For the gas-solid mixture, energy balance is given as follow:

$$\dot{m}_g C_{Pg} \tau_g (T_{g\text{-}init} - T_{g\_out})$$

$$= \int_o^L [(GP_R)' \sigma(T^4_{g\text{-}out} - T^4_P) + h(T_{g\text{-}out} - T_P) 1.5\dot{m}_P/(\rho_P d_P V_P)]dz - m_{resin} H_c \quad (4\text{-}38)$$

Simultaneous resolution of Equations (4-37) and (4-38) gives temperature and resin content axial profiles.

4.3.4 COMPARISON OF THE MODELS

The temperature profiles of the gas and the solid are computed by solving numerically energy conservation equations using Euler's method. The initial value and the other input data

used in the computer program are summarized in Appendix I (Table (I-1)).

This section presents some predicted values of both the temperatures and resin content for the different models discussed before for the same operating conditions. The resin starting combustion temperature is assumed equal to 300^{o}C in all the calculations.

Figure (4-3) presents the predicted values of the heat transfer rate limitation models. Because the resin combustion is assumed instantaneous and there is no other resistance to transfer, the effect of this assumption in the curves is a temperature jump in each model. And the resin conversion curves show that the resin elimination rates are very fast. Furthermore, the different flow regime assumptions have an obvious effect on temperature profiles. The heat transfer rate in the well-stirred model of both phases is the fastest one of the three flow models with respect to resin destruction. And plug-flow in the two phases shows lower heat transfer rate compared with the other models. This characteristic of heat transfer is also shown in the resin conversion curves: the resin starting combustion positions are different.

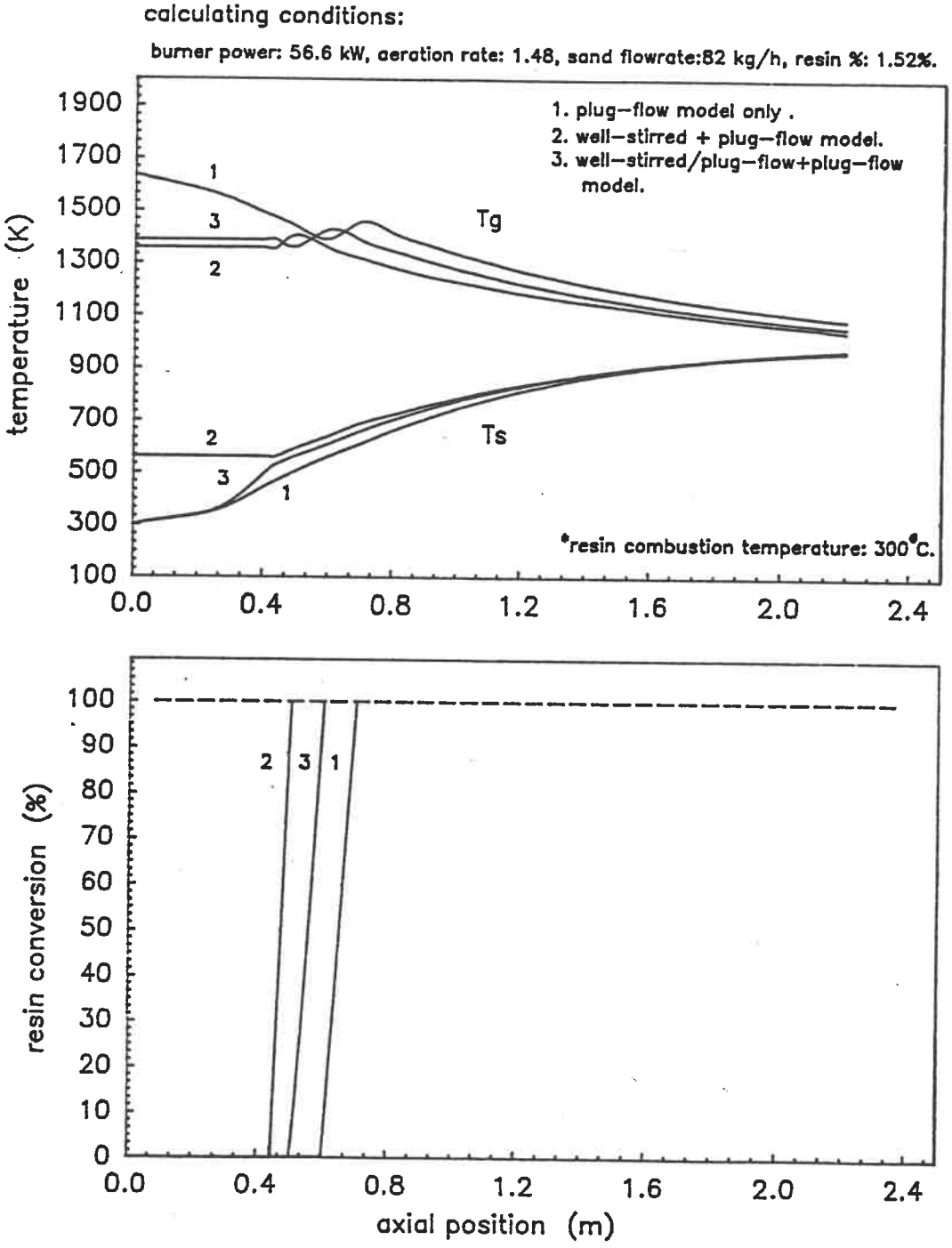

Figure (4-3). Comparison of flow regim models (heat transfer limitation)

4.4 HEAT TRANSFER RATE AND RESIN COMBUSTION PROCESS LIMITATIONS MODELS

In the last section, the heat transfer rate is considered as the only limiting step for the resin combustion process. The heat transfer equations have been given. Here the resin combustion process is considered as another limiting step, equations for different resin combustion processes are given.

4.4.1 RESIN COMBUSTION PROCESS MODELS

As discussed in the theoretical analysis section, there are three possible models for resin combustion process. They will be given respectively.

4.4.1.1 VOLATILE DIFFUSION RATE LIMITATION MODEL

The volatile diffusion rate limitation means that when the particle temperature reaches the resin decomposition temperature, the resin decomposition produces volatiles only. The volatiles diffuse and burn in the gas (Figure (4-2)). The volatile burning rate depends on its diffusion rate. Defining Δm_{resin} [kg/s] as the resin combustion rate. Spalding [1979] gave the following equation:

$$\Delta m_{resin} = 2\ \rho_{vol}\psi_{vol}\ln(1+(\kappa_{vol,0}+\kappa_{ox,\infty}/s)/(1-\kappa_{ox,\infty}))\ \pi\ d_p \qquad (4\text{-}39)$$

where, ψ_{vol} is the diffusion coefficient of the volatile.

$\kappa_{vol,o}$ and $\kappa_{ox,\infty}$ are the concentrations of the volatile on the particle surface and oxygen in the gas phase, respectively.

s is the stoichiometric ratio of the reaction.

Assuming that the decomposition rate is heat transfer limited as in the former section. From thermodynamic equilibrium, the saturated pressure of the volatile on the surface is a function of the particle temperature. Using Clausius-Clapeyron equation, this pressure is:

$$dp_{vol,o}/dT_p = H_p/(\Delta V\ T_p) \qquad (4\text{-}40)$$

where $p_{vol,o}$ is the saturated pressure on the particle surface.

T_p is the particle temperature.

H_p is the decomposition latent heat.

ΔV is the volume change accompanying the phase change at T_p.

From the gas state equation, ΔV can be shown:

$$\Delta V = R\, T_p/(M_{vol}\, P_{vol,o}) \qquad (4\text{-}41)$$

where R is the universal gas constant and M_{vol} is the molecular weight of the volatile.

Equation (4-40) may be integrated with Equation (4-41):

$$\text{Ln}\, P_{vol,o} = -H_p\, M_{vol}/(R\, T_p) \qquad (4\text{-}42)$$

The boundary condition is $T_p \Rightarrow \infty$, $P_{vol,o} = 1$ atm.

Thus the concentration of the volatile ($\kappa_{vol,0}$) is written as:

$$\kappa_{vol,0} = (P_{vol,o}/(R\, T_p))/(\rho_g + P_{vol,o}/(R\, T_p)) \qquad (4\text{-}43)$$

where ρ_g is the density of the gas.

The diffusion coefficient of the volatile (ψ_{vol}) is calculated by the equation of Fuller, Schettler and Giddings [1965]:

$$\psi_{vol} = \frac{10^{-3}\, T_g^{1.75}\, [(M_{vol} + M_{gas})/M_{vol} M_{gas}]^{0.5}}{P\, [(\sum \nu)_{vol}^{1/3} + (\sum \nu)_{gas}^{1/3}]^2} \qquad (4\text{-}44)$$

where M is the molecular weight, $\sum \nu$ is the value of the atomic diffusion volumes. P is the pressure in atmosphere. Subscribes vol and gas refer to the volatile and the gas, respectively.

From characteristics obtained from the company providing us with foundry sand, the resin is constituted by 20% (mole) phenol and 80% (mole) formaldehyde. Although these two components polymerize, it is assumed that they are obtained again when the resin decomposes. Thus the values for Equation (4-44) are [Perry's Chem. Eng. Handbook]:

$$M_{vol} = 42.8, \qquad M_{gas} = 18.29,$$

$$(\sum \nu)_{vol} = 39.98, \qquad (\sum \nu)_{gas} = 17.75,$$

Then the equation of ψ_{vol} is:

$$\psi_{vol} = 7.69*10^{-10}\, T_g^{1.75} \qquad (4\text{-}44a)$$

When the resin burns, the particle diameter reduces gradually. It can be expressed by:

$$d(d_p)/dt=(-4\rho_{vol}\psi_{vol}/\rho_{resin}d_p)\ln(1+(\kappa_{vol,0}+\kappa_{ox,\infty}/s)/(1-\kappa_{vol,0})) \qquad (4\text{-}45)$$

When the particle diameter is equal to the sand diameter ($d_p=d_s$), the resin has been eliminated completely.

4.4.1.2 OXYGEN DIFFUSION RATE LIMITATION MODEL

In the oxygen diffusion rate limitation model, when the particle temperature reaches the resin decomposition temperature, the resin decomposition produces char and a small quantity of volatiles. The volatile combustion process is ignored. When the particle temperature reaches the char burning temperature, the combustion of the char occurs on the surface of the particle. The char burning rate depends on the oxygen concentration on the surface. And oxygen concentration on the surface depends on the oxygen diffusion rate and oxygen concentration in the gas phase. Also defining Δm_{resin} as the resin combustion rate (kg/s), Spalding [1979] gave the following equation:

$$\Delta m_{resin} = 2\ \rho_{ox} \psi_{ox} \ln(1+\kappa_{ox,\infty}/s)\ \pi\ d_p \qquad (4\text{-}46)$$

In which, ψ_{ox} is the diffusion of oxygen, it can be calculated using Equation (4-44) by replacing vol with oxygen. "$\kappa_{ox,\infty}$" and "s" have similar definitions as in Equation (4-39). Assuming char combustion as a "surface combustion", the particle diameter will be reduced gradually. It can be expressed by:

$$d(d_p)/dt=(-4\rho_{Ox}\psi_{Ox}/(\rho_{char}\ d_p))\ln(1+\kappa_{ox,\infty}/s) \qquad (4\text{-}47)$$

When "d_p" is equal to "d_s", all the resin in the used sand is destroyed.

For the oxygen diffusion coefficient (ψ_{ox}),

$M_{ox} = 32$,

$(\sum \nu)_{ox} = 16.6$,

then the equation for ψ_{ox} is:

$$\psi_{ox} = 3.23*10^{-10}\ T_g^{1.75} \qquad (4\text{-}44b)$$

4.4.1.3 VOLATILE/OXYGEN DIFFUSION RATE LIMITATION MODEL

In the volatile/oxygen diffusion rate limitation model, when the particle temperature reaches the resin decomposition temperature, the resin decomposition produces char and volatiles. The volatiles burn around the particle while the resin decomposition happens. When all the volatiles are burned out and the particle temperature is equal or higher than the char burning temperature, the combustion of the char occurs on the surface of particle. This is a two-step combustion process. The volatile burning rate depends on its diffusion rate. And the char burning rate depends on the oxygen concentration on the surface. Also defining Δm_{resin} as the resin combustion rate (kg/s). Equations (4-39) and (4-46) are adopted for this two-

step combustion, respectively. And the particle diameter change is described by Equations (4-45) and (4-47) for each step, respectively.

4.4.2 COMPARISON OF THE MODELS

Due to the three resin combustion models and the three flow models, there are nine possible models that can be derived by combining the equations above for this two limitation models. It is not our purpose here to discuss all of them. They will be discussed by comparing with the experimental data in chapter 6. As a example, plug-flow in the two phases is considered, the three heat transfer rate and resin combustion process limitations models are compared. The general energy conservation equations are shown as:

$$\dot{m}_p C_{pp} dT_p =$$

$$[(GP)'_R \sigma(T_g^4 - T_p^4) + h(T_g - T_p) 1.5\dot{m}_p/(\rho_p d_p V_p)]dz - \Delta m_{resi} H_p \qquad (4\text{-}50)$$

$$(\dot{m}_g/V_g) C_{pg} dT_g = (\dot{m}_p/V_p) C_{pp} dT_p + Q_w/V_g + \Delta m_{resin} H_p/V_p - \Delta m_{resin} H_c/V_p \qquad (4\text{-}51)$$

Equations for calculating Δm_{resin} depends on different resin combustion process assumptions.

As mentionned before, the temperature profiles of the gas and the solid are computed by solving numerically energy conservation equations using Euler's method. The initial value and the other input data used in the computer program are summarized in Appendix I (Table (I-1)).

Figure (4-4) shows the predicted values of the temperatures and resin conversion profiles of the three different combustion models under the same operating conditions. The plug-flow in the two phases is assumed in this comparison. From the predicted results, the volatile diffusion limitation model shows the fastest resin elimitation rate. The oxygen diffusion limitation model under assumption that the stoichiometry of the reaction is equal to 10 is a slower rate than the first case. For the volatile /oxygen two diffusion limitations model, there is a resin conversion jump at the begining of the resin combustion process due to the quick volatile combustion.

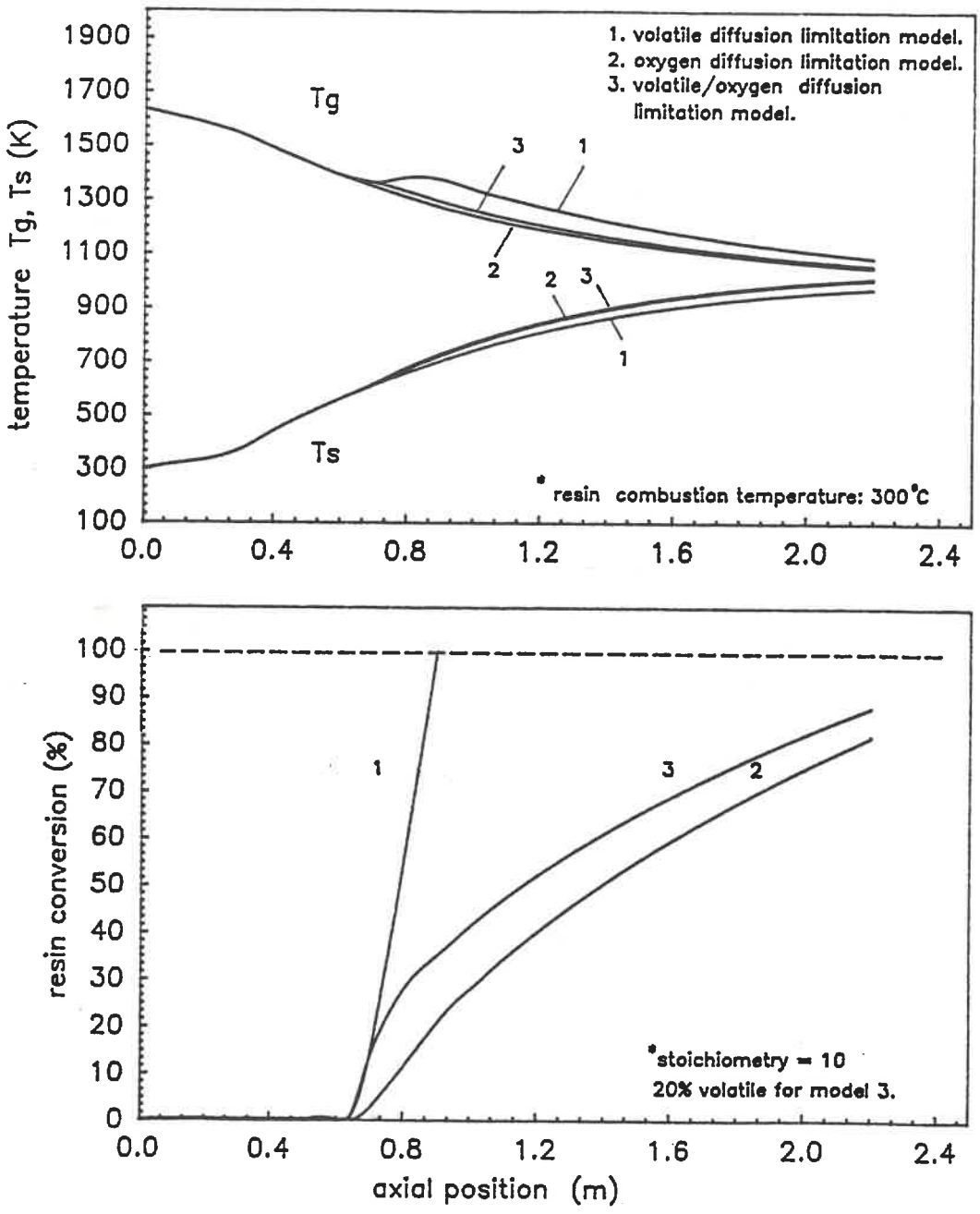

Figure (4–4). Comparison of resin combustion models (plug–flow model for flow regime)

4.4.3 EFFECT OF DIFFERENT RESIN CONTENT ON THE PREDICTIONS OF THE MODELS

Figure (4-5) shows the effect of the resin content on one model. The chosen model is: volatile/oxygen diffusion limitation and well-stirred plus plug-flow in the gas phase, plug-flow in the solid phase. There is no effect on the temperature profiles of the gas and the particle as the contribution of the resin combustion to the overall heat transfer is low compared to the energy input from the burner. The resin conversion predictions are as expected: a higher resin content has a lower resin conversion.

4.5 CONCLUSION

Modeling the gas contact process encompasses two modeling levels. For the hydrodynamics, two regions are considered in the unit: the burner and the entrance region of the furnace where the flow of each phase can be well-stirred and plug-flow, the remaining of the furnace where both phase flows are plug-flow. For the heat and mass transfer, it is proposed that:

—— heat transfer is by convection and radiation. The amount of resin does not affect much the temperature profiles.

—— mass transfer is limited by various steps according to

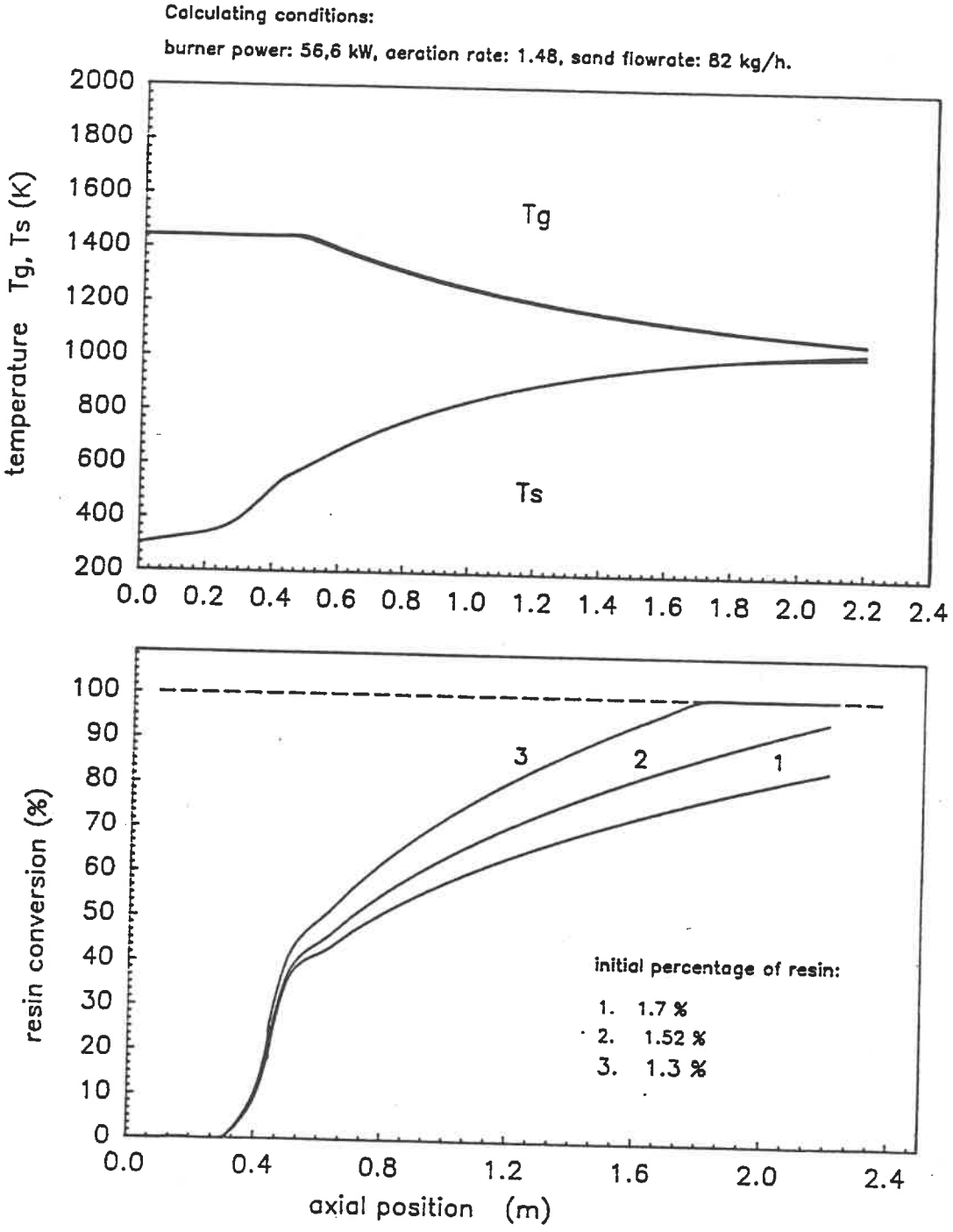

Figure (4–5). Effect of resin content in one model

different assumptions (heat transfer limitation, volatile diffusion limitation, oxygen diffusion limitation or all of them). The combustion reaction is considered instantaneous. In chapter 6, all these models will be verified with the experimental results.

CHAPTER 5. EXPERIMENTAL INSTALLATION AND DATA ACQUISITION

5.1 INTRODUCTION

The vertical Gas-Contact Process installation was designed and constructed to meet the following objectives:

— Because the GCP is a continuous process, stable and continuous supplies of gas and particles are required. The literature review showed that the flowrate of both gas and particle are two of the main factors that affect the gas-solid flow regime and the heat transfer between gas and solid. Therefore, the power of the unit and the flowrate of particle need to be adjusted in a certain range. The present installation is designed to do so by using a screw feeder for the sand, and a counter rotation burner . Its nominal power is 58 kW, and can be changed in the range 58±15 kW.

— Analysis of heat transfer in GCP is based on the gas and particle temperature axial profiles. It requires to measure gas and particle temperature at different axial positions in the unit. For measuring particle temperature, a specific device has been designed. this device is also used for obtaining the sample of particles at different axial positions of the unit. From these samples, the remaining amount of resin can be measured.

— The oxygen content is also a main factor that affects the resin combustion rate. A control system of aeration rate has been designed in the present installation. At the same time, analysers of O_2, combustible and CO_2 are also used to check the exhaust gas.

This chapter describes the installation used in foundry sand reclamation. In addition to the installation characteristics, operating procedures, measurement techniques are described.

5.2 GAS-CONTACT INSTALLATION AND PROCEDURE

5.2.1 GENERAL DESCRIPTION

The vertical Gas-Contact installation is shown schematically in Figure (5-1). It consists of a counter-rotation burner, a vertical furnace, a combustion system, a solid screw feeder, a gas-solid injector, an expansion chamber for particle disengaging and an exhaust gas system. The overall height of unit is around 5m.

Counter-rotation burner. The characteristics of the counter-rotation burner have been described in Chapter 1.

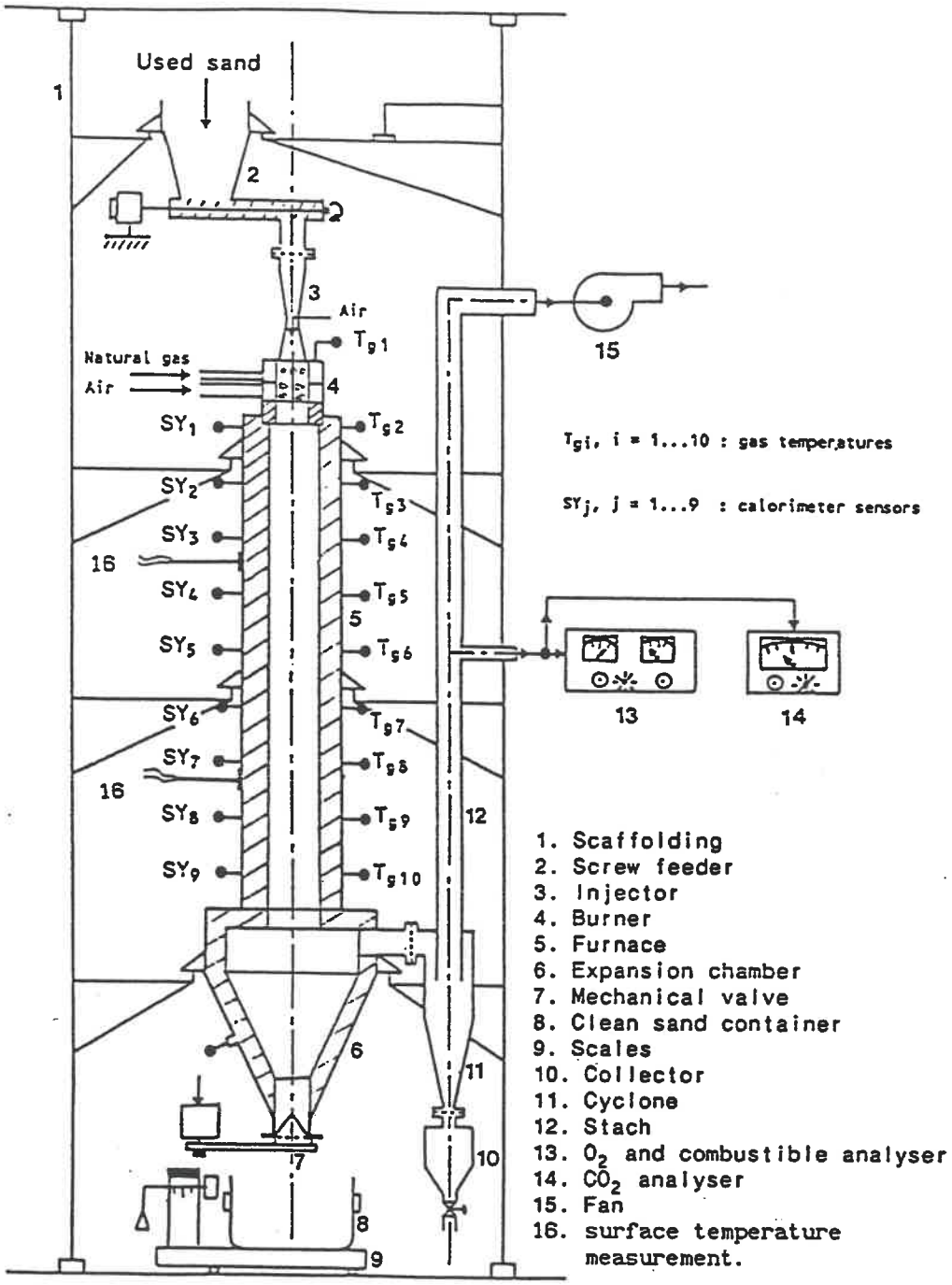

Figure (5-1). Schematic view of the Gas-contact unit

(Figure (1-2)).The main dimensions of the burner are shown in Figure (5-2). The nominal power of the burner is 58 kW, and the power range is 40 kW - 70 kW. The burner also includes an automatic ignition and flame checking system.

Furnace and expansion chamber. The furnace and expansion chamber are composed of a steel shell and a refractory wall with a thickness of 80mm. Refractory cement is used, and its maximum temperature is 1482°C. The inside diameter of the furnace is 0.2 m.

Combustion control system. The flowrate of natural gas and the aeration rate can be adjusted. The system schematics are shown in Figure (5-3) with all its measurement devices for gas and air flowrate and pressure.

Exhaust gas system. The exhaust gas system (Figure (5-3)) includes the fan, orifice and analyser of O_2, combustible and CO_2. It also includes a collector of the particles (Figure (5-1)).

Injector. The schematic view of the injector is shown in Figure (5-4). The Venturi injector is used to obtain a satisfactory feeding of solid particles. The main effects of such a device is to avoid the return of the flame and to improve

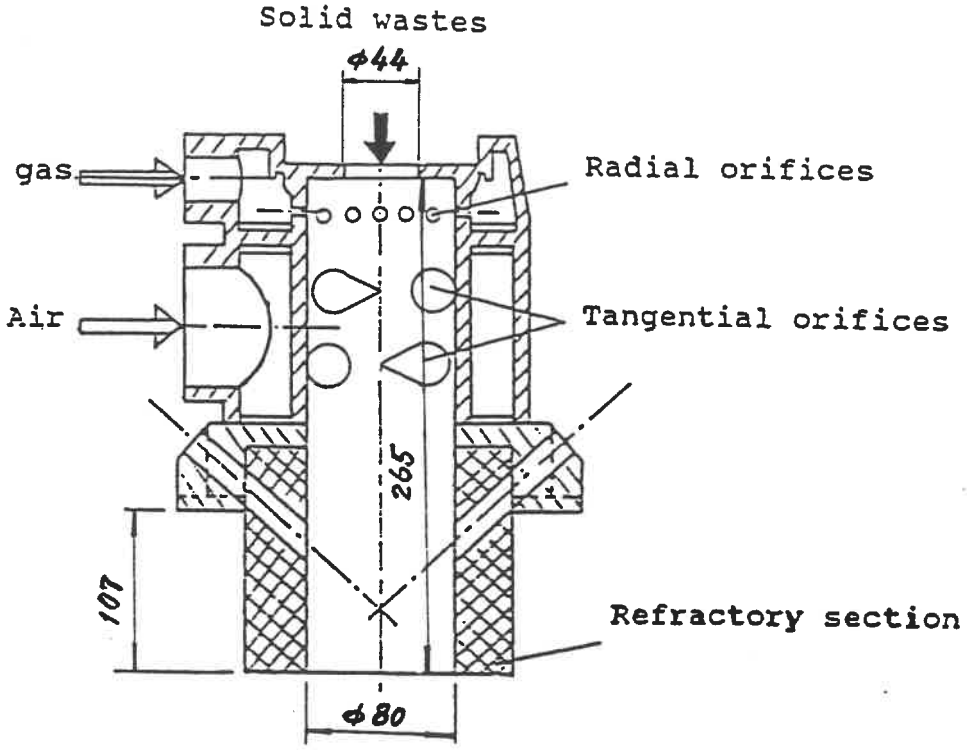

Figure (5-2). Overall size of the "counter-rotation" burner

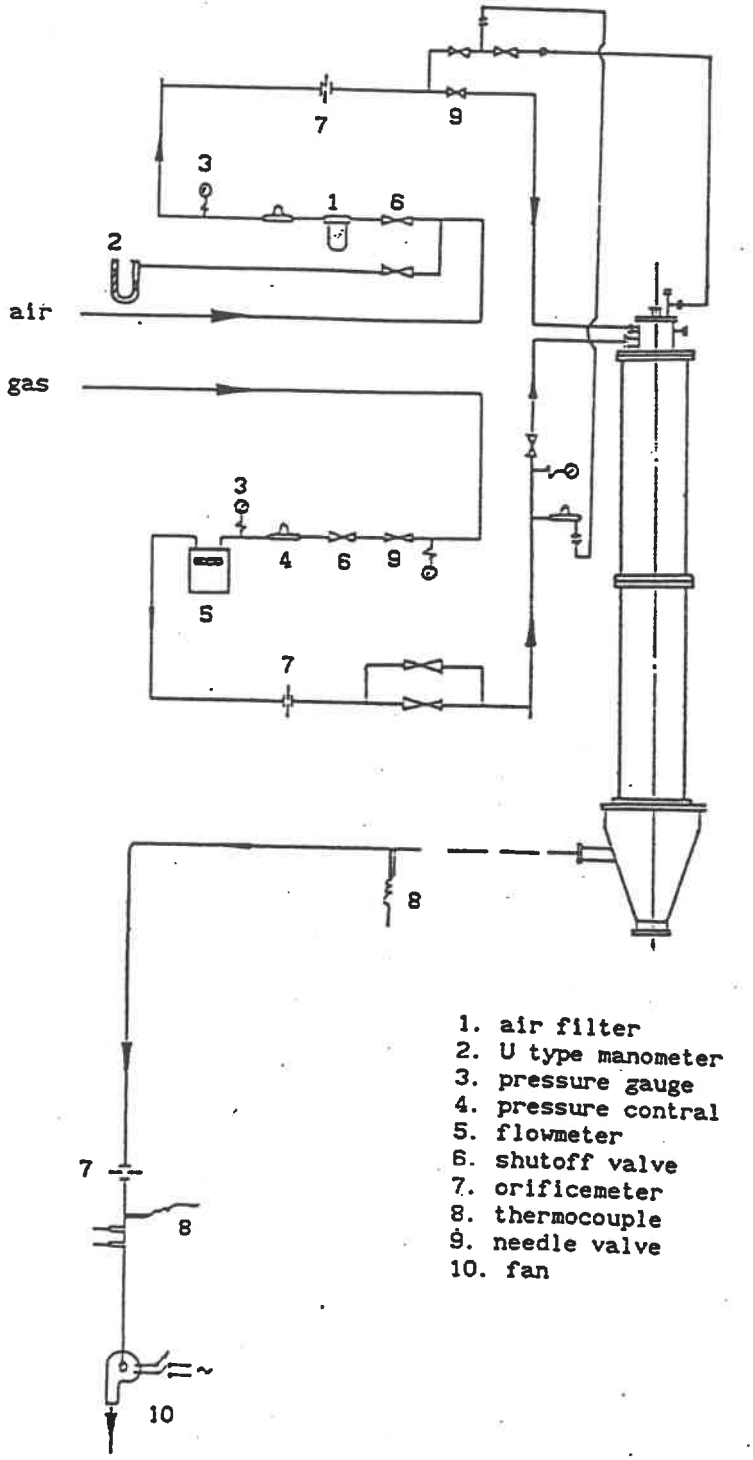

Figure (5-3). Draft of combustion control system and exhaust gas system.

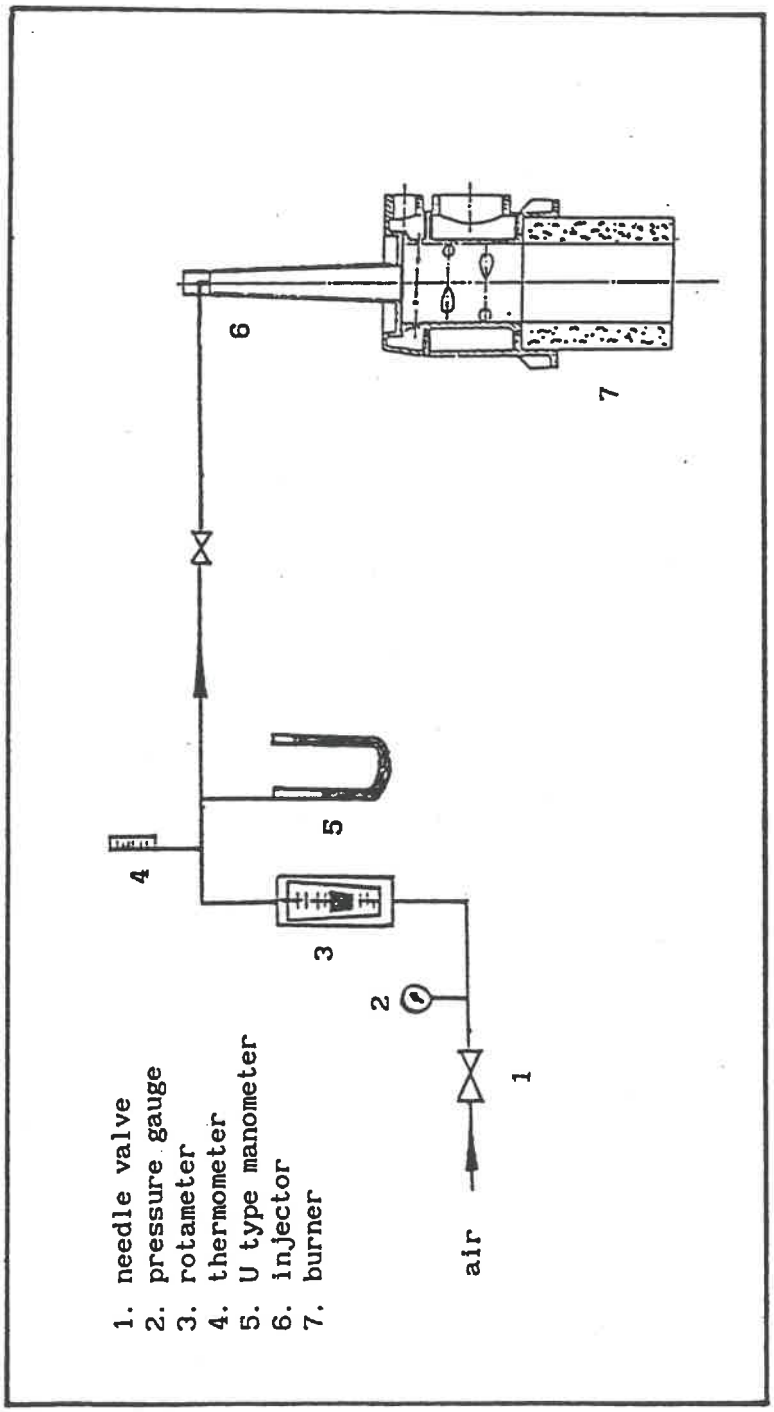

Figure (5-4). Schematic view of injector system

the dispersion of the particles. The aeration pressure is around 250 mbar.

Solid flow system. Solid flow rate is controlled by a calibrated screw feeder (Figure (5-1)). The solid flows through the furnace and is collected by the expansion chamber.

Calorimetric sensor system. The calorimetric sensor system (Figure (5-5)) is composed of a stainless steel probe, a container insulated with a glass wool and aluminum, a vacuum system. It is used to draw out a sample of solid particles. By this method, the solid particle temperature can be measured by calculating the thermal equilibrium of the system. (see section 5.5.2).

5.2.2 OPERATING PROCEDURES

Before starting a GCP experiment, a safety check need to be done to ensure that there is no flammable material near the unit. For the experiments of foundry sand reclamation, the probe and the container (see section 5.2.5.2) must be prepared before starting the burner. If necessary, the probe can be cleaned by pressure air for ensuring that the gas-solid flow can go through it freely. A certain quantity of water (usually 300-400g) is put in the container.

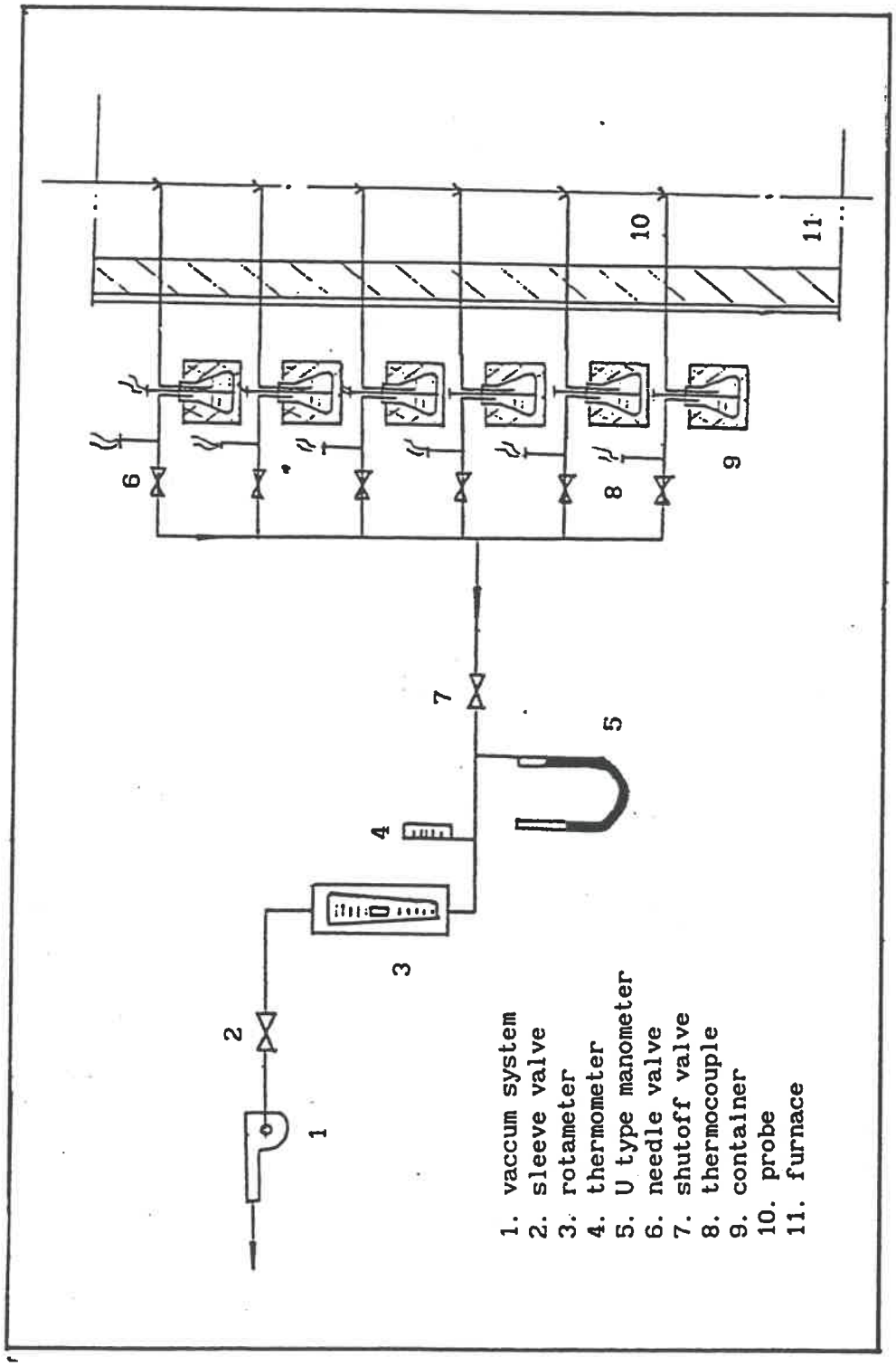

Figure (5-5). Calorimetric sensor system.

The first step is igniting the burner. Using lower power for the burner ignition (around 40 kW). When the burner is operated, the flowrate of natural gas and air are adjusted to required values. Then, the process is operated about 60 minutes without the sand feeding. Observing gas temperatures from computer screen, when the temperature change is smaller than 10°C/minute, the quasi-steady operation state is achieved. In this case, the screw feeder can be started, and the sand flowrate can be adjusted to a required value. Few minutes are needed for reaching the steady state sand flow. Then measurements can be taken:

—— record the gas temperature,

—— open the vaccum system, draw out the sand from the furnace to the container, and record the water temperature change, gas temperature before the gas enters the container and after the gas exits the container. At the same time, record the flowrate of gas in the vaccum system and the operating time (usually 3 minutes),

—— record the concentration of O_2 and CO_2 in the exhaust gas.

Regular shut down is simple: first the screw feeder is turn off, then the natural gas flow and last air flow, when the temperature is low enough.

Emergency shut down is possible by turning off the gas

flow. Emergency switches are available at the bottom and at the top of the unit.

Regular maintenance and checkings are carried out on the installation to insure the precision of measurements and the overall integrity of the system. In addition, gas leak checks are carried out on a monthly basis.

5.3 GAS FLOW MEASUREMENTS

The aim of gas flow measurement in this experiment is measuring the gas flowrate. The gas here includes the natural gas and air. There are several systems concerned by gas flowrate measurements:

—— Combustion system (includes natural gas and combustion air).

—— Exhaust system.

—— Injection system.

—— Calorimetric sensor system.

In the combustion system and the exhaust gas system (Figure (5-3)), orifice-meters are used to measure the gas flowrate. In the injection system and the calorimetric sensor system the rotameters are used to measure the gas flowrate. All the calibration curves are given in Appendix II.

5.4 MEASUREMENT OF SOLID FLOW

A screw feeder is used in the solid flow system (Figure (5-1)). The feeder is not a standard screw feeder. A balance is used to calibrate this feeder. The flowrate of solid particle depends on the rotation rate of the motor of the feeder. The calibration curve of the feeder is shown in Appendix II. Figure (5-6) shows the effect of injection air on the sand flowrate. The experiment results demonstrate that this effect can be ignored.

5.5 TEMPERATURE MEASUREMENT

5.5.1 MEASUREMENT OF GAS TEMPERATURE

The measurements include the gas temperature in the burner, furnace, and calorimetric sensor system.

Gas temperature in the burner. Based on the structure of the burner, we use a moving-thermocouple in this region. Figure (5-7) shows the structure of the moving-thermocouple. A type B, unexposed junction is chosen.

Gas temperature in the furnace. The measuring points of gas temperature along the axial position of the furnace are

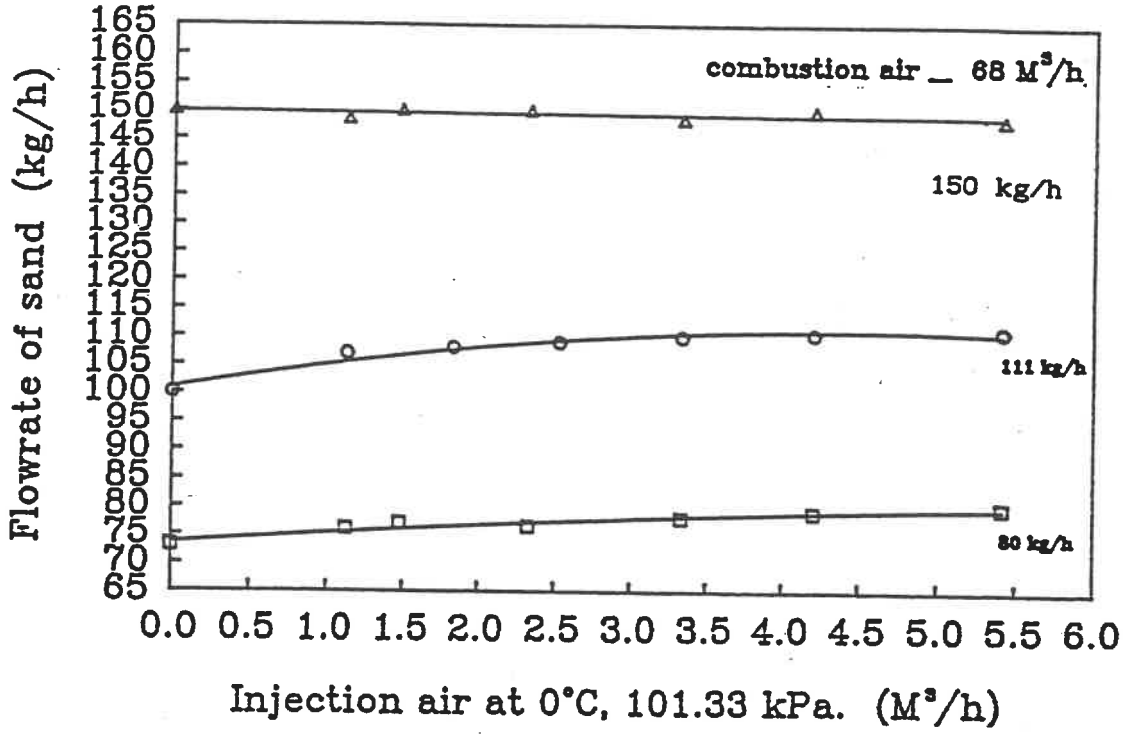

Figure (5-6). Effect of injection air on the sand flowrate

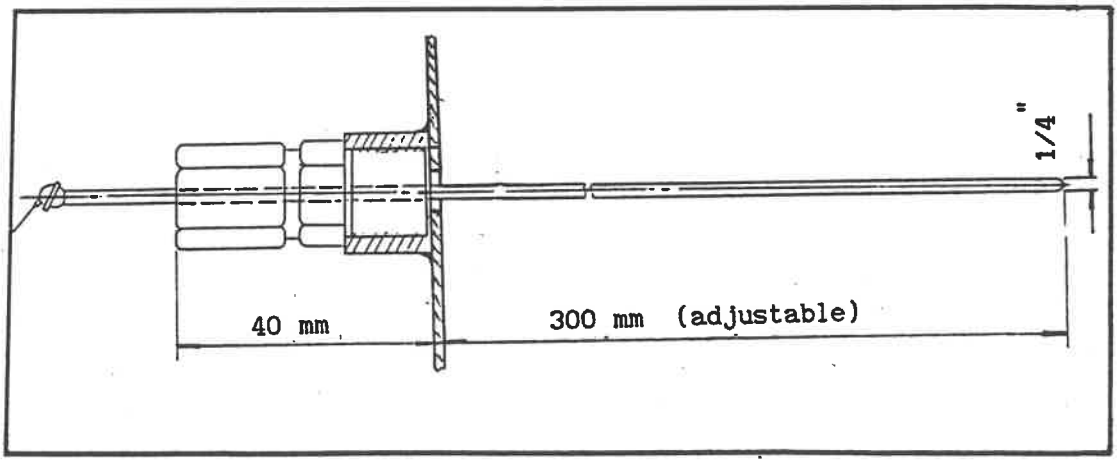

Figure (5-7). Fixture of the thermocouple

shown in Figure (5-1). B type thermocouples are used in the two top positions. K type is used below. The installation of the probe is the same as in Figure (5-7). The error of the gas temperature measurement is -10°C to -20°C. Analysis of the error is given in Appendix III.

Gas temperature in calorimetric sensor system. There are six measuring points of the gas temperature in the vacuum system. K type exposed junction thermocouples are chosen.

5.5.2 MEASUREMENT OF PARTICLE TEMPERATURE

Usually the measurement of the solid particle temperature is a tough problem. In our experiments, a specific experimental method is used. The basic principle of this method is the same as in the calorimeter. A vacuum system is used for obtaining the sample quickly. Figure (5-8) shows the schematic view of the method. The main parts of this system are the probe tube and a container as a specific calorimeter.

For the probe tube, three different types of probe have been tested. The probe used in this experiment is the fastest for obtaining the sample among these three types of probe.

The container is made of glass with a 1 liter capacity

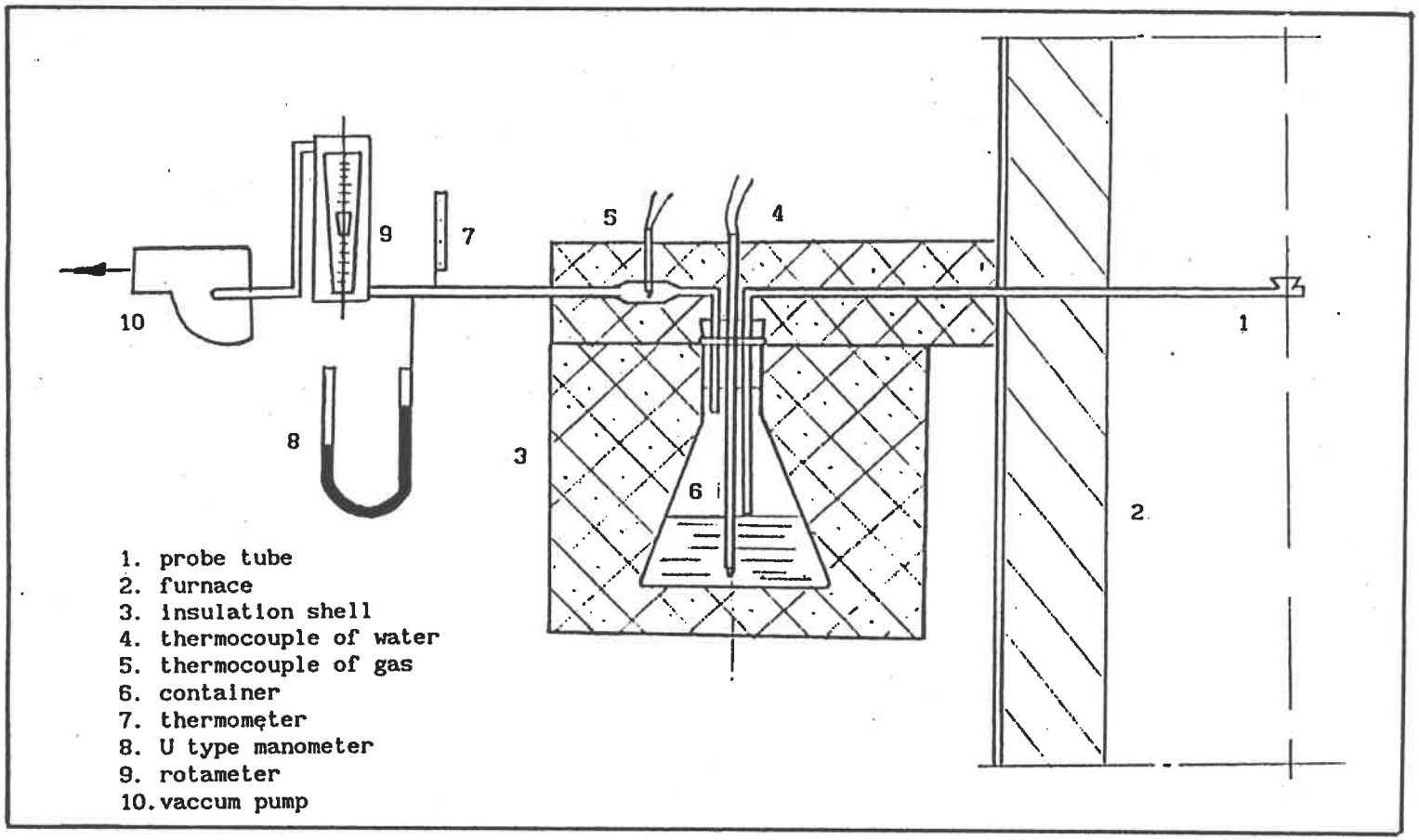

Figure (5-8). Schematic view of calorimetric sensor system

and uses 300-400g of water. The vacuum pressure for each probe is 0.025 atm. The time for getting one sample is 3 minutes. The sample is 12g and the water temperature change is 40-60°C, because of the small quantity of the sample. The insulation shell of the system is thick enough, and the heat loss is ignored. The energy balance of the system is written as:

$$W_p C_{pp} (T_p - T_{H2O}) + \dot{m}_g C_{pg} (T_{g\text{-}in} - T_{g\text{-}out})\, t = W_{H2O} C_{pH2O} (T_{H2O} - T_{H2O\text{-}init}) + (W_{H2O} - W_{H2O\text{-}init})\, H_{H2O} \quad (5\text{-}3)$$

where W is the weight of matter, m_g is the gas flowrate. C_p is the specific heat. H_{H2O} is latent heat of water evaporation. Subscript "p" is sand phase, "g" is gas phase, "H2O" is water.

From equation (5-3), the temperature of solid particle can be calculated:

$$T_p = T_{H2O} + [W_{H2O} C_{pH2O} (T_{H2O} - T_{H2O\text{-}init}) + (W_{H2O} - W_{H2O\text{-}init})\, H_{H2O} + \dot{m}_g C_{pg} (T_{g\text{-}in} - T_{g\text{-}out})\, t\,] / W_p C_{pp} \quad (5\text{-}4)$$

The error of the solide temperature measurement is ±0.5°C. Analysis of the error is given in Appendix III.

5.5.3 MEASUREMENT OF WATER TEMPERATURE

For the measurement of solid particle temperature, water temperature is a important value. Type K, exposed junction thermocouples are put in the water.

5.5.4 MEASUREMENT OF THE OUTSIDE SURFACE TEMPERATURE OF THE FURNACE

As the heat loss of the furnace is to be calculated, the temperature of the outside surface of the furnace needs to be measured. Two points are chosen for measuring the surface temperature (see Figure (5-1)). K thermocouple are used. The average value of temperatures of these two points is used for Equation (4-30):

$$T_{surf} = (T_{1\text{-}surf} - T_{2\text{-}surf}) / 2 \qquad (5\text{-}5)$$

5.6 MEASUREMENT OF RESIN CONVERSION

The resin coating the sand disappears gradually. The method for measuring the temperature of the solid particle can also be used for getting the sample at different position in the furnace (Figure (5-8). From gravimetry analysis, before and after leaving the sample in an oven, the quantity of resin is obtained.

5.7 PHYSICAL PROPERTIES OF GAS AND SOLID

5.7.1 GAS PROPERTIES

5.7.1.1 NATURAL GAS PROPERTIES

The gas used in the GCP is natural gas. Its composition and its physical properties are shown in Table (5-1) and Table (5-2), respectively.

Table (5-1) : Composition of natural gas, Gaz Métropolitain (% volume)

Hydrocarbons				Inertes	
CH_4	C_2H_6	C_3H_8	C_4H_{10}	N_2	CO_2
95.527%	2.064%	0.117%	0.01%	1.942%	0.340%

Table (5-2) : Physical properties of natural gas, Gaz Métropolitain

PCI MJ/Nm^3	PCS MJ/Nm^3	V^0_a m^3/m^3	V^0_{fh} m^3/m^3	$\beta_0(H_2O)$ %	$\alpha_0(CO_2)$ %	ρ_g kg/Nm^3
34.75	39.7 (37.55)*	9.5	10.51	18.8	9.5	0.75 (0.707)*

PCI : lower heating value

PCS : higher heating value

V^0_a : stoichiometriy of air

V^0_{fh} : stoichiometry of flue-gas

β_0 : volume percentage of water in flue-gas

α_0 : volume percentage of CO_2 in flue-gas

ρ_g : gas density

* : at 15°C and 101.325 kPa

5.7.1.2 FLUE-GAS PROPERTIES

The composition of flue-gas is given in Table (5-3). The values are volume percentage.

Table (5-3) : Composition of flue gas (% volume)

	CO_2	H_2O	N_2
Flue gas	9.5%	18.8%	71.7%

The physical properties are determined by the composition and temperature (Perry and Chilton, 1989).

All the physical pproperties of flue-gas are determined as a function of the composition of the gas from the following expression:

$$M = (CO_2\%\ M_{CO2} + H_2O\%\ M_{H\ O} + N_2\%\ M_{N2}) / 100 \qquad (5\text{-}6)$$

where M is a physical property.

The heat capacity of flue-gas is determined as a function of temperature from the following expression derived from data (Perry, 1984):

$$Cp_g = 880.21 + 0.23\ T_g \qquad (5\text{-}7)$$

where T_g is in unit ($^\circ$K) and Cp_g is in unit (J/kg $^\circ$K).

The flue-gas thermal conductivity as a function of temperature is determined by the following expression derived from data in Perry's Handbook [1984]:

$$\lambda_g = (-8.138\times10^{-2} + 7.816\times10^{-3}T_g) / 100 \qquad (5\text{-}8)$$

where T_g is in unit (K) and λ_g is in unit (J/s m K).

The viscosity of flue-gas is determined by the following expression derived from data in Perry's Handbook [1984]:

$$\mu = 4.68\times10^{-5} \times (T_g/1173)^{0.65} \qquad (5\text{-}9)$$

where T_g is in the unit (K) and μ is (kg s/m^2).

The density of flue-gas is determined by the following expression derived from data in Perry's Handbook [2984]:

$$\rho_g = 2.407 - 5.276\times10^{-3}T_g + 4.554\times10^{-6}T_g^2 - 1.342\times10^{-9}T_g^3 \qquad (5\text{-}10)$$

wher T_g is in the unit (K) and ρ_g is (kg/m^3).

5.7.2 SOLID PROPERTIES

The particle size distribution of both used sand and clean sand are determined by sieving. Care is taken in these

determinations to select appropriate samples and sieving times and a series of experiments are carried out to ensure that the selection has been correctly made.

The size distributions of the clean and used particle are shown in Figure (5-9), (5-10). According to these figures, the mean diameters are:

used sand: $\bar{D}_{Pres} = 297\ \mu m$

clean sand: $\bar{D}_{Ps} = 275\ \mu m$

Sand density is measured by using a graduate cylinder and a scale. The sand is put in the water. The values are:

used sand: $\rho_{s+r} = 2651\ kg/m^3$

clean sand; $\rho_s = 2597\ kg/m^3$

The mass percentage of the resin is measured by gravimetry using an oven. The mass percentage is obtained from the mass change between the used sand and the sand out after a prolonged stay in the oven at 600°C. The average value of different measurements is 1.52%. Table (5-4) shows the results of the experiments.

Table (5-4) : Percentage of resin

Run No.	1	2	3	Average
Resin % (mass)	1.45	1.49	1.62	1.52

Figure (5-11) is the result of thermo-balance test. It shows the initial temperature for resin beginning decomposition. From this curve, the temperature for resin decomposition is around 180^{o}C.

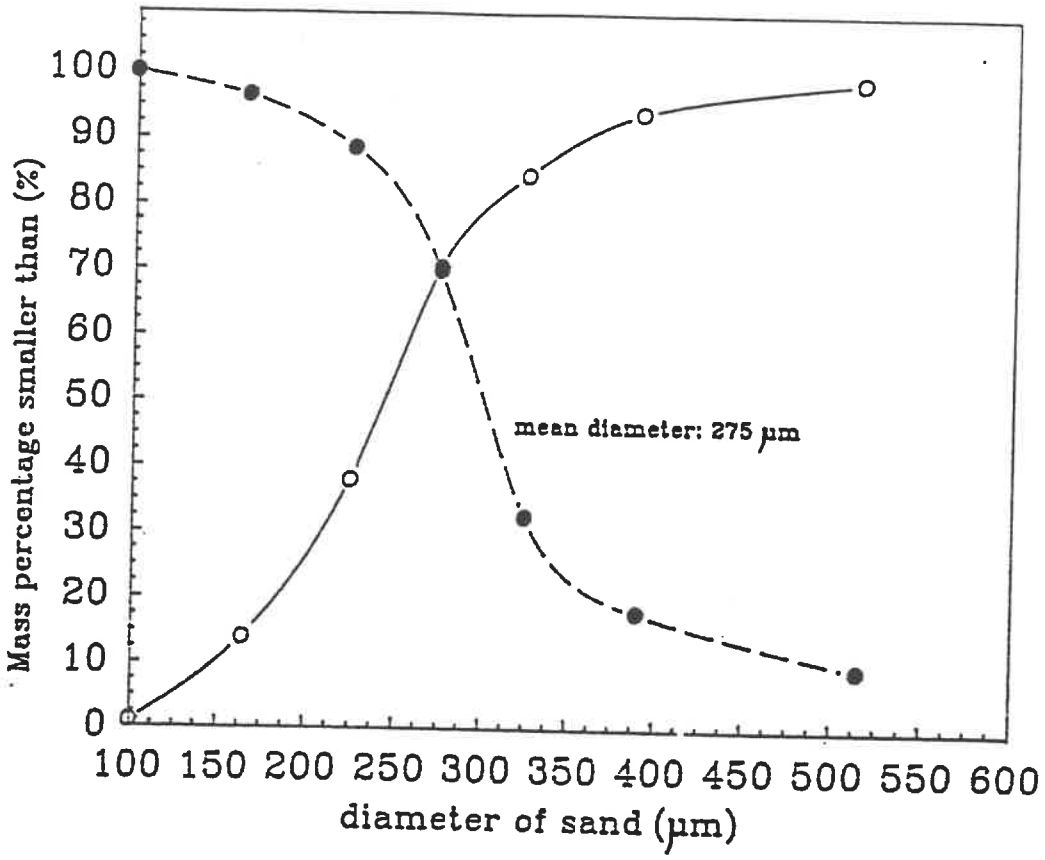

● : downward cumulative curve
○ : upward cumulative curve

Figure (5-9). Clean sand particle size distribution

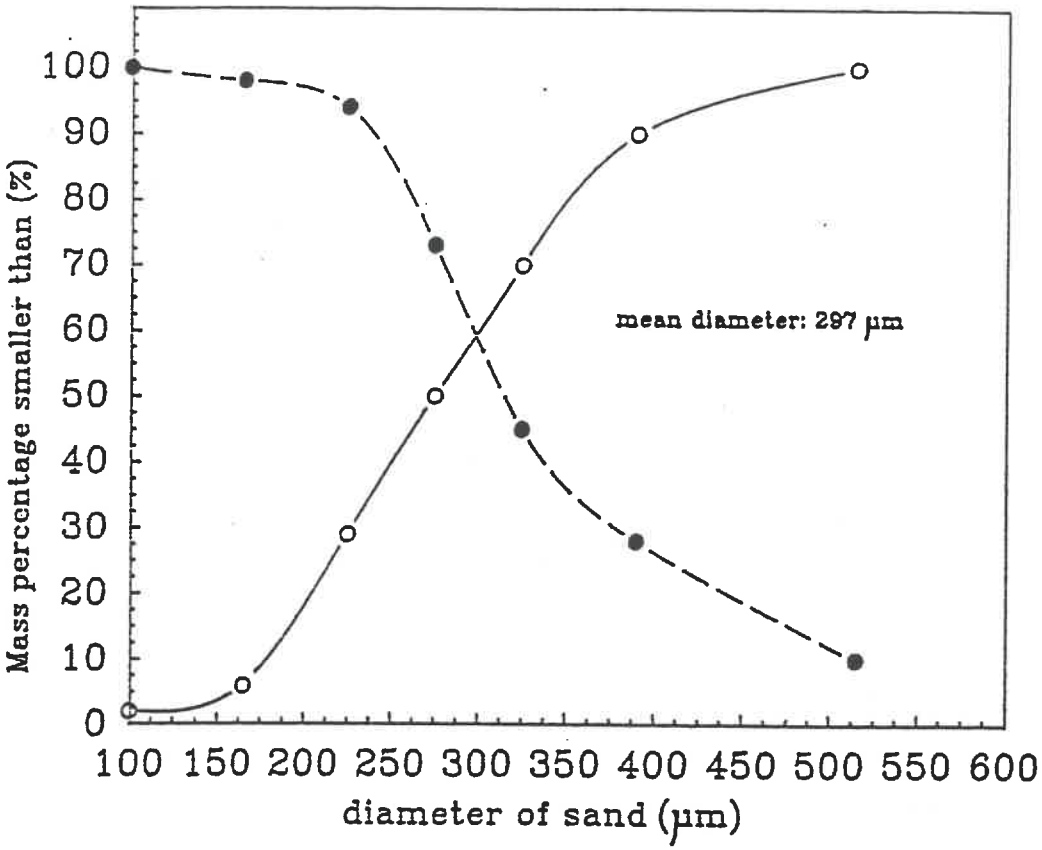

● : downward cumulative curve
o : upward cumulative curve

Figure (5-10). Used sand particle size distribution

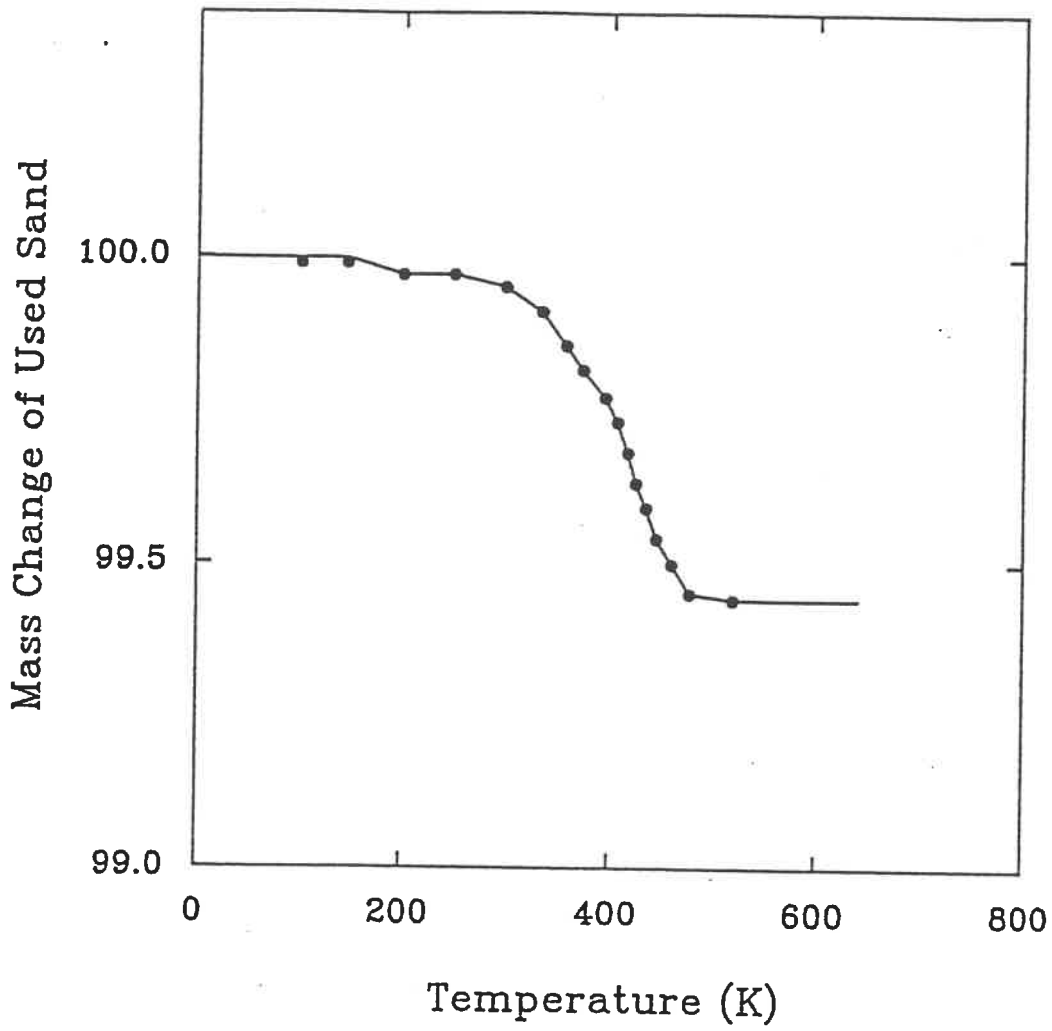

Fig (5–11) Mass Variation of Used Sand vs Temperature

CHAPTER 6. EXPERIMENTAL RESULTS, DISCUSSION AND COMPARISON WITH MODELING RESULTS

6.1 INTRODUCTION

In this chapter, the heat and the mass transfer mechanism and hydrodynamics behaviour of the GCP are selected by using the experimental results. The flow regimes and limitative process of resin combustion in the GCP are characterized, and the models described in Chapter 4 are distinguished. An optimum model for foundry sand reclamation is proposed.

6.2 EXPERIMENTAL RESULTS

Experiments are performed on the pilot-scale unit described in Chapter 5. The experimental program is divided in three parts:

—— Operation of the unit without sand. It is used to check the working state of the unit, get the heat and hydrodynamics behaviour of the gas, and calculate the heat losses.

—— Heating of clean sand, it is used to analyse the flow regimes of gas-solid flow, and obtain the heat transfer behaviour between the gas and solids.

—— Reclamation of the used sand, it is used to model the resin combustion process in the GCP.

All the data in this section are obtained while the experimental unit is operated under steady state conditions which is reached after 60 minutes of preheating and 20 minutes of operation. The maximum time of recording all the data for one experiment is around 20 minutes.

6.2.1 OPERATION OF THE UNIT WITHOUT SAND

The preliminary test is the heating of the furnace. This initial phase has the objective of verifying the operation of the experimental installation. The initial furnace temperature is as same as the laboratory temperature. When the burner power is around 40 kW to 60 kW, it needs about one hour to reach steady state which is characterized by a maximum 10°C variation of the gas temperature over 10 minutes. Under these conditions, the average outside surface temprature of the furnace is in the range of 150°C - 185°C.

Figure (6-1) shows the gas temperature profile in the unit under the following operating conditions: 56.6 kW burner power and 1.48 aeration rate. The essential characteristics of the combustion and gas hydrodynamics in the burner and the furnace can be obtained. The highest temperature region is in the lower part of the burner and the top of the furnace, at an

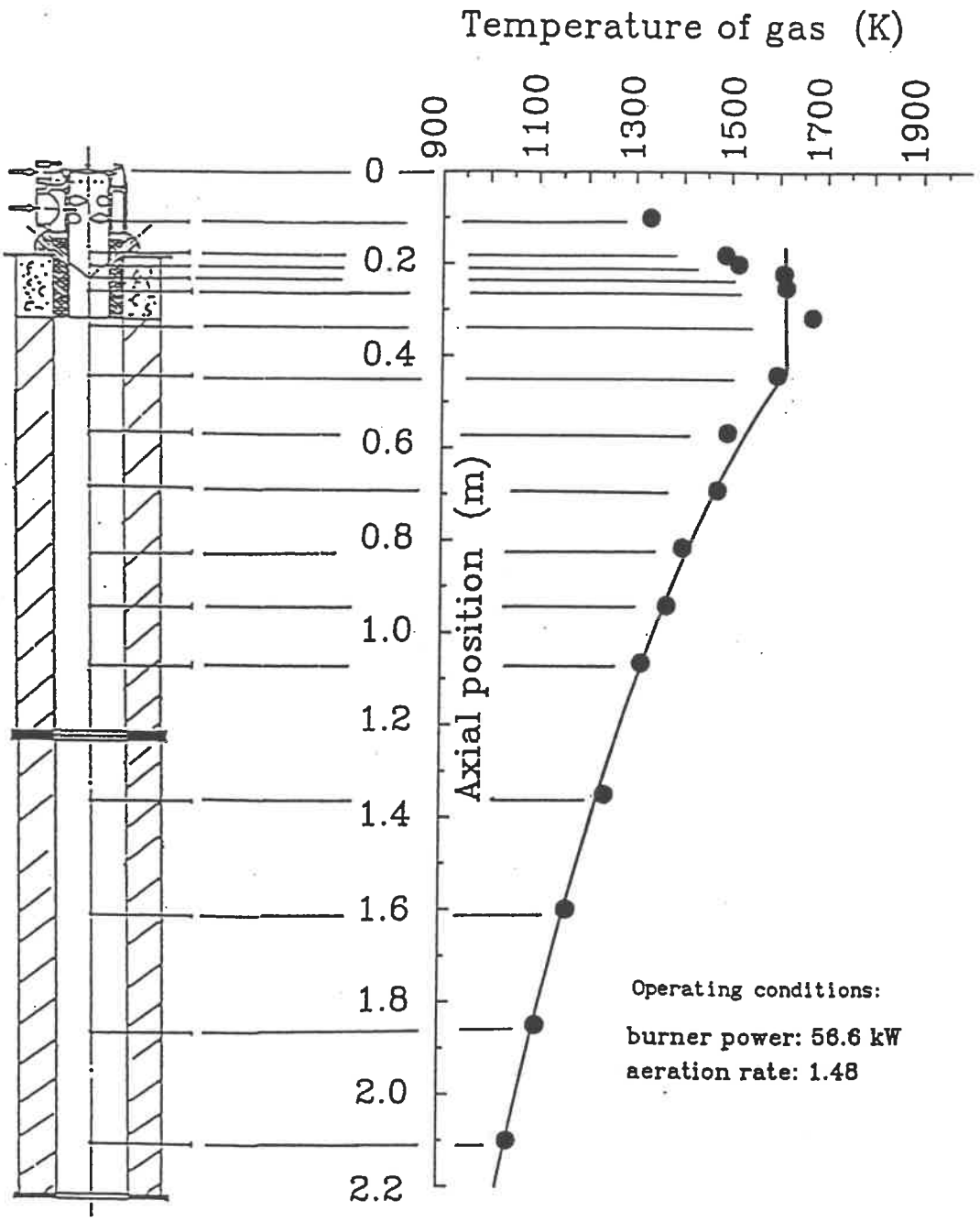

Figure (6-1) Axial gas temperature profile without sand

axial position between 0.18m and 0.4m. Combustion of natural gas occurs in this zone, and the flame is fully developed in the refractory section of the burner. Near the entrance orifices of natural gas and air (axial position: 0 - 0.15m), the gas temperature is lower, since there is no flame.

Although the gas temperature is not completely uniformed in the high temperature zone, a constant value shown by the straightline in Figure (6-1) can be used to approximate the temperature.

After this temperature region, the gas temperature drop is about 500°C over the 2.1 meter length of the furnace. It means that the heat loss from the wall can not be ignored, it has been considered in Chapter 4. From the value mentioned above, the overall heat loss from the wall of the furnace is around 30% to 40%.

6.2.2 HEATING OF CLEAN SAND

Experiments have been done for heating of clean sand. The operating conditions are shown in Table (6-1). And the experimental results are shown in Figure (6-2) and (6-3).

Table (6-1) : Experimental conditions for clean sand

	Burner power	Aeration rate	sand flow rate
Test 1	56.6 kW	1.25	82 kg/h
Test 2	56.6 kW	1.25	125 kg/h
Test 3	56.6 kW	1.48	82 kg/h

There is not a big difference in the shape of the gas temperature profiles for these experiments, and the one without sand. There is still a flat temerature zone at the top of the unit. And the length of this zone is around 5 times the burner diameter (D_{burner} = 80mm). So the well-stirred assumption for gas phase in this region is suitable.

The sand temperature raised about 300°C in the first 0.44 meter, and another 300°C is obtained on the following 1.7 meter. It shows that the heat transfer rate in the first region between the two phases is higher than in the rest. But the sand temperature does not show the well-stirred characteristics in the first region.

Figure (6-2) shows the effect of sand flowrate. The sand temperature obviously decreases as the mass flowrate of sand increases about 52%. The equilibrium temperature of the two

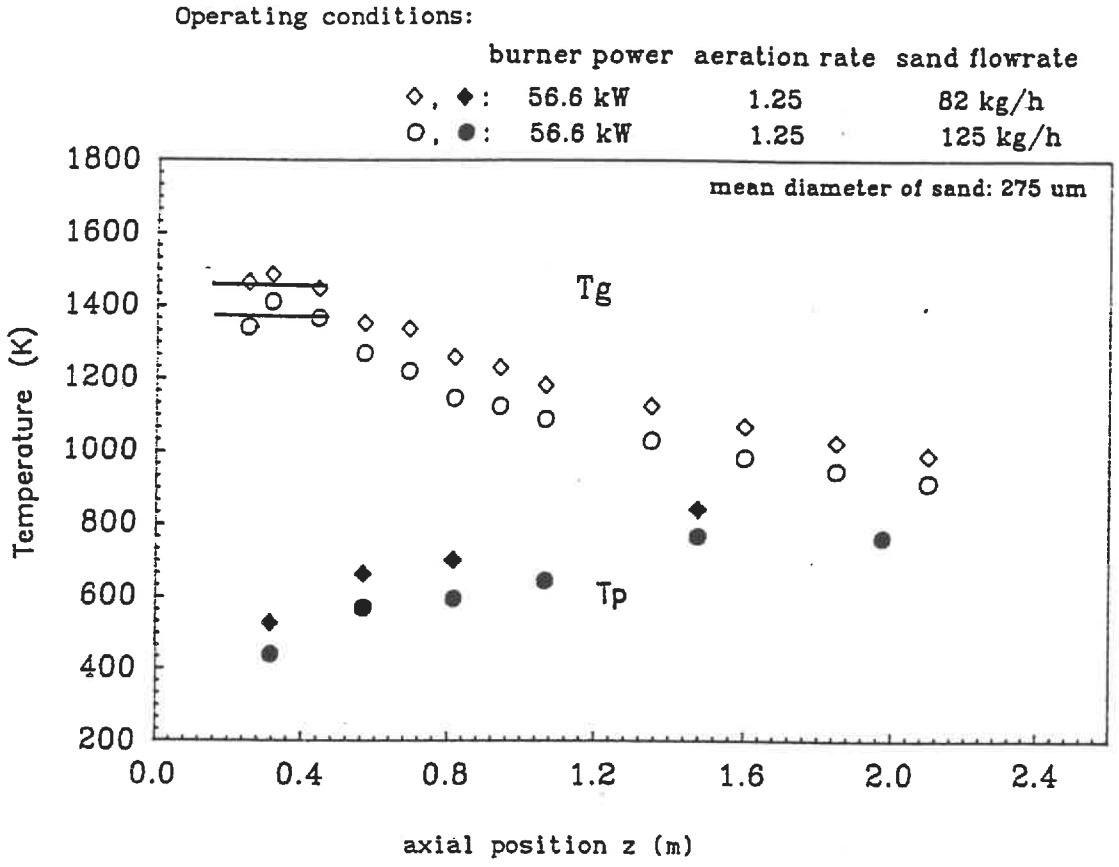

Figure (6-2) Experimental results of sand flowrate effect for heating clean sand

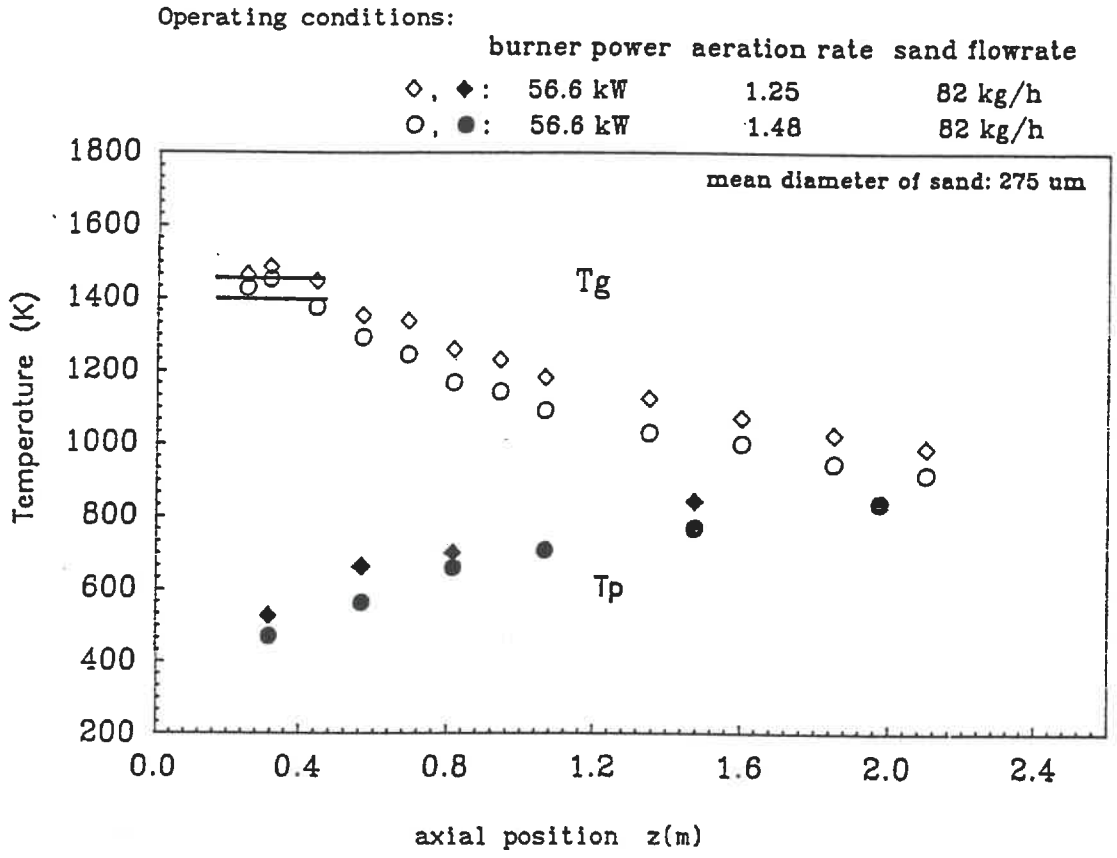

Figure (6-3) Experimental results of aeration rate effect for heating clean sand

phases decreases about 120°C. Figure (6-3) presents the effect of aeration rate. As the areation rate increases about 20%, the equilibrium temperature of two phases decreases about 60°C. Increasing the aeration rate shows three opposite effects. First it reduces the heat transfer driving force due to the initial gas temperature drop. Second is that the quantity of flue-gas is increased, and therefore, its velocity which results in a higher convective heat transfer coefficient between the two phases. Third, this higher velocity reduces the residence time of the sand in the furnace and therefore limits the heat transfer.

6.2.3 RECLAMATION OF USED SAND

Only four experiments have been done to check the effect of different operating conditions due to the availability of used sand. The operating conditions are shown in Table (6-2).

Table (6-2) : Experimental conditions for used sand

	Burner power	Aeration rate	Sand flow rate
Test 1	56.6 kW	1.48	82 kg/h
Test 2	56.6 kW	1.48	125 kg/h
Test 3	56.6 kW	1.30	82 kg/h
Test 4	64.45 kW	1.48	82 kg/h

The experimental results including the gas and solid temperature profiles, and resin conversion are shown in Figure (6-4), (6-5), and (6-6). The gas phase temperature keeps the same characteristics as in the heating clean sand process: a 5 burner diameter long zone where the gas is well mixed appears at the top of the unit. The presented data show the effect of different operating conditions. For resin conversion, the effects are obvious : for a given power input and a given aeration rate (Figure (6-4)), an increase of the sand flowrate results in a lower temperature and a much lower resin distribution rate. For a given power input and a given sand flowrate (Figure (6-5), an increase in the aeration rate results in slightly lower temperatures but in a much higher resin destruction rate. For a given sand flowrate and a given aeration rate (Figure (6-6), an increase in the burner power results in slightly higher temperatures and in a higher resin destruction rate. Figure (6-7) summarizes the resin conversion profiles. Two of the limitations for resin distribution are clear. One is the heat transfer rate, because the changes in burner power and sand flowrate affect the heat transfer rate between the two phases. Another is the oxygen concentration. Increasing the aeration rate will raise the oxygen concentration in the flue-gas, and allow for a better combustion of the resin.

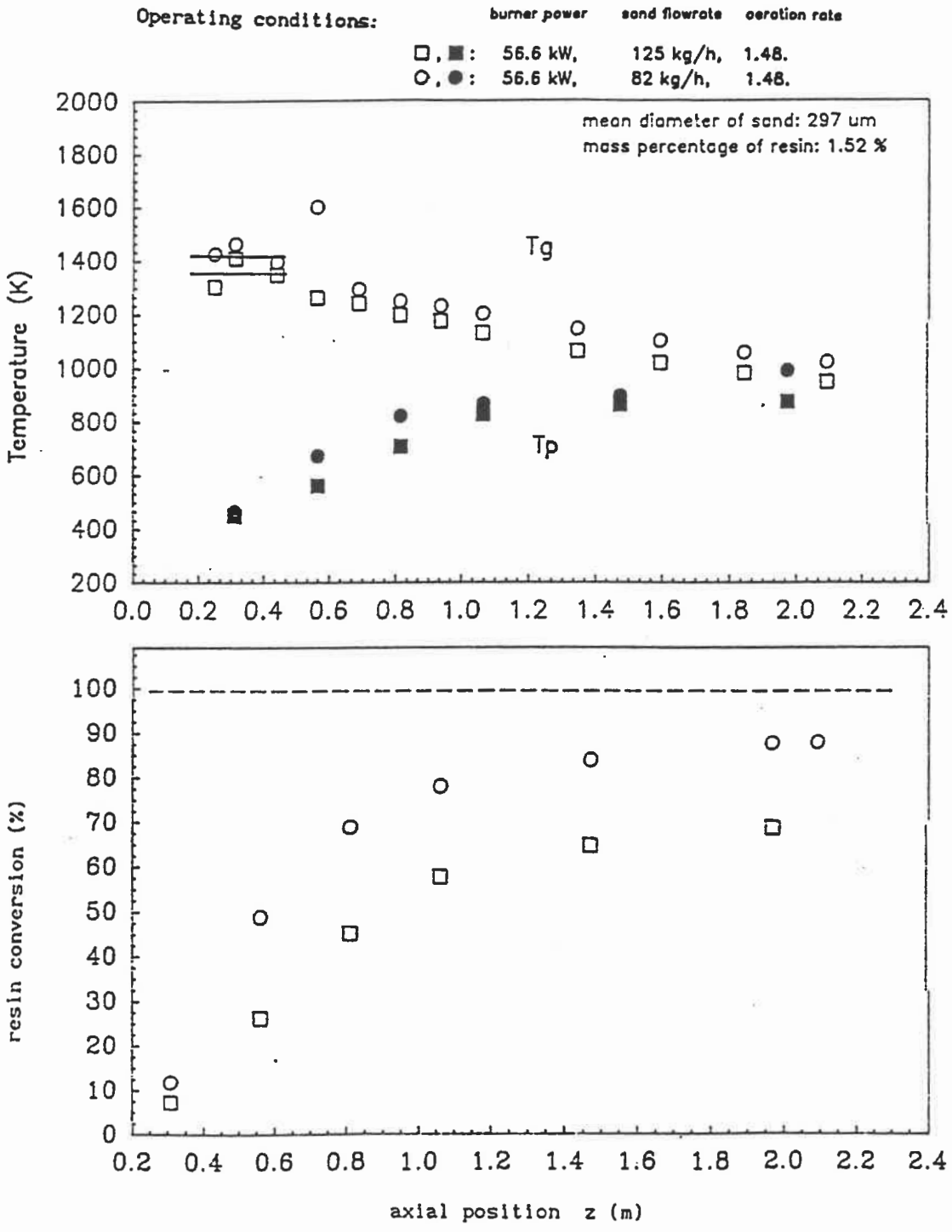

Figure (6-4) Effect of used sand flowrate

- Experimental data

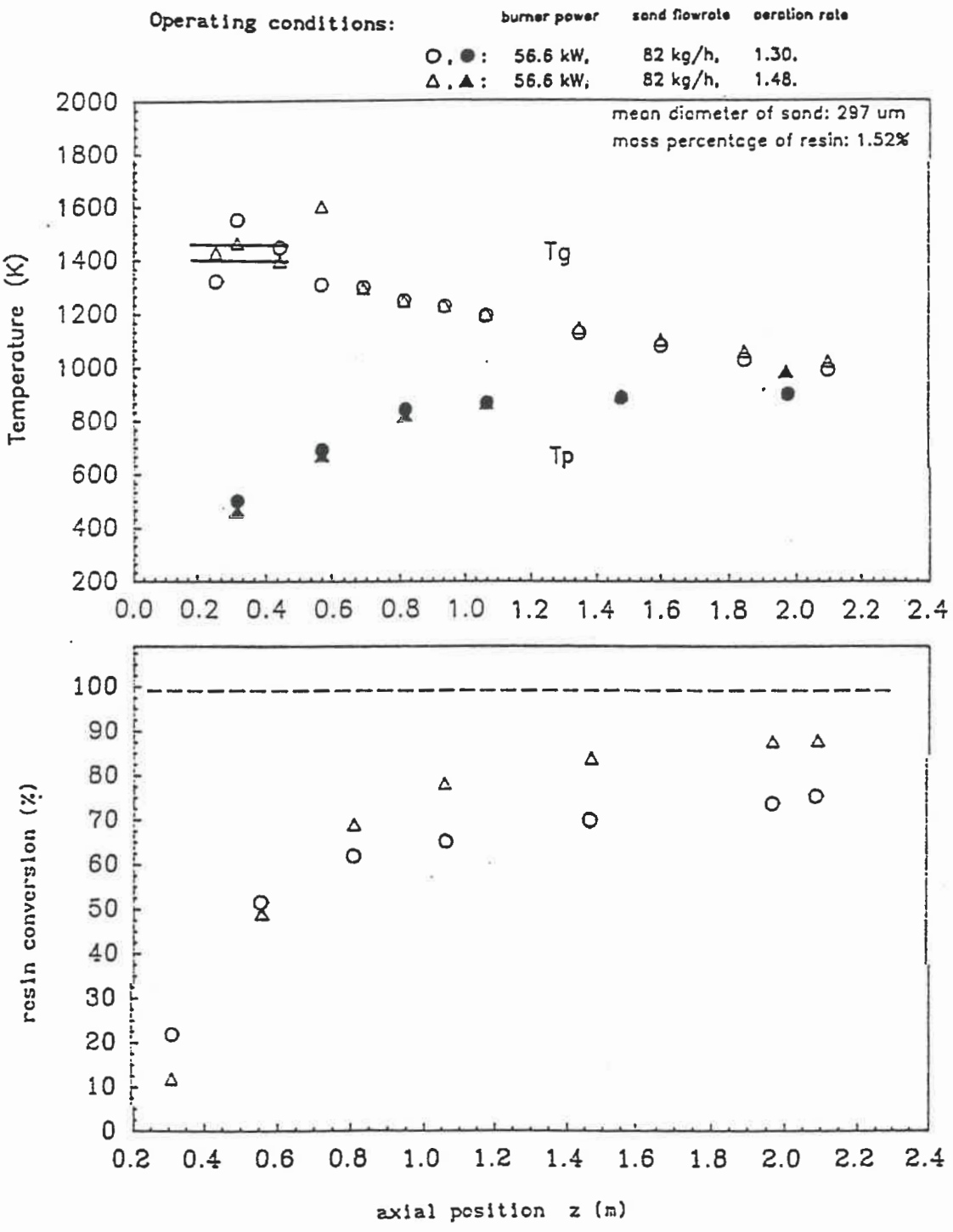

Figure (6-5) Effect of aeration rate - Experimental data for used sand

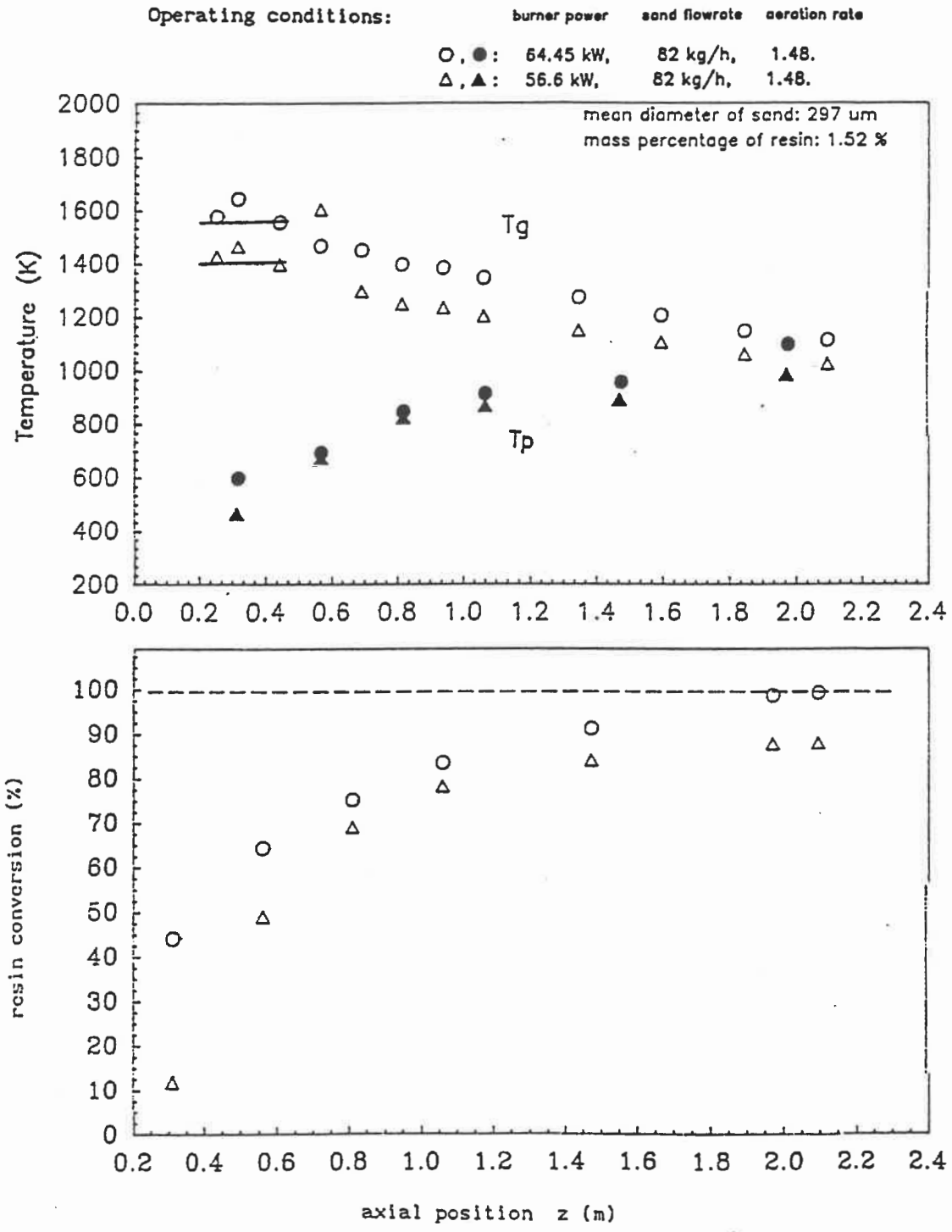

Figure (6-6) Effect of burner power - Experimental data for used sand

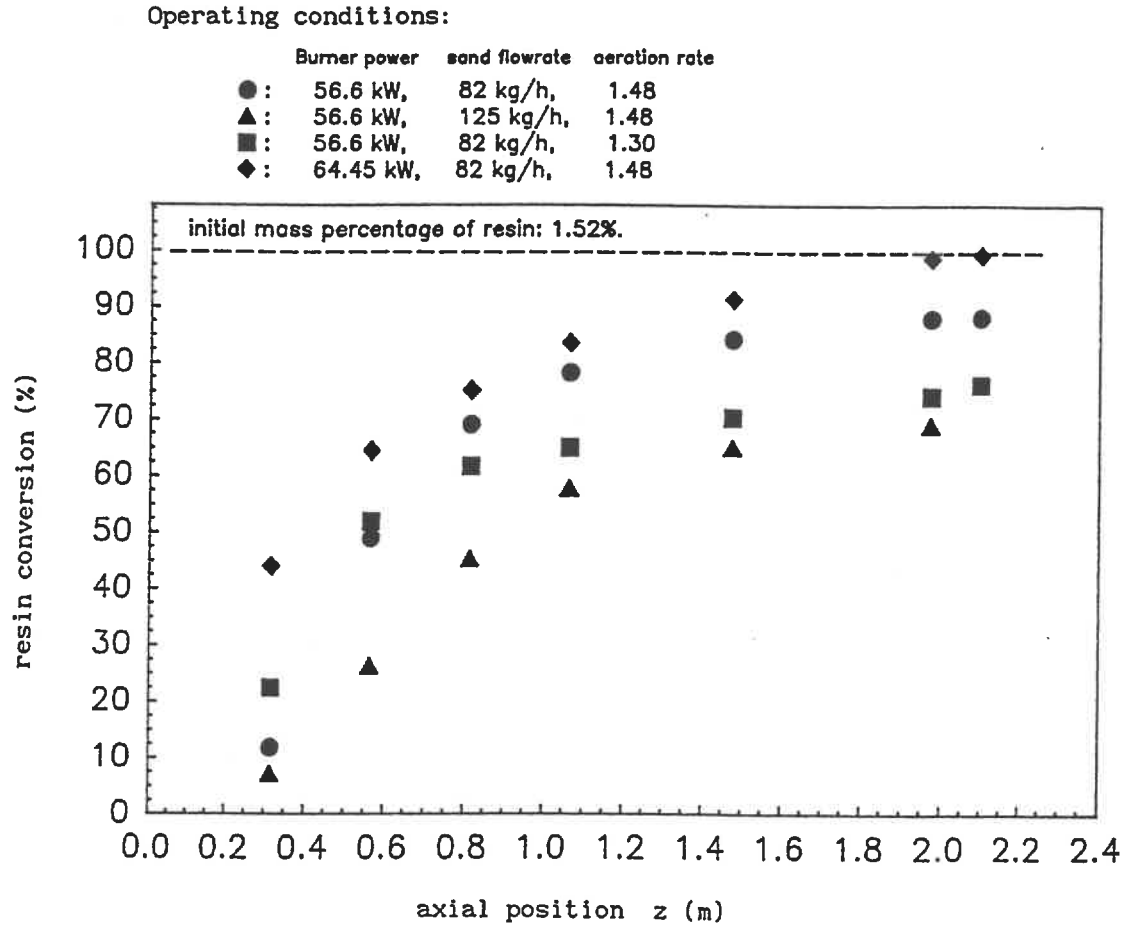

Figure (6-7) Conversion of resin under different operating conditions

The best result in resin destruction in these experiments are for the following conditions: 64.45 kW burner power, 1.48 aeration rate and 82 kg/h sand flowrate. The resin conversion is more than 99.3%.

The effect of aeration rate is sensitive for resin destruction. A further investigation has been carried out (Figure (6-8)): two burner powers have been chosen with various aeration rates. The resin conversion was measured on the sand at the exit of the unit. Figure (6-8) shows that, the higher burner power the better the resin destruction. There exists an optimum aeration rate for which resin conversion, at any given burner power, is maximum. This optimum value does not depend on the burner power; it depends on the amount and the type of resin. This optimum aeration rate is 1.48 for this used sand. If the aeration rate is lower, not enough oxygen is available to burn the resin. This does not, however, reflect the actual stoichiometry of the incineration reaction as oxygen is still detected in the exhaust gas, it merely indicates that oxygen transfer is a limiting step. If the aeration rate is higher than 1.48, the exit resin conversion drops. This may be due to the lower temperature in the furnace or to the lower residence time of the solid.

To check the reproducibility of the experiments, one

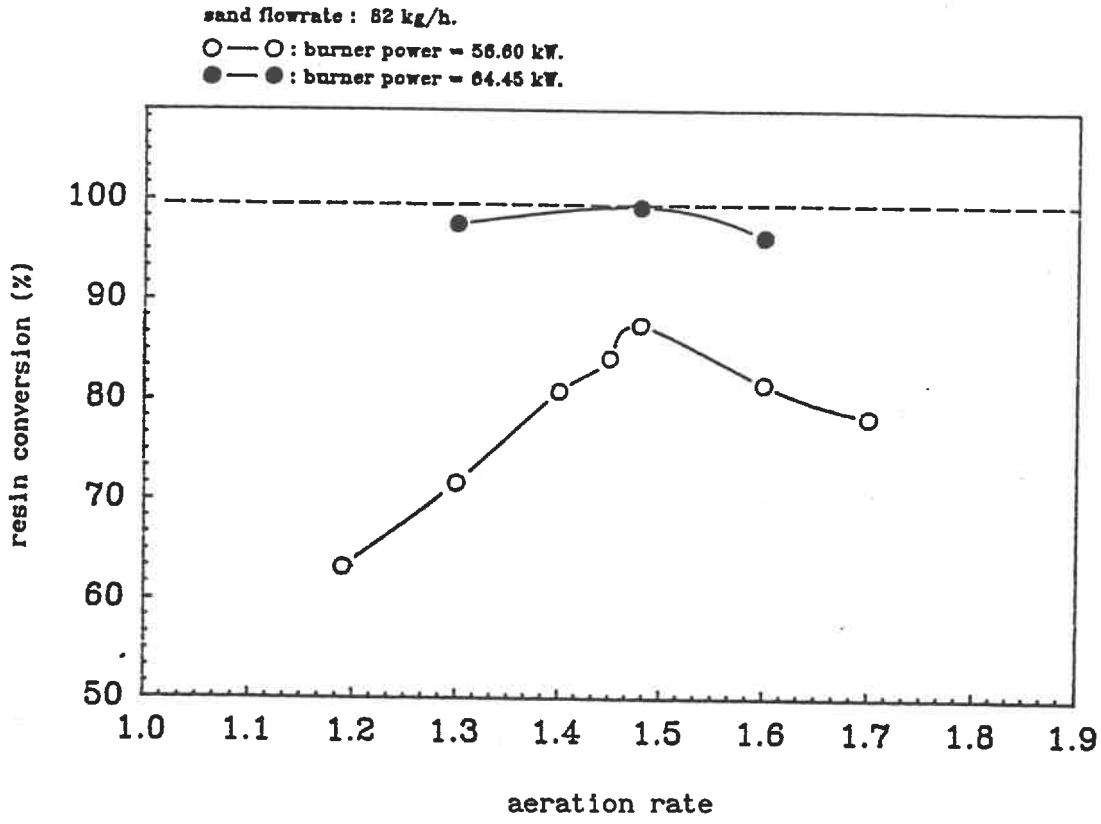

Figure (6-8) Effect of aeration rate for resin conversion

experiment has been done again. The same operating conditions are taken, and the test is repeated twice. The results are shown in (figure (6-9)), and indicates that the reproducibility is very good.

The composition of the exhaust gas is checked by using the O_2, CO_2, and combustible analysers. The result is shown below under the operating conditions of 56.6 kW burner power, 1.48 aeration rate, 82 kg/h sand flowrate.

	O_2	CO_2	Combustible
% mass	3.6%	14.8%	0.15%

The value of combustible shows the good combustion conditions in the process.

6.3 COMPARISON OF EXPERIMENTAL AND MODELING RESULTS

Chapter 4 has presented the theoretical approach of modeling the GCP. Several models have been advanced. According to the experimental results, the assumptions of different models will be checked in this chapter. And one model will be selected for modeling used sand reclamation process by GCP.

6.3.1 MODELING THE FLOW REGIMES

From discussion of the experimental results, clean sand heating or used sand reclamation process showed the same flow

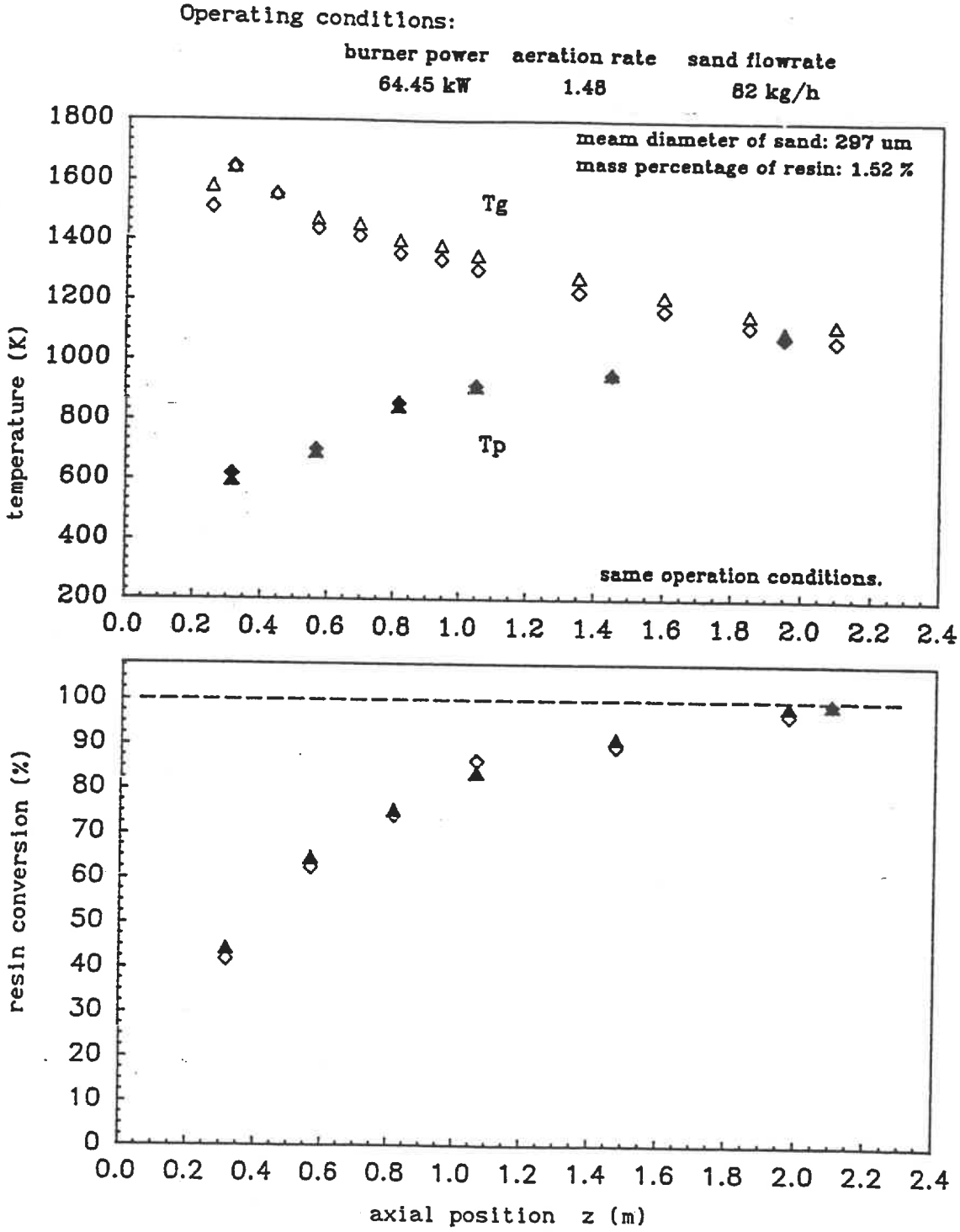

Figure (6-9) Reproducibility test for used sand

behaviour. It is possible to consider only the clean sand heating process for comparing with the model predictions.

There are three models for flow regime as mentioned in Chapter 4. Figure (6-10) shows the predicting data of these models comparing with the experimental results. The assumptions for these models are:

– Model I considers that both the gas and the solid phases are in plug-flow through the whole process.

– Model II considers that both the gas and the solid phases are in well-stirred flow in the first region which length is 0.44 m (5 burner diameters) and plug-flow in the second region.

– Model III considers that the gas phase has two flow forms. One is well-stirred flow in the first region, then is plug-flow in second region. The solid phase is plug-flow through the whole process.

In Figure (6-10), as expected from the respective assumptions of the models, the obvious differences are in the first region. Model III gives the most satisfactory prediction of the experimental data.

Figure (6-11) and (6-12) show that model III is able to predict satisfactorily the effects of aeration rate and sand flowrate on the thermal behaviour of the unit. Model III which considers a well-stirred zone only for the gas which length is equal to 5 times diameter is therefore chosen.

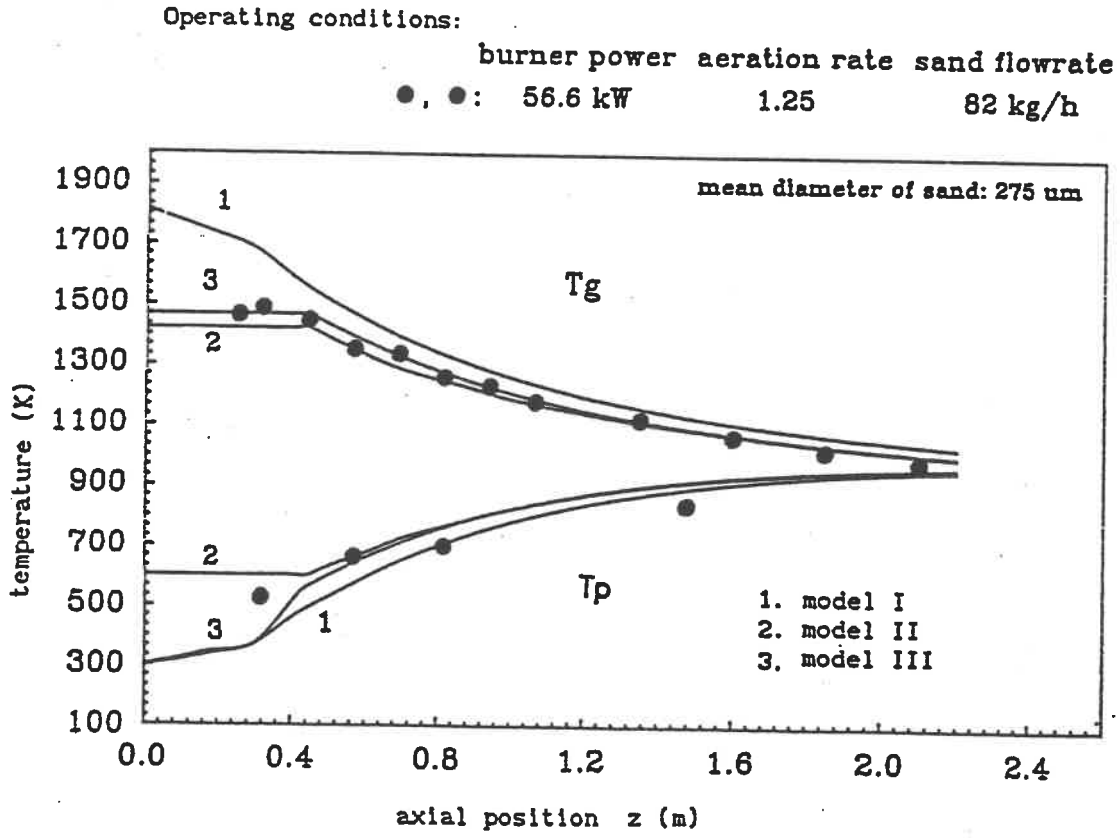

Figure (6-10) Comparison of the different models (clean sand)

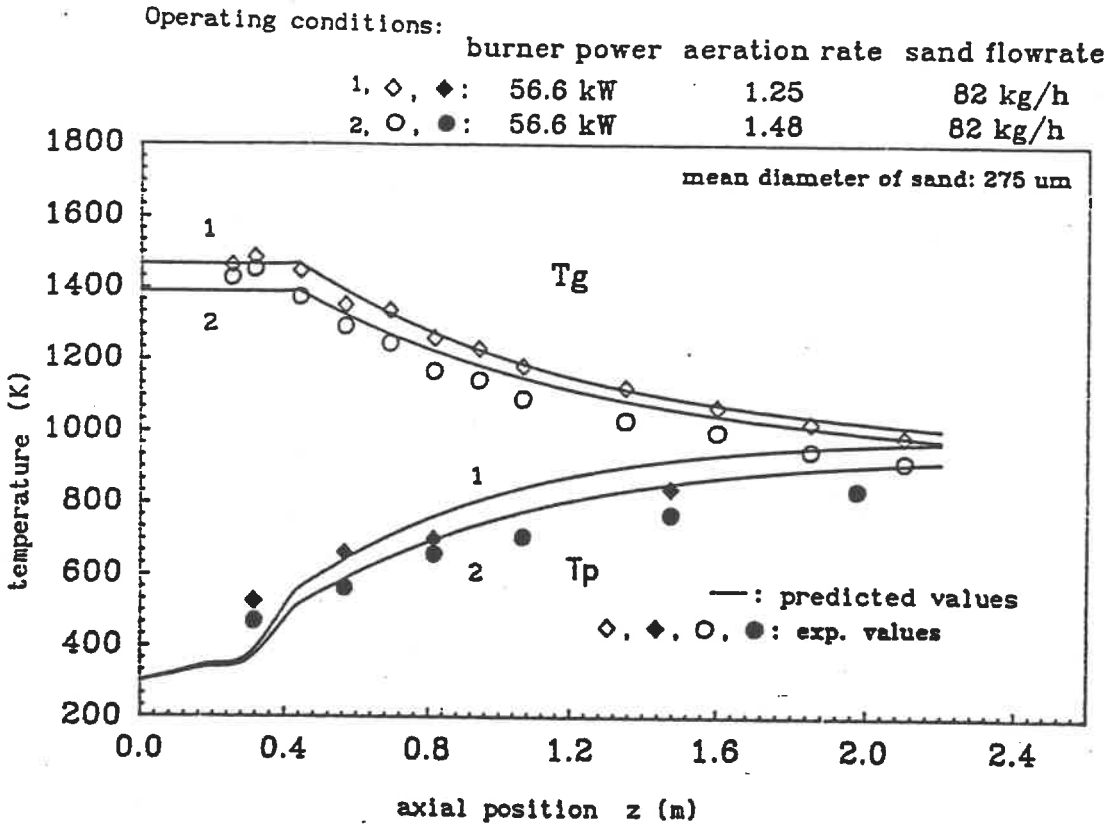

Figure (6-11) Modeling the effect of aeration rate for clean sand

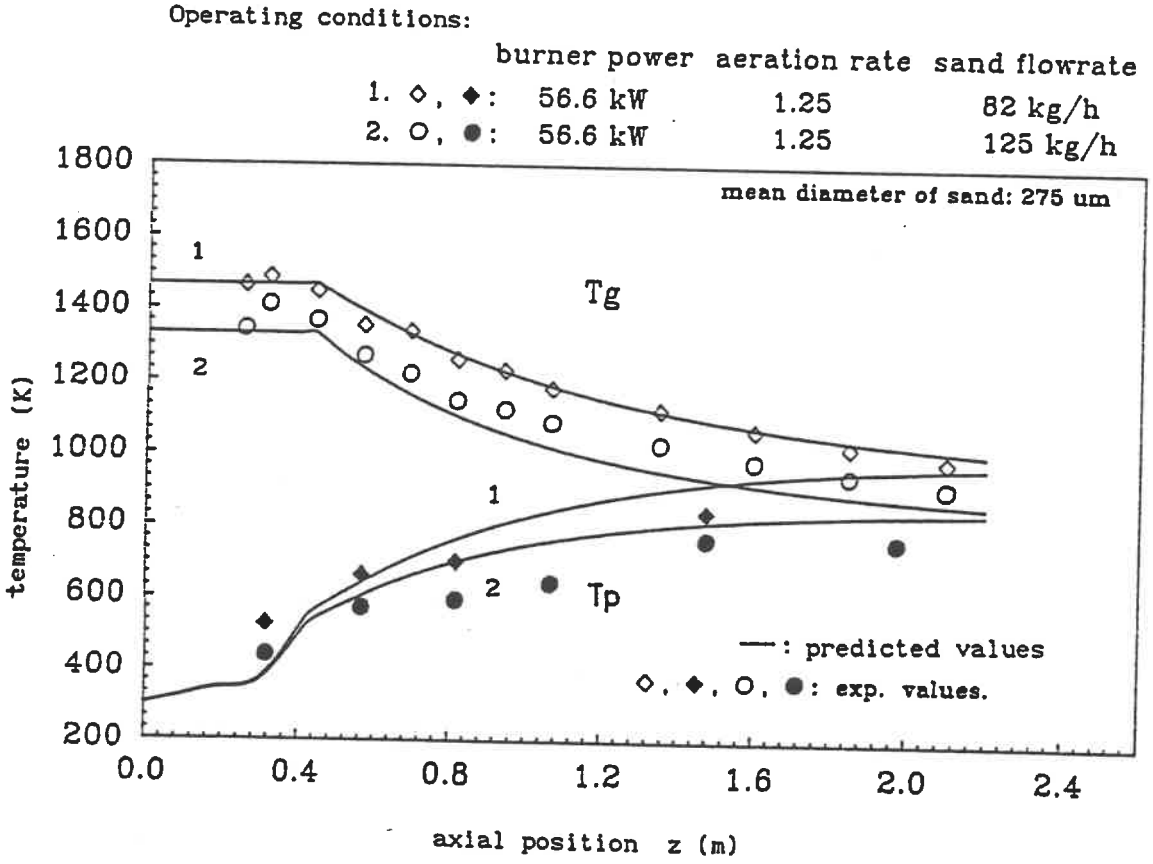

Figure (6-12) Modeling the solid flowrate effect for clean sand

6.3.2 MODELING THE RESIN COMBUSTION PROCESS

In Chapter 4, the resin combustion process is considered according to two categories. One assumes that the resin combustion rate is infinite, and that the process is controlled by the heat transfer rate only. The second assumes that both the heat transfer rate and the resin elimination rate are limitations of the process. It is very clear from the resin conversion results (Figure (6-7)), that the heat transfer rate is not the only one limitation of the process. Thus the resin combustion limitation needs to be considered.

Three models for the resin combustion process are proposed in chapter 4. Taking the same operating conditions, the predicting results of these three models are shown in Figure (6-13) comparing with the experimental data. For the thermal behaviour, there are no big difference between the three models. but from the resin conversion results, only the volatile/oxygen diffusion model tends to give a satisfying result. The volatile diffusion model shows a very fast rate of resin elimination. The oxygen diffusion model does not have a resin conversion jump in the begining of the process that is shown in experimental results. Thus the volatile/ oxygen diffusion model is chosen as the resin combustion process.

The volatile/oxygen diffusion model is assumed when the

Operating conditions:

burner power: 56.6 kW, aeration rate: 1.48, sand flowrate: 82 kg/h

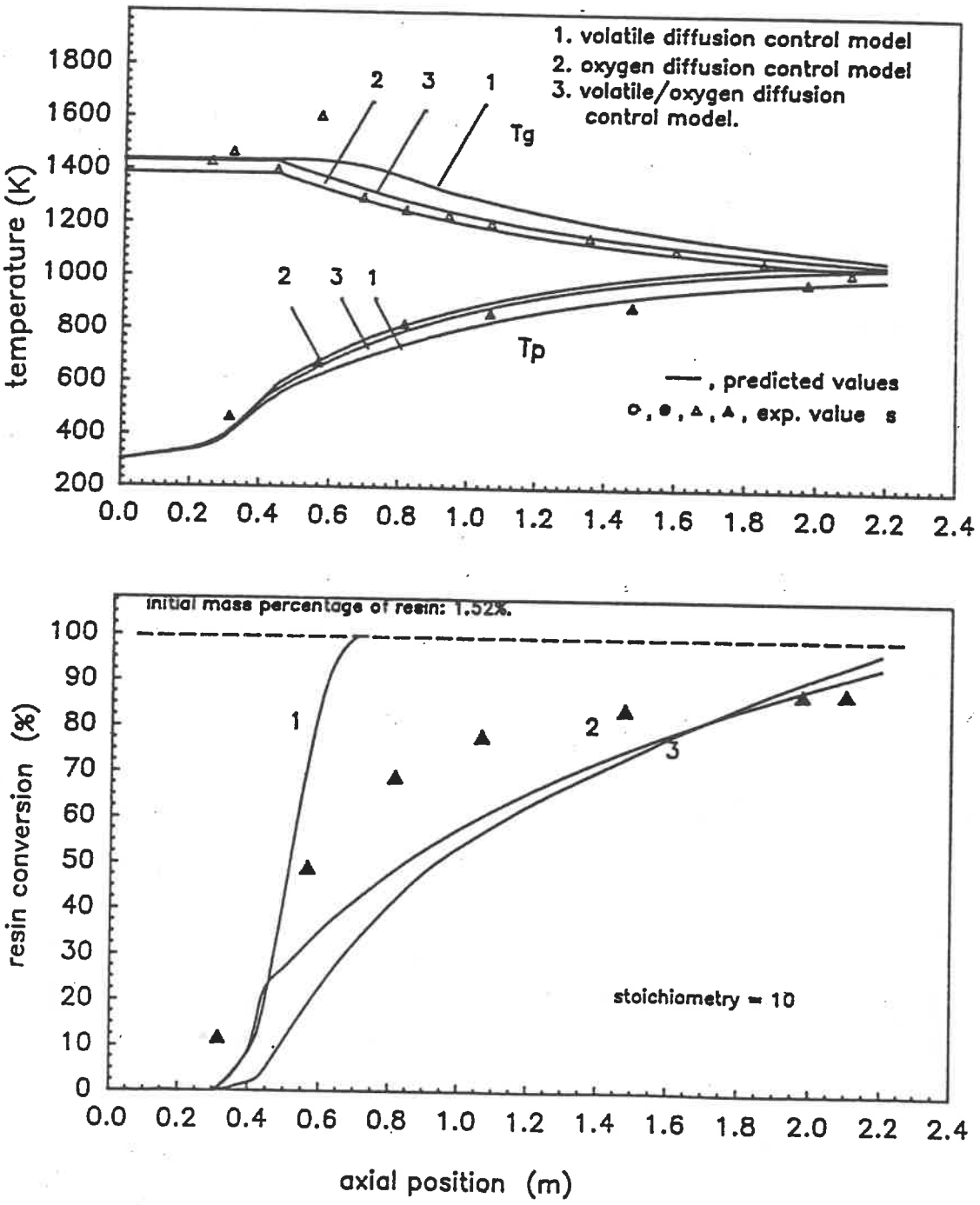

Figure (6–13). Comparison of resin combustion models

particle temperature reaches the resin decomposition temperature, volatiles and char are produced. Then volatiles diffuse to the atmosphere and burn around the particle. After volatiles burn out, char begins its combustion on the surface of the particle. The fuel droplet combustion model is adopted for volatile combustion. The limitation of this combustion is the volatile diffusion rate. Volatile evaporation starts at 180°C as was determined in paragraph 5.7.3. For char burning on the surface of the particle, the limitation process is oxygen diffusion rate. The heat of combustion of the volatile is assumed given to the gas while the heat of combustion of the char is assumed given to the solid.

Now the mass percentage of volatile and char need be estimated. It is not easy to use a simple method for obtaining the quantity of volatile. It is also almost impossible to get the stoichiometry of both the volatile and the char combustion. So in the model for used sand, the percentage of volatiles and the stoichiometry of the combustion are treated as two adjusted parameters. However, percentage of volatiles is expected to be in the range 10 to 30%.

Figure (6-14) presents the effect of stoichiometry. From the temperature profiles of the two phases, there is almost no effect. But the resin combustion is drastically affected. Among the change range of the stoichiometry, the value of 10 appears to

be the best although it does not fit properly the experimental data. Figure (6-15) shows the effect of the percentage of volatiles at a stoichiometry of ten. From this figure, no drastic effect of the percentage of volatile is found. More couples of these two parameters are tested in the model for different operating conditions. The results are shown in Figure (6-16), (6-17), (6-18) and (6-19). The values of these two parameters are shown in Table (6-3):

Table (6-3) : Values of feeding parameters

Figure	Volatile	Stoichoimetry
(6-16)	15%	10
(6-17)	30%	12
(6-18)	30%	10
(6-19)	20%	10

Considering all the experimental results, an amount of volatiles equal to 20% and a stoichiometry equal to 10 seems to adequate (Figure (6-18)). this percentage of volatiles agrees with the expexted range.

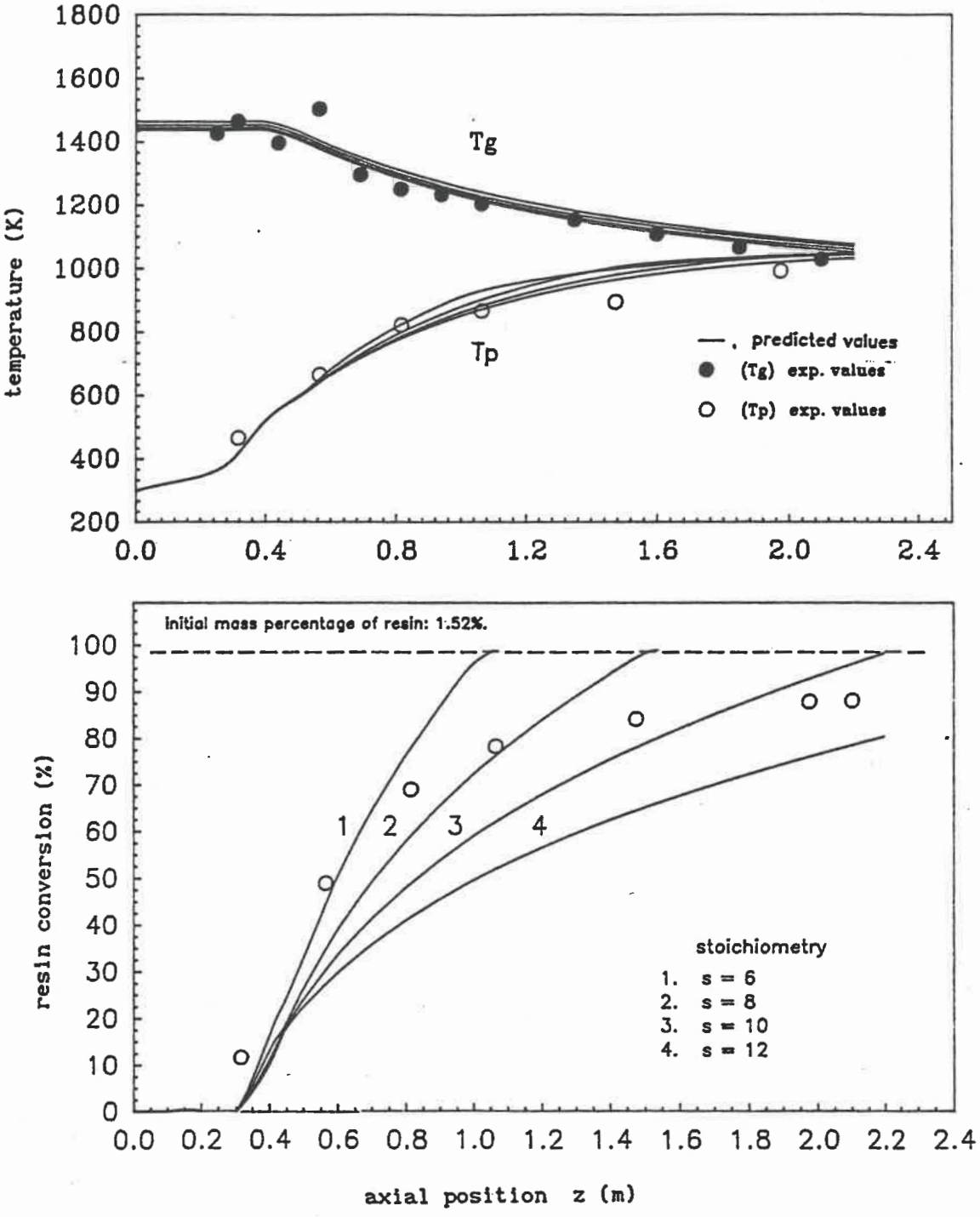

Figure (6-14) Effect of stoichiometry (volatile = 15%)

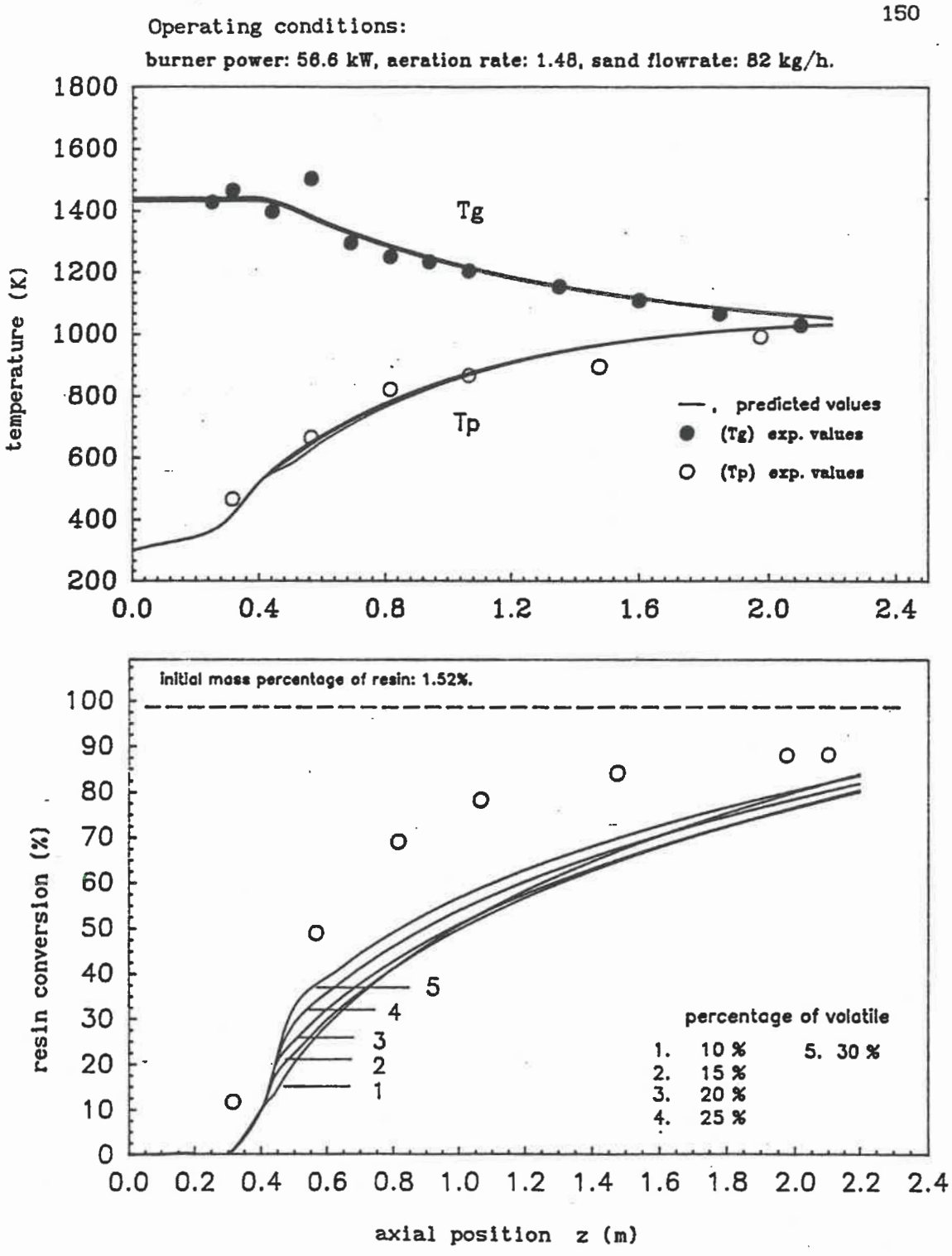

Figure (6-15) Effect of mass percentage of volatile (stoichiometry = 10%)

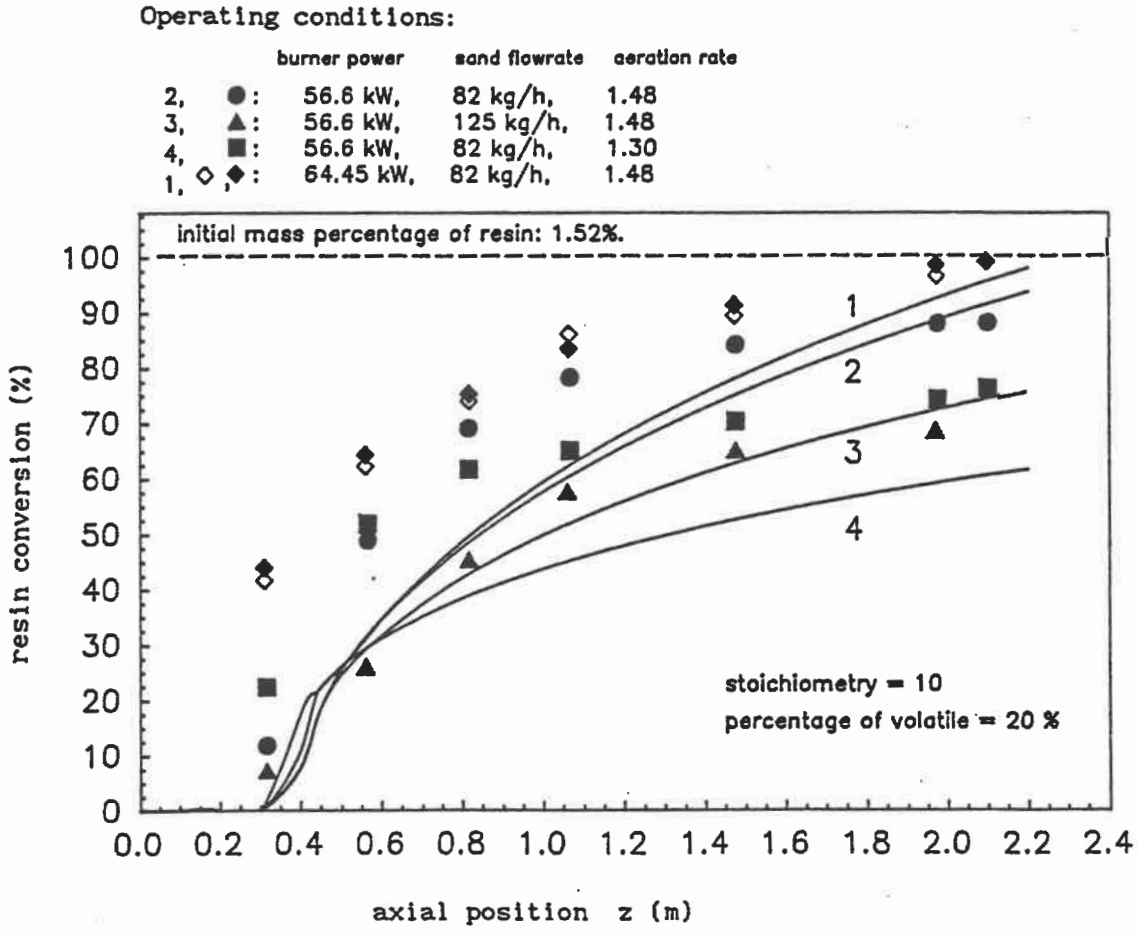

Figure (6-19) Resin conversion (stoichiometry = 10 volatile = 20%)

Operating conditions:

	burner power	sand flowrate	aeration rate
2, ●:	56.6 kW,	82 kg/h,	1.48
3, ▲:	56.6 kW,	125 kg/h,	1.48
4, ■:	56.6 kW,	82 kg/h,	1.30
1, ◆:	64.45 kW,	82 kg/h,	1.48

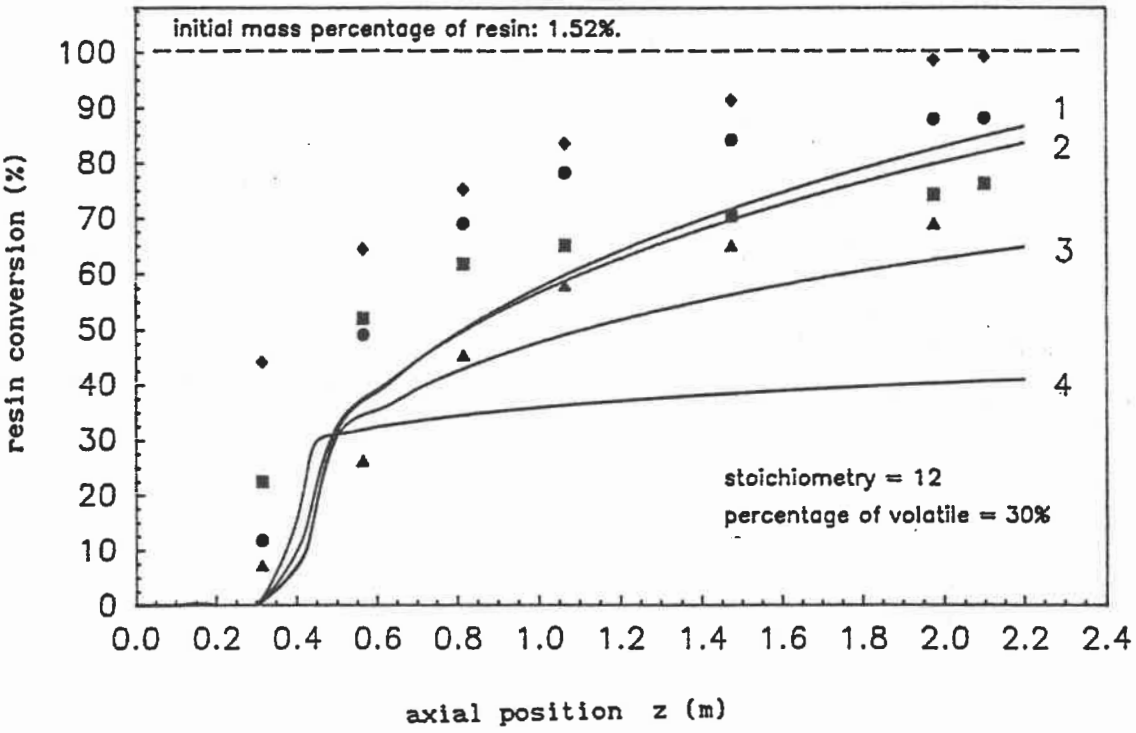

Figure (6-17) Resin conversion (stoichiometry = 12, volatile = 30%)

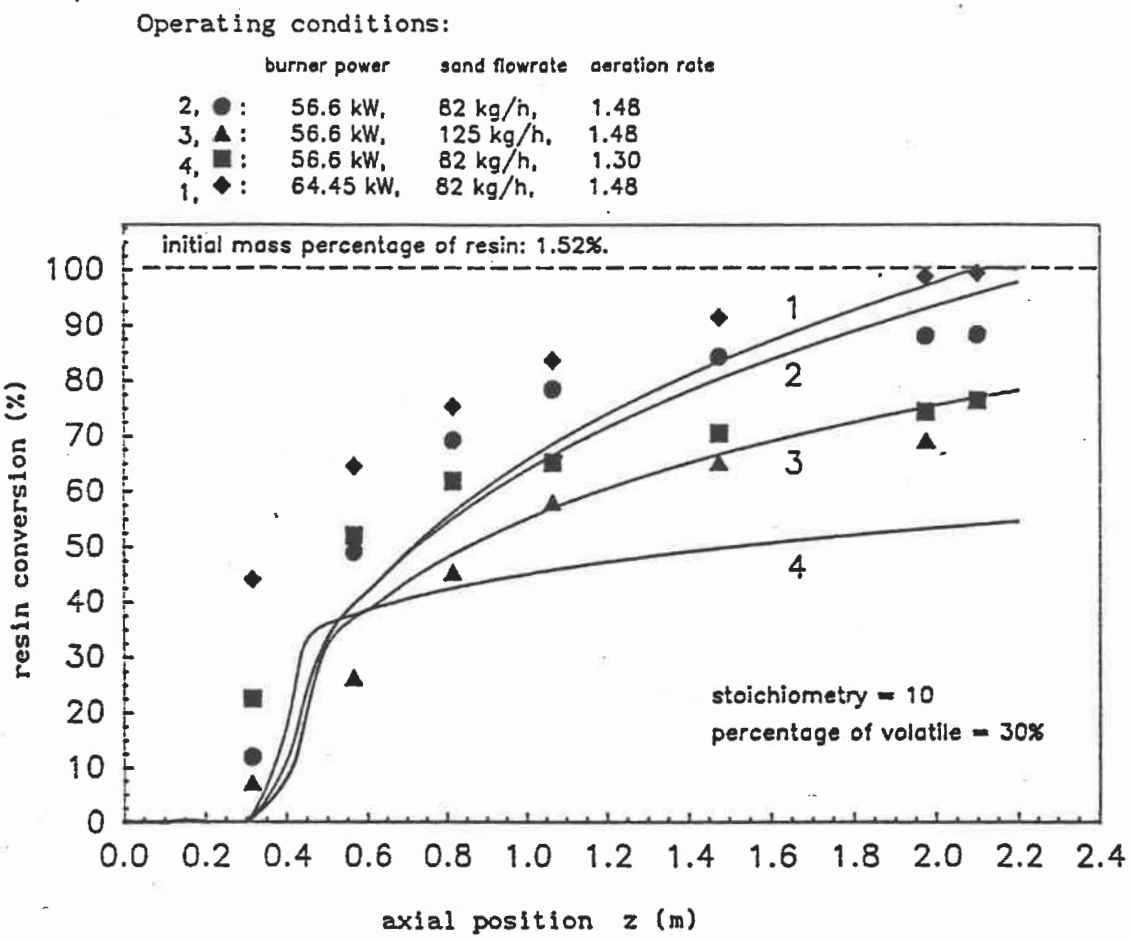

Figure (6-18) Resin conversion (stoichiometry = 10)

volatile = 30%)

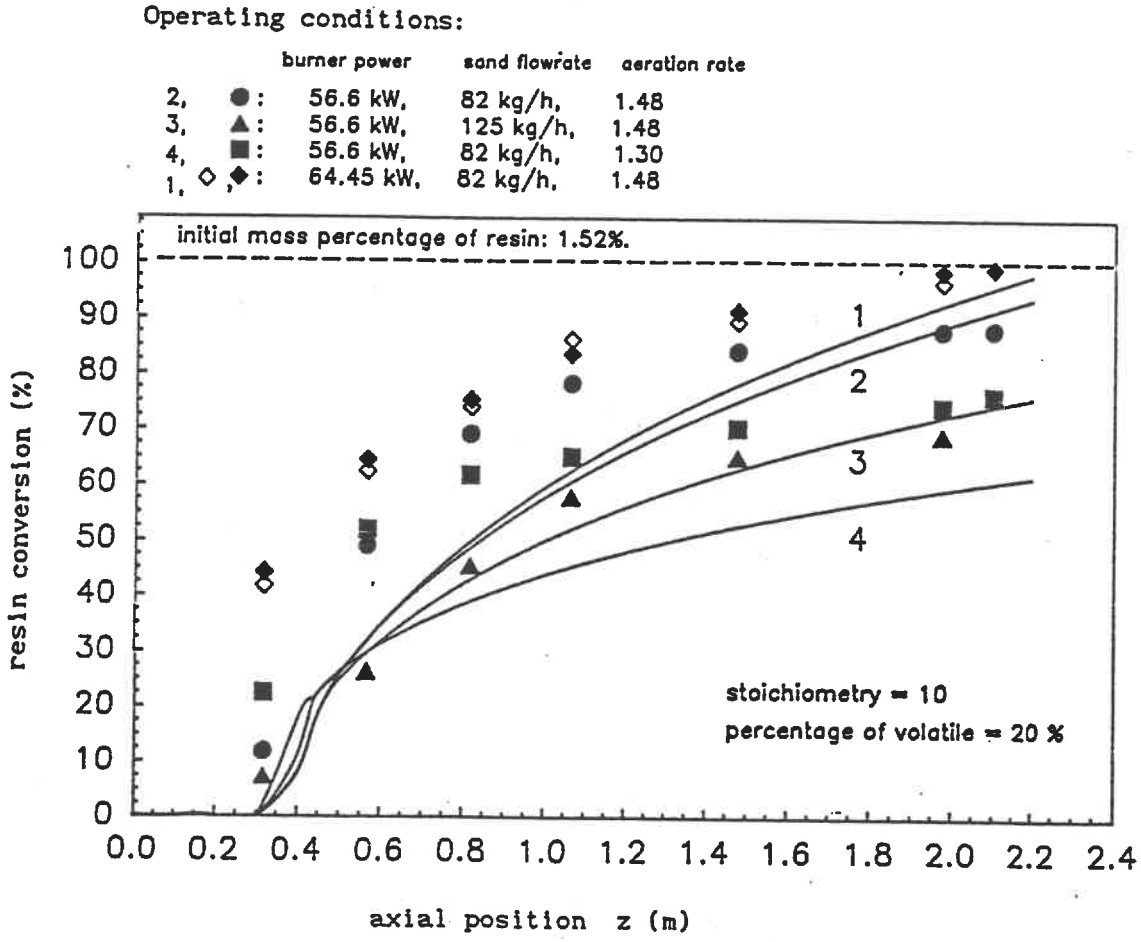

Figure (6-19) Resin conversion (stoichiometry = 10 volatile = 20%)

6.3.3 OPTIMUM MODELING RESULTS FOR USED SAND

It is found that the model which considers:

- a well-stirred zone for the gas (length: 5 burner diameters) at the top of the unit, then a plug-flow zone,
- a plug-flow zone for the solid all over the unit,

satisfactorily describes the temperature axial profiles of both gas and solid as well as the resin conversion profiles in a GCP unit. It is found that the heat transfer between the two phases occurs by convection and radiation and that the mechanism for resin destruction is:

- volatile evaporation and combustion in the gas phase which starts when the particle reaches the volatilizing temperature of 180°C. The amount of volatile is 20% in mass of the resin;
- char combustion on the surface of the particle.

The overall oxygen stoichiometry is found to be 10 mol O_2/mol resin. Model predictions are shown in Figure (6-20), (6-21) and (6-22). For the temperature profiles, the model predicts fairly well the experimental data. For the resin combustion, the model predicts the same trend as the experimental results. The exit resin conversion is predicted quite satisfactorily.

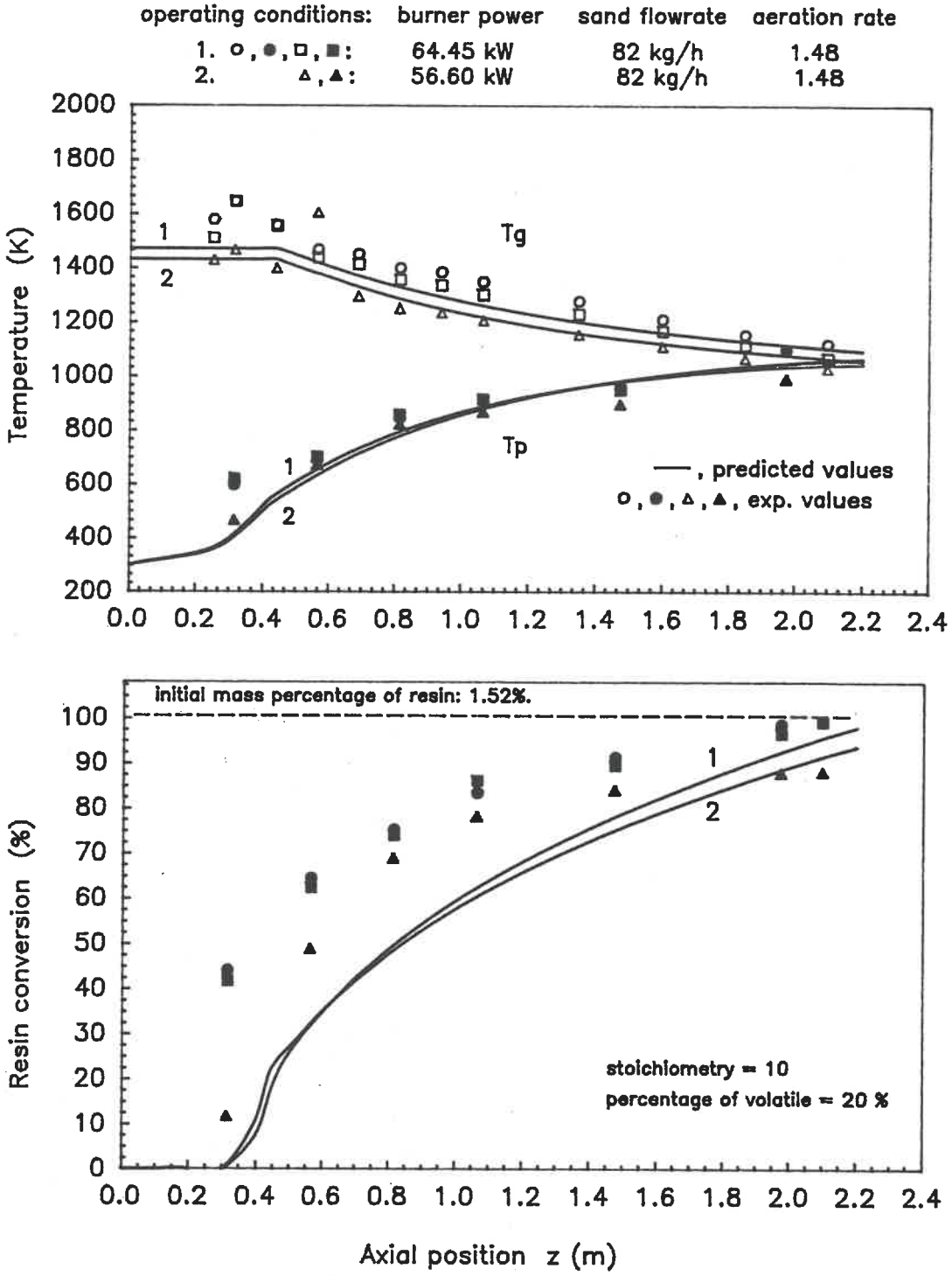

Figure (6–20). Modeling of burner power effect for used sand

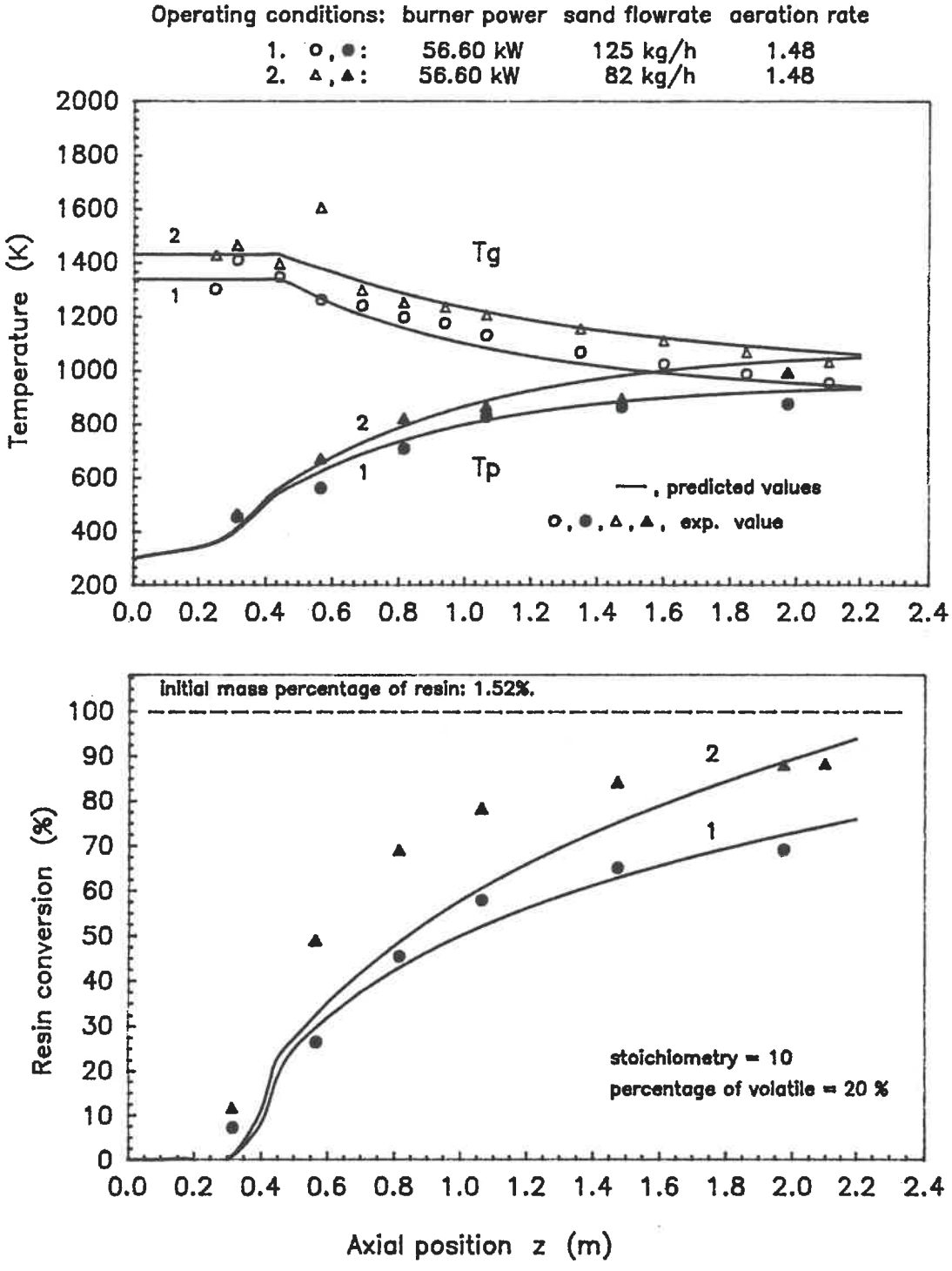

Figure (6-21) Modeling of sand flowrate effect for used sand

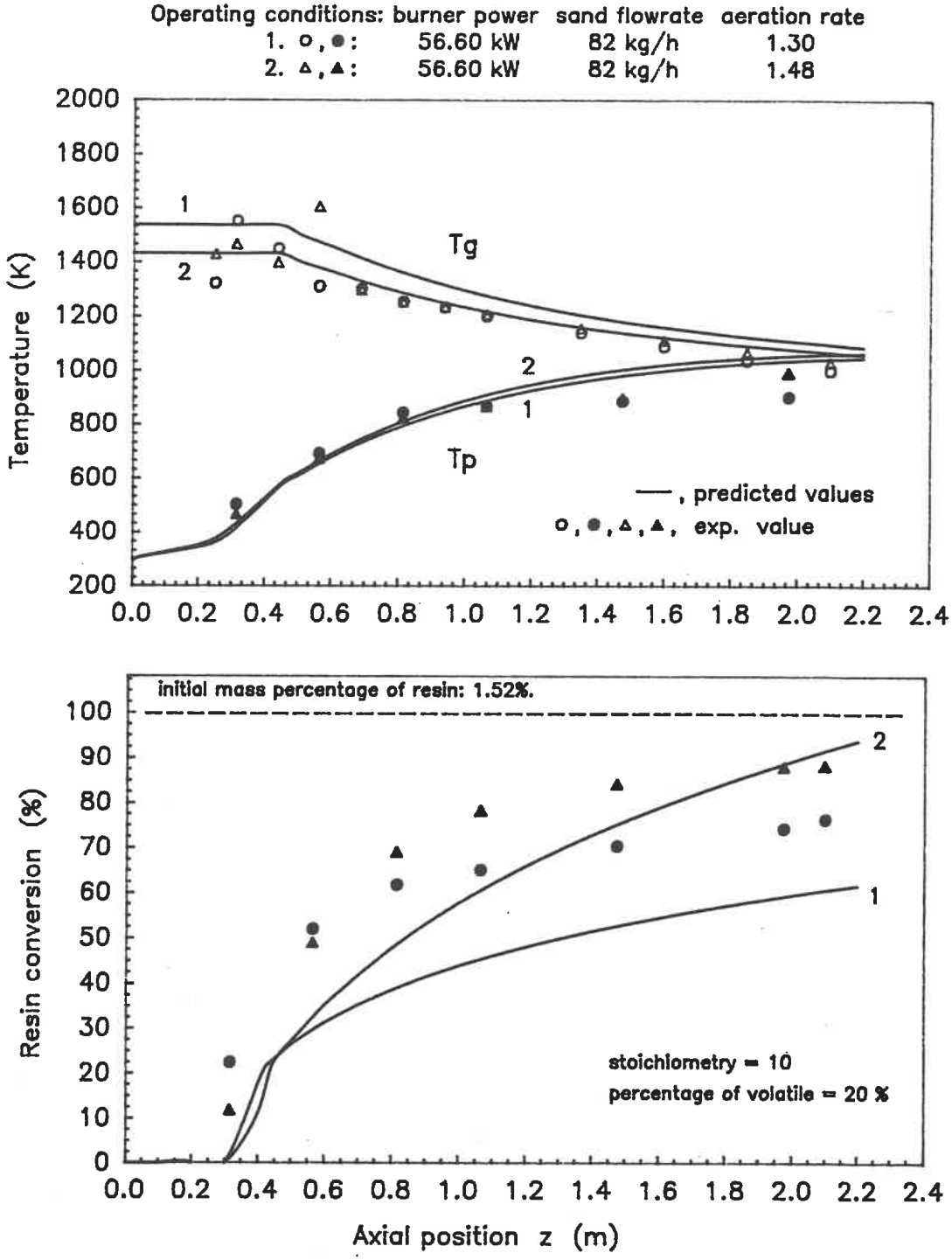

Figure (6-22) Modeling of aeration rate effect for used sand

CHAPTER 7. CONCLUSIONS

The objective of this project is to apply the Gas-Contact Process to foundry sand reclamation. The study is concerned with a two phases (gas and solid) flow, direct contact heat transfer between the gas and the perticle and resin combustion process. A developed model is given for design purposes.

This research is conducted in two stages. Through the theoretical approach, the possible models are advanced under the resonable assumptions. Then comparing with the experimental data, optimum assumptions are chosen. An optimum model is then obtained.

For flow regime and heat transfer:

1. The flow regime in the GCP is dilute fluidized solid flow. The sand particle flow is fully developed.
2. The gas phase is in a well-stirred region at the beginning of the process. The length of this region is 5 times the burner diameter.
3. Taking the assumption of plug-flow in solid phase and well-stirred flow plus plug-flow in gas phase, the model predicts axial temperature profiles of both phases in the furnace that are in good agreement with the experimental results.
4. The heat transfer in the GCP includes force convection and rediation. The sand temperature can be raised more than 650°C

from room temperature in seconds.

For resin combustion process:

1. Resin combustion in cludes resin decomposition and the burning process of the decomposed products. The volatile and char are are considered as two products of resin decomposition in the model.
2. Resin combustion rate is not only limited by the heat transfer, it is also a function of the particle temperature, concentration of oxygen and diffusion rate of volatiles and oxygen.
3. The predicted values of resin conversion are in satisfactory agreement with the experimental data.

For foundry sand reclamation:

1. The GCP shows a very good performance for foundry sand reclamation. The sand temperature can be raised more than 650°C; most of the resin is destroyed as conversion rates of up to 99.3% are obtained.
2. The specify comsumption of natural gas in the experiments is about 0.7 kWh/kg (used sand). This value can be much improved by integrating recovery units especially on the exhaust gas and exit treated sand.
3. The model can be used for the calculation of the size of a GCP unit used to foundry sand reclamation. When the sand flowrate is determined, from the specify comsumption of natural gas

(0.7 kWh/kg), the burner power can be determined. Then taking the value of the optimum aeration rate (1.48), the flowrate of the flue gas can be calculated. Taking a gas velocity equal to 2.5 m/s, as in our study, the inside diameter of the furnace is determined. Feeding the initial values which are shown in the Table (I-1) to the model, the length of the furnace will be obtained under the condition that the resin conversion is more than 99.99%.

Recommendations for further work:

1. Detailed reseach for resin decomposition products needs to be done. This work includes getting the composition and the concentration of the products as well as the stoichiometry and the various heats of change of phase and reaction.
2. More types of foundry sand need to be tested to compare with the predictions of the model.
3. Experiments on a large scale unit need to be undertaken to assess the validity of the model for scale-up and design.

REFERENCES

ABRAMRON B.M., RIVKIND YA V. and FISHBEIN G.A., *J. Eng. Phys. (USSR)*, **30**, 1-73 (1976).

ABRAMRON B. M. and BORDE I., "Particle-fluid heat transfer in two-phase flow", **vol 4**, 1921-1928 (1979).

AYYASWAMY P.S., "Combustion dynamics of moving droplets", Encyclopedia of Envi. Control Tech., **vol 1, 20**, 479-533 (1989).

BENALI M., "Analyse hydrodynamique du ruissellement des particules grosses et denses à contre courant d'une suspension fines particules, à travers une colonne garnie", Ph.D. thesis Université de Technologie de Compiègne, France, (1989).

BENALI M., GUY C. and CHAOUKI J., " Thermal treatment of divided solid wastes by the Gas-contact process", *Chem.Eng. Process.*, submitted for publication, (1991a).

BENALI M., SHAKOURZADEH-BOLOURI K. and LARGE J. F., "Flow of a suspension of fine particles around a steel ball fixed in a cylindrical pipe", *Powder Technol.*, 66, 285-292 (1991b).

BIRD R.B., STEWART W.E. and LIGHTFOOT E.N., "Transport phenoment" *John Wiley and sons,* N.Y. (1960).

BOOTHROYD P.G. "Flowing of Gas Solid Suspensions", *Chapman and Hall Ltd.*, London (1971).

CHEREMISINOFF P.N., "Hydrodynamics of gas-solid fluidization", *Gulf Pub. Corp.,* **11**, 471-535, Texas (1984).

CLIFT R. and GAUVIN W.H., "The motion of particles in turbulent gas flow", *Chemeca*, **14**, (1970).

CLIFT R., GRACE J.R. and WEBER M.E., "Bubbles, drops and particles", *Academic Press Inc.,* N.Y. (1978).

CLIFT R. and FARROKHALACE T., "Fluidization", *Plenum Press.*, N.Y. (1980).

EDWARDS D.K., "Molecular gas band radiation", *Advances in Heat Transfer*, *Academic Press*, N. Y., **vol 12**, 115-193 (1976).

EDWARDS D.K. and MATAVOSION R., "Scaling rules for total absorptivity and emissivity of gases", *J. Heat Transfer*, **106**, 684 (1984).

FAETH G.M. and LAZAR R.S., "Evaporation and combustion of a fuel droplet", *A.I.A.A.J.* **9**, 2165 (1971).

FENIMORE C.P. and MARTIN F.J., "Burning of polymers", "The Mechanisms of Pyrolysis, Oxidation, and Burning of Organic Materials", Wall L.A. Ed., 159-191 (1972).

FERNANDEZ-PELLO A.C., "Convective droplet combustion", 1986 Fall Technical Meeting, East Section of the Combustion Institute, San Juan, Puerto Rico, D 1-D 14 (1986).

FLAMANT G., MENIGANLT T and SCHWANDER D., "Combined heat transfer in a semitransparent mutilayer packed bed", *J. Heat Transfer*, **110**, 463-467 (1988).

FRISCH V., TESCHAR R. and POTKE W., "Computation of radiant heat transfer in rectangular furnace chamber", *Gas Warme International*, **31**, 421 (1982).

GAURIER L., " Applications du procédé gaz-contact au traitement des déchets industriels", *Rev. Gen. Therm. Fr.*, **26**, (1987).

GAURIER L., "Some applications of the gas-contact process in the treatment of industrial waste", *French/Italian Days of Flames*, 15-17 March, Italy (1989).

GELDART D. and RHODES M.J., " From minimum fluidization to pneumatic transport - a critical review of the hydrodynamics", *Circulating Fluidized Bed Tech.*, (1986).

GRAY W.A., KILHAM J.K. and MIILLER R., "Heat transfer from flames", *Elek Science,* London (1976).

GROBER H., ERK S. and GRIGULL U., "Fundamentals of heat transfer", *McGraw-Hill,* N.Y. (1960).

HAM R.K., BOYLE W.C. and FERO R.L.,"Evaluation of organic compounds in ground water of ferrous foundry wastes landfills", *AFS Transactions*, **95**, 693-695 (1987).

HOTTEL H.C. and SAROTIM A.F., "Radiation transfer", *McGraw-Hill*, N. Y. (1967).

HOTTEL H.C., "First estimates of industrial furnace performance - the one-gas-zone model reexamined", Heat Transfer in Flames, *Scripta Book Corp.*, Washington DC, 5-28 (1974).

ISHII M. and KOCAMUSTAFAOGULLARI G., "Two-phase flow models and their limitations", *Argonne National Lab. Report,* U. of Wisconsin at Milwaukee, ANL-80-111 (1981).

KANE J.M., "Foundry air pollution: a status report", *Foundry M.T.*, **50**, 50-55 (1968).

KUNII D. and LEVENSPIEL O., "Fluidization Engineering", *John Wiley and Sons*, N.Y. (1969).

LEUNG L.S. and JONES P.J., "Gas-solid downflow in standpipes", *Mutil. Sci. and Tech. Series, Hemisphere Pub. Corp.*, London (1980).

LUDWIG C.B., MALKMUS W., Reardon J.G. and Thomson J.A.L., "Handbook of infrared radiation from combustion gases", *NASA SP-3080*, Washington DC (1973).

MATSUMOTO S. and PEI C.T.D., "A mathematical analysis of pneumatic drying of grains - I. Constant drying rate", *Int. J. Heat Mass Transfer.*, **6**, 843-849 (1984).

PERRY's "Chemical Engineers Handbook", 6th ed., McGraw Hill (1984).

RANZ W.E. and MARSHALL W.R., "Evaporation from drop, Part II", *Chem. Eng. Prog.*, **48**, 173-180 (1952).

REISS H., "Radiative transfer in nontransparent dispersed media", *Springer-Verlag*, Brelin (1988).

SIEGEL R. and HOWELL J.R., "Thermal radiation heat transfer", Second Ed., *McGraw-Hill*, N. Y. (1981).

SMOOT D.L. and SMITH P.J., "Coal Combustion and Gasification", *Plenum Press*, N. Y. (1985).

SOO S.L., "Fluid dynamics of multiphase systems", *Blaidshell Pub Corp.*, Mass. (1967).

SPALDING D.B., "Combustion and mass transfer", *Pergamon Press*, N. Y. (1979).

STAUB F.W., 'Steady-state and transient gas-solid flow characteristics in vertical transport lines", *Powder Tech.*, **26**, 147-159 (1980).

TAYLOR P.B. and FOSTER P.J., "The total emissivities of luminuous and no-luminuous flames", *Int. J. Heat Mass Transfer*, **17**, 1591-1605 (1974).

TIEN C.L. "Thermal radiation properties of gases", Advances in Heat Transfer, *Academic Press*, N. Y., **5**, 258-324 (1978).

TIEN C.L., "Thermal radiation in packed and fluidized beds", *J. Heat Transfer*, **110**, 1230-1242 (1988).

TIEN C.L. and DROLEN B.L., "Thermal radiation in particulate media with dependent and independent scattering", in Annual review of numerical fluid mechanics and heat transfer, Chawla T.C. Ed., *Hemisphere*, Washington DC, **vol 1**, 1-34 (1987).

TSUJI Y., MORIKAWA Y. and SHIOMO H., "LDV measurements of an air-solid two-phase flow in a vertical pipe", *J. Fluid Mech.*, (1986).

VISKANTA R. and MENGEUC M.P., "Radiation heat transfer in combustion systems", *Prog. Energy and Combust. Science*, **13**, 97 (1987).

VISKANTA R. and MENGUC M.P., "Modeling of radiative heat transfer", in Encyclopedia of Environmental Control Technology, **vol 1**, Cheremisnoff P.N. Ed., 599-646 (1989).

VORTMEYER D., "Radiation in packed solids", *Heat Transfer, Hemisphere*, Washington DC, **vol 4**, 525-539 (1978).

VORTMEYER D., "Warmestrahlung in dispersen feststollsystemen", *Chem. Ing. Tech.*, **51**, 839-851 (1979).

WILLIAMS A., "Combustion of droplets of liquid fuels: A review", *Combust. and Flame*, **21**, 1-31 (1973).

APPENDIX I. COMPUTER CODE OF THE MODELS

I.1 INITIAL PARAMATERS OF THE MODELING PROGRAM

Table (I-1) Initial parameters of the modeling program

Name	Symbol	Value
Internal diameter of furnace	D_f	0.2 m
Outside diameter of furnace	D_{f-out}	0.36 m
Length of furnace	L_f	2.2 m
Temperature of resin decomposition	T_d	180 °C
Resin decomposition latent heat	H_p	6.75×10^5 J/kg
Heat of combustion of resin	H_c	3.6×10^7 J/kg
Net heat value of natural gas	PCI	34.75×10^6 J/m^3
Calorific capacity of sand	C_p	1840 J/kg.K
Density of resin	ρ_r	1130 kg/m^3
Calorific capacity of volatile	C_{pvol}	2521 J/kg.K
Density of clean sand	ρ_s	2597 kg/m^3
Density of used sand	ρ_{s+r}	2651 kg/m^3
Partial pressure of CO_2	P_{CO2}	0.1 atm

I.2 COMPUTER CODE OF WELL-STIRRED MODEL IN THE GAS PHASE AND PLUG-FLOW MODEL IN THE SOLID PHASE

```
Program Gas_Contact_Model;
{Well_stirred in Gas and Plug_flow in Particles}
uses crt,dos;
Const
Pi        = 3.1415;
sigma     = 5.67e-8;
g         = 9.81;
R         = 8.3143; {J/mol K}

Var
Reynolds1: real;    Vt         : real;      mg         : real;
ms       : real;    ms_init    : real;      Dp         : real;
Dps      : real;    Dp_init    : real;      Mp         : real;
dt       : real;    t          : real;      Tao_s      : real;
Ar       : real;    Ap         : real;      Tao_g      : real;
At       : real;    Df         : real;      Cps        : real;
Ts       : real;    Tg         : real;      Emis_G     : real;
Emis_S   : real;    Emis_r     : real;      Abso_G     : real;
q_convec : real;    q_rad      : real;      Reynolds   : real;
Rho_s    : real;    Cvap       : real;      Lambda_r   : real;
Rho_r    : real;    Hsub       : real;      Hcomb      : real;
Vg       : real;    Vp         : real;      visco      : real;
dens     : real;    Prandtl    : real;      Cp_gas     : real;
Lambda_gas: real;   Coef_h     : real;      DataFile   : text;
Name_of_file : string;                      i          : integer;
mode_of_out : integer;                      dz_out     : real;
fract_resin:real;   calc_rate  : integer;   Ut         : real;
Lf       : real;    aa         : real;      bb         : real;
Hsub1    : real;    Hcomb1     : real;      cc         : real;
Wg       : real;    Ca         : real;      G1         : real;
G2       : real;    As         : real;      Ag         : real;
ss       : real;    Rho_ox     : real;      Ae         : real;
X_ox     : real;    X_vap      : real;      D_ox       : real;
Go       : real;    Dp1        : real;      dz         : real;
z        : real;    m_gas      : real;      Aeration   : real;
Pco2     : real;    Ts_in      : real;      B2         : real;
Lm       : real;    X_ox1      : real;      D_vap      : real;
X_vapo   : real;    Cpvap      : real;      ab         : real;
Rho_vap  : real;    Rho_ox1    : real;      Resin      : real;
number   : real;    Tg_in      : real;      Tg_out     : real;
dalta_g  : real;    dalta_s    : real;      Tg1        : real;
Ts1      : real;    A1         : real;      B1         : real;
C1       : real;    D1         : real;      D2         : real;
```

```
D3       : real;    D4       : real;       Q        : real;
Q1       : real;    X_oxo    : real;       dalta    : real;
Tg_in1   : real;    Cp_gas1  : real;       Q3       : real;
Q2       : real;    Cp_air1  : real;       P_vap    : real;
Sc       : real;    Reynoldg : real;       Sh       : real;
Kc       : real;    X_vapoo  : real;       K        : real;
X_oxf    : real;    K1       : real;       K2       : real;


Function Cpg ( x : real )   : real;
 Begin
   Cpg := 880.21+0.23*X;    {J/(kg K)}
 end;

Function Cpa ( x : real )    : real;    {air}
 Begin
   Cpa := 949.98+0.182*X;     {J/(kg K)}
 end;

Function Rho_g ( x : real )   : real;
 Begin
   Rho_g := 2.4073-5.276e-3*X+4.5539e-6*X*X-1.342e-9*X*X*X*X; {kg/m3}
 end;

Function Mu ( x : real )  : real;   { viscosite du gaz }
 Begin
   Mu := 4.68e-5*exp(0.65*ln(x/1173));  {kg s/m2}
 end;

Function Lambda ( T : real ) : real;
 Begin
   Lambda := (-8.138e-2+7.3161e-3*T)/100;  {J/(s m K)}
 end;

Function h ( T , Vt , Dp_init : real ) : real;
 Begin

   h:=(Lambda_gas/dp)*(2.0+0.6*exp(0.5*ln(Reynolds))

      *exp(0.333*ln(Prandtl)));

 end;
```

```
Procedure initial_data;

Begin
 dz     := 0.01;
 Df     := 0.2;
 Emis_S:= 0.80;

 Emis_r:= 0.47;

 Rho_s := 2651;          { kg/m3 }
 Cps    := 1740;         { J/kg K}
 i      := 0;
 Hsub   := 675000;       { J/kg }
 Hcomb := 36000000;      { J/kg }
 Rho_r := 1130;          { kg/m3 }
 ss     := 10;
 Rho_ox:= 1.42846;       { kg/m3 at 0 C }
 Cpvap := 2521;          { J/kg K }
 Pco2   := 0.1;          { bar }
 Go     := 0;
 dalta_g:= 100;
 Ts      := Ts_in;
 Tg      := 1438;
 Tg_in   := 1600;
 dalta   := 10;
end;


Procedure Set_file;
begin
Writeln (' interval for writting file ');
Readln  ( dz_out);
Writeln (' Name of the file ');
Readln  ( Name_of_file );
Assign  (datafile, name_of_file );
Rewrite ( datafile );
end;



Procedure Write_in_file;
begin
  if z >= i*dz_out then
  begin
    Writeln (datafile, z:10, Ts:10, Tg:10, Dp:20, X_ox:20,

             Resin:20, Dps:10);

    i := i+1;
  end;
end;
```

```
Procedure proprietes;

Begin
  aa := (fract_resin-1)*Rho_r*Dp_init*Dp_init*Dp_init
        /(fract_resin*(Rho_r-Rho_s)-Rho_r);
  Dps   := exp(1/3*ln(aa));
  Mp    := 1/6*pi*((Dp_init*Dp_init*Dp_init-Dps*Dps*Dps)
           *Rho_r+Dps*Dps*Dps*Rho_s);
  if fract_resin < 10e-8 then
  begin
  Mp    := 1/6*pi*Dp_init*Dp_init*Dp_init*Rho_s;
  end;
  number:= ms_init/Mp; {Number/s}
  ms    := ms_init;    {kg/s}
  mg    := m_gas*(10.65+9.6*(aeration-1))*1.295;  {kg/s}

   while dalta > 1 do
   begin
     Cp_gas1 := Cpg(Tg_in);
     Cp_air1 := Cpa(Tg_in);
     Tg_in1  := (34750000+9.6*aeration*1.293*1005*300
                +1*0.75*1044*300)/(Cp_gas1*10.65*1.295+9.6
                *(aeration-1)*Cp_air1*1.293);
     dalta   := Tg_in-Tg_in1;
     if dalta > 0 then
     begin
       Tg_in := Tg_in-1;
     end;
     if dalta < 0 then
     begin
       Tg_in := Tg_in+1;
     end;
     dalta := abs(dalta);
   end;

   Tg_in := Tg_in1;

  X_oxo := 9.6*(Aeration-1)*0.21*Rho_ox/(10.65+9.6
           *(Aeration-1))/1.295;  { by mass }
  Resin := fract_resin;
  X_ox  := X_oxo;
end;
```

```
Procedure calculation ;

Begin
  While  dalta_g > 1 do
  Begin
    i        := 0;
    Q        := 0;
    Q3       := 0;
    Ts       := Ts_in;
    z        := 0;
    Resin    := fract_resin;
    X_ox     := X_oxo;
    Dp       := Dp_init;
    Wg       := (10.65+9.6*(aeration-1))*m_gas*Tg/273;   {m3/s}
    D_ox     := 3.23e-10*exp(1.75*ln(Tg));
    D_vap    := 7.69e-10*exp(1.75*ln(Tg));
    Rho_vap  := 0.82*500/Tg;
    Rho_ox1  := 0.78*500/Tg;
    Visco       := Mu ( Tg );
    Dens        := Rho_g ( Tg );
    Cp_gas      := Cpg ( Tg );
    Lambda_gas  := Lambda ( Tg );

    While z < Lf do
    begin
    Lm   := pi*Df*dz/(2*dz+pi*Df);
    Ut   := dp*exp(0.333*ln(4*(Rho_s-Dens)
           *(Rho_s-Dens)*g*g/225/Dens/Visco));
    Emis_G := (0.266+7.19e-5*Tg)*(1-exp(-6*0.69*Pco2*Lm))
              +(0.252-7.41e-5*Tg)*(1-exp(-6*7.4*Pco2*Lm))
              +(0.118-4.52e-5*Tg)*(1-exp(-6*80*Pco2*Lm));
    Abso_G      := Emis_G;
    Reynolds    := Dens*Dp*Ut/Visco;

    if z < 0.265 then
    begin
      Ae := 0.25*pi*0.08*0.08;
    end;
    if z > 0.265 then
    begin
      Ae   := 0.25*pi*Df*Df;
    end;

    Vg          := Wg/Ae;
    Prandtl     := Cp_gas * Visco / Lambda_gas;
    Coef_h      := h(Tg,Ut,Dp);
    Tao_s       := dz/Vg;
```

```
Tao_g       := 0.265/(Wg/0.25/pi/0.08/0.08)
               +(Lf-0.265)/(Wg/0.25/pi/Df/Df);

if z < 0.265 then
begin
  Ar        := pi*0.08*dz;
end;
if z > 0.265 then
begin
  Ar        := pi*Df*dz;
end;
Ap          := 0.25*pi*Dp*Dp*number*Tao_s;
At          := Ar+Ap;
Ca          := Ap/At;
G2          := 1/ca/emis_s+1/emis_G-1/abso_g+((1/abso_g)-1)
               /(ca*emis_s+(1-ca)*emis_r);
G1          := At/G2;

A1     := G1*sigma;
B1     := ms*Cps;
B2     := mg*Cp_gas;
C1     := Coef_h*pi*Dp*Dp*number*Tao_s;

P_vap := -Hsub*42.8/1000/R/Ts;
P_vap := exp(P_vap)*101330;
X_vapo:= P_vap/R/Ts*42.8/1000;
X_vapo:= X_vapo/(Dens+X_vapo);

Hsub1 := 0;
Hcomb1:= 0;
Go    := 0;

if resin > 10e-8 then
begin
if X_ox > 0 then
begin
if Ts > 453 then
begin
If Dp > Dps then
Begin
 Go := 2*Rho_vap*D_vap*ln(1+(X_vapo+X_ox/ss)/(1-X_vapo))*pi*Dp;

if (fract_resin-resin)/fract_resin*100 > 20 then
begin
  Go := 2*Rho_ox1*D_ox*ln(1+X_ox/ss)*pi*Dp;
end;
```

```
Dp1 := exp(1/3*ln(6/pi*(1/6*pi*Dp*Dp*Dp-Go*Tao_s/Rho_r)));
     if Dp1 < Dps then
     begin

      Go    := 1/6*pi*(Dp*Dp*Dp-Dps*Dps*Dps)*Rho_r/Tao_s;
     end;
     Dp     := Dp1;
     if Dp1 < Dps then
     begin
       Dp   := Dps;
     end;
     X_ox1  := (mg*X_ox-Go*ss*number*Tao_s)
                /(mg-Go*ss*number*Tao_s);
     X_ox   := X_ox1;
     Resin  := 1/6*pi*(Dp*Dp*Dp-Dps*Dps*Dps)*Rho_r;
     Resin  := Resin/(1/6*pi*Dps*Dps*Dps*Rho_s+Resin);

     Hsub1  := Go*Hsub*number*Tao_s;
     Hcomb1 := Go*Hcomb*number*Tao_s;
    end;
    end;
    end;
    end;

     Ts1 := (A1*(Tg*Tg*Tg*Tg-Ts*Ts*Ts*Ts)+C1*(Tg-Ts))/B1
            -Hsub1/B1+Ts;

     if resin > 10e-8 then
     begin
     if (fract_resin-resin)/fract_resin*100 > 20 then
     Begin
       Ts1 := (A1*(Tg*Tg*Tg*Tg-Ts*Ts*Ts*Ts)+C1*(Tg-Ts))
              *dz/B1-Hsub1/B1+Hcomb1/B1+Ts;

     end;
     end;

       Q1 := Tao_g*B1*(Ts1-Ts)+Hsub1*Tao_g;
       Q  := Q+Q1;
       Q2 := Hcomb1*Tao_g;
       Q3 := Q3+Q2;
       Ts := Ts1;
       z  := z+dz;

     GotoXY (1,19);
     WriteLn('    z       Ts        Dp         X_ox
              Resin       Tg_in      X_oxf');
```

```
          GotoXY (1,20);
          Writeln(z:10,'  ',Ts:10,'  ',Dp:10,'  ',X_ox:10,'  ',
                  Resin:10,'  ',Tg_in:10,
                 '',X_oxf:10,'',K:10,'',K2:10);

          if mode_of_out=2 then Write_in_file;
       end;

          Tg1 := Tg_in-Q/B2/Tao_g+Q3/B2/Tao_g;

          dalta_g := Tg-Tg1;

          if dalta_g > 0 then
          begin
            Tg := Tg-0.5;
          end;

          if dalta_g < 0 then
          begin
            Tg := Tg+0.5;
          end;

          dalta_g := abs(dalta_g);

          GotoXY (1,21);
          Writeln('    Tg          Tg1          dalta_g        X_ox
                   Go       K2 ' );
          GotoXY (1,22);
          Writeln(Tg:10,'  ',Tg1:10,' ',dalta_g:10,'
                  ',X_ox:10,'',Go:10,'',K2:10);
      end;
end;


Procedure Write_on_screen;

Begin
GotoXY (1,17);
Writeln (  '  z      T solide      T gas        Dp
            Resin          Dps      X_ox' );
GotoXY (1,18);
Writeln (z:10,'  ',Ts:10,'  ',Tg:10,' ',Dp:10,' ',Resin:10,'  ',
         Dps:15,'  ',X_ox:15,'',X_vapo:10,'',bb:10,
         '',cc:20,'',D_vap:20);
end;
```

```
Procedure Operating_condition;
Begin
  Clrscr;
  GotoXY  ( 1 , 1 );
  Writeln (' burner power (kW) ');
  Readln  ( m_gas );
  m_gas:= m_gas/34.75/1000;  {nm3/s}
  Writeln (' Particle flowrate (kg/h)');
  Readln  ( ms_init );
  ms_init := ms_init/3600; {kg/s}
  Writeln (' Aeration rate ');
  Readln  ( Aeration );
  Writeln (' Initial particles temperature (K)');
  Readln  ( Ts_in );
  Writeln (' diametre de particule  (mm) ');
  Readln  ( dp ); dp := dp / 1000;
  Writeln (' initial diameter of particule (mm)');
  Readln  ( Dp_init ); Dp_init := Dp_init / 1000;
  Writeln ( ' Mass percentage of the resin (%) (For clean sand put
              value=10e-9) ' );
  Readln  ( fract_resin ); fract_resin := fract_resin / 100;
  Writeln ( ' Length of region ( m ) ' );
  Readln  ( Lf );
  Writeln ( ' Write on screen ( 1 ) or write in file ( 2 ) ' );
  Readln  ( mode_of_out );
  if mode_of_out = 2  then set_file;
end;



BEGIN
operating_condition;
Initial_data;
Proprietes;

Write_on_screen;
calculation;
Write_on_screen;
if mode_of_out=2 then Write_in_file;
if mode_of_out=2 then close(datafile);
end.
```

I.3 COMPUTER CODE OF PLUG-FLOW MODEL

```
Program Gas_Contact_Model;
{plug_flow in the both phases}


uses crt, Printer;

Const

Pi          = 3.1415;
sigma       = 5.67e-8;
g           = 9.81;
R           = 8.31;

Var
Reynolds1       : real;  Pco2          : real;  Ut            : real;
mg              : real;  ms            : real;  ms_init       : real;
Dp              : real;  Dp1           : real;  Dps           : real;
Dp_init         : real;  Mp            : real;  dz            : real;
z               : real;  z_max         : real;  As            : real;
Df              : real;  Df1           : real;  Cps           : real;
Ts              : real;  Tg            : real;  Abso_g        : real;
Emis_G          : real;  Emis_S        : real;  Emis_r        : real;
q_convec        : real;  q_rad         : real;  Reynolds      : real;
Vp              : real;  Rho_s         : real;  Lambda_r      : real;
Rho_r           : real;  Hsub          : real;  Hcomb         : real;
V_gas           : real;  visco         : real;  dens          : real;
Prandtl         : real;  Cp_gas        : real;  Lambda_gas    : real;
Coef_h          : real;  DataFile      : text;  Name_of_file  : string;
i           : integer;   out_mode  :integer;  dz_out         : real;
Cte             : real;  calc_rapid:integer;  aa             : real;
bb              : real;  cc            : real;  Hvap1         : real;
Hcomb1          : real;  Hloss         : real;  fract_resin   : real;
Rho_vap         : real;  Aera          : real;  Wg            : real;
Tw              : real;  Tamb          : real;  Lambda_w      : real;
Taog            : real;  Taop          : real;  At            : real;
Ap              : real;  Ca            : real;  G1            : real;
G2              : real;  Re1           : real;  Gr            : real;
h_out           : real;  h_in          : real;  Qw            : real;
Ag              : real;  X_ox          : real;  X_vapo        : real;
ss              : real;  D_vap         : real;  Go            : real;
m_gas           : real;  Aeration      : real;  T_out         : real;
Resin           : real;  D_ox          : real;  Rho_ox        : real;
Cpvap           : real;  Rho_ox1       : real;  Lm            : real;
X_ox1           : real;  fract_resin1: real;  Number          : real;
Tm              : real;  Dens_air      : real;  visco_air     : real;
Lambda_air      : real;  GrPr          : real;  Rep           : real;
```

```
Reynolds_g     : real;  P_vap       : real;  Sc            : real;

Reynoldg       : real;  Sh          : real;  Kc            : real;
X_vapoo        : real;  K           : real;  K1            : real;
K2             : real;  X_oxf       : real;

Function CPg ( x : real )   : real;
Begin
  Cpg  := 880.21+0.23*x;
end;

Function Rho_g ( x : real )   : real;
Begin
  Rho_g := 2.407-5.276e-3*X+4.554e-6*X*X-1.342e-9*X*X*X;
end;

Function Mu ( x : real )  : real;
Begin
  Mu := 4.68e-5 * exp ( 0.65 * ln ( x / 1173 ) ) ;
end;

Function Lambda ( T : real ) : real;
Begin
  Lambda := (-8.138e-2+7.3161e-3*T)/100;
end;

Function h ( T , Vt , Dp_init : real ) : real;
Begin
  h:=(Lambda_gas/Dp)*(2.0+0.6*exp(0.5*ln(Reynolds))
      *exp(0.333*ln(Prandtl)));
end;


Procedure Initiation;

Begin
z      := 0.44;
Df     := 0.2;
Emis_S := 0.80;
Emis_r := 0.47;
Rho_s  := 2651;
Cps    := 1740;
Hsub   := 6.75e5;
Hcomb  := 3.6e7;
i      := 0;
dz     := 0.01;
Df1    := 0.36;
```

```
Tamb   := 300;
Rho_r  := 1130;
Lambda_w:=18.6;
ss     := 10;
Rho_ox := 1.42846;
T_out  := 473;  {K}
Pco2   := 0.1;   {bar}
Cpvap  := 2521;  {J/kg K}
Go     := 0;
end;


Procedure Properties;
Begin
  aa:= (fract_resin1-1)*Rho_r*Dp_init*Dp_init*Dp_init
       /(fract_resin1*(Rho_r-Rho_s)-Rho_r);
  Dps:=exp(1/3*ln(aa));
  Mp:=1/6*pi*((Dp_init*Dp_init*Dp_init-Dps*Dps*Dps)
      *Rho_r+Dps*Dps*Dps*Rho_s);
  if fract_resin < 10e-8 then
  begin
  Mp:=1/6*pi*Dp_init*Dp_init*Dp_init*Rho_s;
  end;
  Number:=ms_init/Mp;  {number of particles /s}
  ms:=ms_init; {kg/s}.
  Resin := fract_resin;
  mg:=m_gas*(10.65+9.6*(aeration-1))*1.295; {kg/s}
end;


Procedure Physical_properties;

Begin
  D_ox      := 3.23e-10*exp(1.75*ln(Tg));
  D_vap     := 7.69e-10*exp(1.75*ln(Tg));
  Rho_vap   := 0.82*500/Ts;
  Rho_ox1   := 0.78*500/Ts;
  if z < 0.265 then
  begin
  Df := 0.08;
  end;
  if z > 0.265 then
  begin
  df := 0.2;
  end;
```

```
Aera       := 0.25*pi*Df*Df;

Wg         := (10.65+9.6*(aeration-1))*m_gas*Tg/273;

Visco       := Mu ( Tg );
Dens        := Rho_g ( Tg );
Cp_gas      := Cpg ( Tg );
Lambda_gas  := Lambda ( Tg );
Lm          := pi*Df*dz/(2*dz+pi*Df);
Emis_G      := (0.266+7.19e-5*Tg)*(1-exp(-6*0.69*Pco2*Lm))
                +(0.252-7.41e-5*Tg)*(1-exp(-6*7.4*Pco2*Lm))
                +(0.118-4.52e-5*Tg)*(1-exp(-6*80*Pco2*Lm));
Abso_G      := Emis_G;

P_vap := -Hsub*42.8/1000/R/Ts;
P_vap := exp(P_vap)*101330;
X_vapo:= P_vap/R/Tg*42.8/1000;
X_vapo:= X_vapo/(Dens+X_vapo);

Ut := dp*exp(0.333*ln(4*(Rho_s-Dens)
      *(Rho_s-Dens)*g*g/225/Dens/Visco));


Rep := Dp*Dens*Ut/Visco;

If Rep < 0.4 then
begin
Ut    := exp(0.5*ln(3.1*g*(Rho_s-Dens)*dp/Dens));
end;

Reynolds    := Dens*dp*Ut/Visco;
V_gas       := Wg/Aera;
Vp          := Ut+V_gas;
Reynolds_g  := Dens*Df*V_gas/Visco;
Prandtl     := Cp_gas * Visco / Lambda_gas;
Coef_h      := h ( Tg, Ut, Dp );
Taog        := dz/V_gas;
Taop        := dz/Vp;
At          := 0.25*pi*Dp*Dp*number/Vp+pi*Df;
Ap          := 0.25*pi*Dp*Dp*number/Vp;
Ca          := Ap/At;
G2 :=1/Ca/emis_s+1/emis_g-1/abso_g+((1/abso_g)-1)
     /(ca*emis_s+(1-ca)*emis_r);
G1 :=At/G2;

{ Heat loss from the wall }
h_in  := 0.026*exp(0.8*ln(Reynolds_g))
         *exp(0.4*ln(0.59))*Lambda_gas/Df;
```

```
  Tm          := (T_out+Tamb)/2;
  Dens_air    := 0.972*363/Tm;
  Visco_air   := 2.15e-5*Tm/363;
  Lambda_air  := 3.126e-2*Tm/363;
  Gr          := Dens_air*Dens_air*g*dz*dz*dz/visco_air
                 /visco_air/Tm*(T_out-Tamb);
  GrPr        := Gr*0.697;
  h_out       := 0.59*exp(0.25*ln(Gr*0.697))*Lambda_air/dz;
  Qw          := (Tg-Tamb)*pi*dz/(1/Df/h_in+ln(Df1/Df)/2
                  /Lambda_w+1/Df/h_out);
end;


Procedure Key;

Var

Tg1             : real;
Ts1             : real;

Begin

q_convec    := Coef_h*(Tg-Ts)*pi*dp*dp*number/Vp;
q_rad       := G1*sigma*(Tg*Tg*Tg*Tg-Ts*Ts*Ts*Ts);

As          := ms*Cps*Taop;
Ag          := mg*Cp_gas*Taog;

Hvap1       := 0;
Hcomb1      := 0;
Go          := 0;

if X_ox > 0 then
begin
if Ts > 453 then
begin
If Dp > Dps then
Begin

  Go := 2*Rho_vap*D_vap*ln(1+(X_vapo+X_ox/ss)/(1-X_vapo))*pi*Dp;

  if resin > 10e-8 then
  begin
  if (fract_resin-resin)/fract_resin*100 > 20 then
  begin
    Go := 2*Rho_ox1*D_ox*ln(1+X_ox/ss)*Pi*Dp;
  end;
  end;
```

```
  Dp1 := exp(1/3*ln(6/pi*(1/6*pi*Dp*Dp*Dp-Go*dz/V_gas/Rho_r)));
  if Dp1 < Dps then
  begin
    Go   := 1/6*pi*(Dp*Dp*Dp-Dps*Dps*Dps)*Rho_r*V_gas/dz;
  end;
  Hvap1 := Go*Hsub*number*Taop;
  Hcomb1      := Go*Hcomb*number*Taop;
  Dp          := Dp1;
  if Dp1 < Dps then
  begin
    Dp        := Dps;
  end;
  end;
  end;
  end;


Ts1 := Ts+(q_rad+q_convec)*dz*Taop/As-Hvap1*Taop/As;
Tg1 := Tg-(Ts1-Ts)*As/Ag-Qw*Taog/Ag-Hvap1*Taop/Ag+Hcomb1*Taop/Ag;

if resin > 10e-8 then
begin
if (fract_resin-resin)/fract_resin*100 > 20 then
Begin
Ts1 := Ts+(q_rad+q_convec)*dz*Taop/As-Hvap1*Taop/As+Hcomb1*Taop/As;
Tg1 := Tg-(Ts1-Ts)*As/Ag-Qw*Taog/Ag-Hvap1*Taop/Ag+Hcomb1*Taop/Ag;
end;
end;

Ts  := Ts1;
Tg  := Tg1;
X_ox1 := (mg*dz/V_gas*X_ox-Go*ss*number*dz/Vp*dz/Vp)
         /(mg*dz/V_gas-Go*ss*number*dz/Vp*dz/Vp);
X_ox  := X_ox1;
Resin := 1/6*pi*(Dp*Dp*Dp-Dps*Dps*Dps)*Rho_r;
Resin := Resin/(1/6*pi*Dps*Dps*Dps*Rho_s+resin);
end;


Procedure Write_results_on_screen;

Begin
GotoXY ( 1 , 18 );
Writeln (  '    z          T solide      T gas
           Dp          Dps      Resin    ' );
```

```
GotoXY ( 1 , 20 );
Writeln ( z:10,'    ',Ts:10,'    ',Tg:10,'    ',Dp:15,'   ', Dps:10,'
        ',Resin:10,'   ',X_ox:10,'   ',X_vapo:10,'    ',Go:10);
end;


Procedure Writefile;

Begin
Writeln ( ' interval for writing file ' );
Readln ( dz_out );
Writeln ( ' Name of the file ? ' );
Readln ( Name_of_file );
Assign ( datafile, Name_of_file );
Rewrite ( datafile );
end;



Procedure Information;
Begin
  Clrscr;
  GotoXY  ( 1 , 1 );
  Writeln (' Burner power (kW) ');
  Readln  ( m_gas ); m_gas:=m_gas/34.75/1000; {nm3/s}
  Writeln (' Particle flowrate  (kg/h) ');
  Readln  ( ms_init ); ms_init:= ms_init/3600; {kg/h}
  Writeln (' Aeration rate ');
  Readln  ( aeration );
  Writeln (' Particle diameter  (mm) ');
  Readln  ( Dp ); Dp := Dp / 1000;
  Writeln (' initial diameter of particule (mm)');
  Readln  ( Dp_init ); Dp_init := Dp_init / 1000;
  Writeln ( ' percentage of resin %' );
  Readln  ( fract_resin ); fract_resin := fract_resin / 100;
  Writeln ( 'initial percentage of resin %');
  Readln  ( fract_resin1 ); fract_resin1 := fract_resin1/100;
  Writeln ( ' concentration of oxygen ');
  Readln  ( X_ox );
  Writeln ( ' Initial gas temperature  ( K ) ');
  Readln  ( Tg );
  Writeln ( ' Initial particle temperature ( K )');
  Readln  ( Ts );
  Writeln ( ' distance Z_max ( m ) ' );
  Readln  ( Z_max );
  Writeln ( ' Write on screen ( 1 ) or on file ( 2 ) ' );
  Readln  ( out_mode );
  if out_mode = 2  then Writefile;
```

```
  Writeln ( ' calcul precis 1 or approximatif 2 ');
  Readln  ( calc_rapid );
end;


Procedure Write_results_on_file;


Begin
  if z >= i * dz_out  then
  Begin

  Writeln  ( Datafile, z:10, Ts:10, Tg:10, Dp:20,resin:20 );


  i := i + 1;
  end;
end;



Procedure Choose_dz;

Begin

  dz := 0.01;
  if z < 1      then  dz := 0.001;
  if calc_rapid = 2  then dz := 0.001;
end;



Begin    { principal programme }

Information;
Initiation;
Properties;

if out_mode = 2  then  Write_results_on_file;
Write_results_on_screen;


While z <= z_max  do
Begin
  Choose_dz;
  Physical_properties;
  Key;
  Z := Z + dz;
```

```
  Write_results_on_screen;
  if out_mode = 2  then Write_results_on_file;
end;

  if out_mode = 2  then close(datafile);


end.
```

APPENDIX II. CALIBRATION CURVES

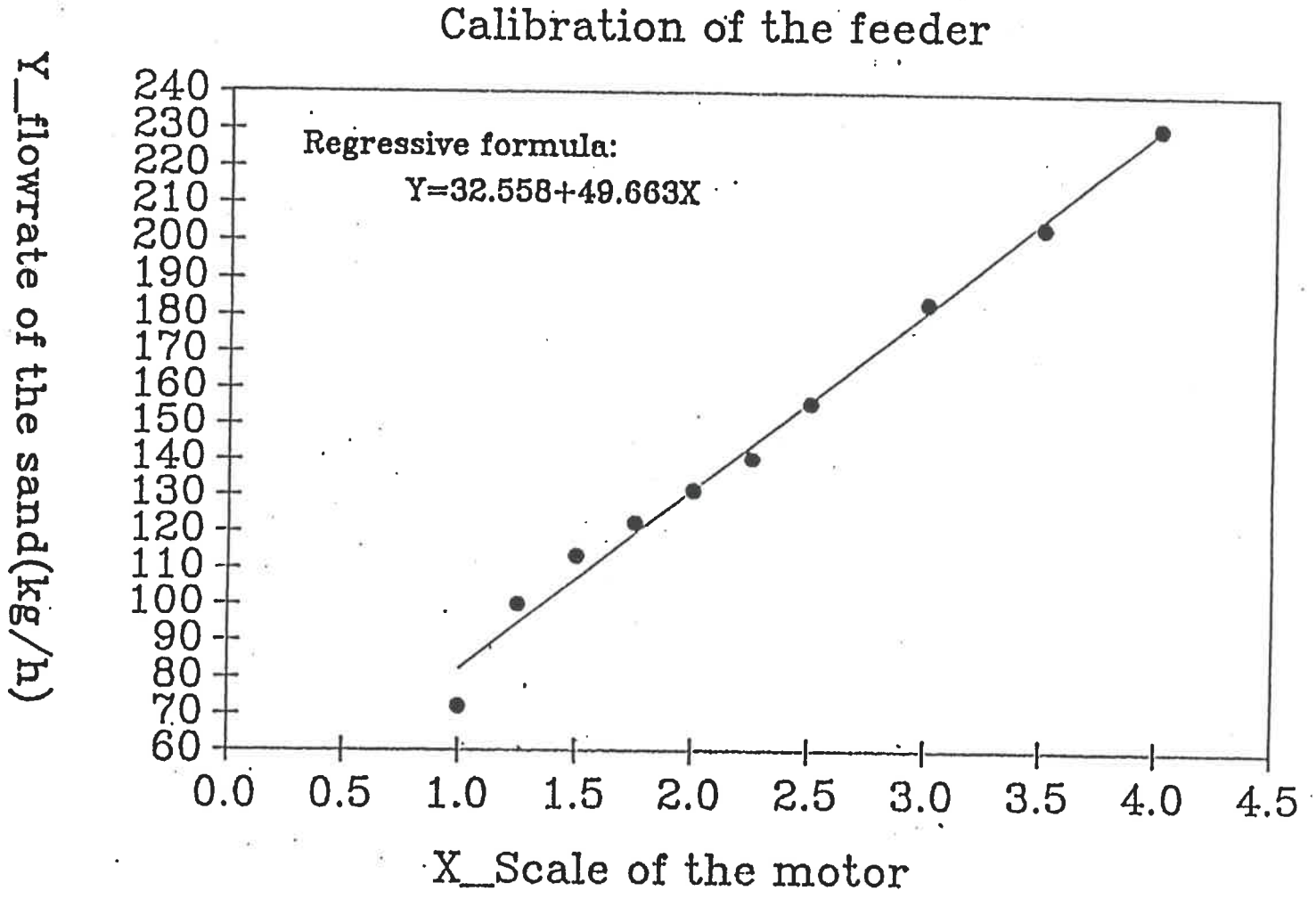
Calibration of the feeder
Regressive formula:
Y=32.558+49.663X
Y_flowrate of the sand(kg/h)
240
230
220
210
200
190
180
170
160
150
140
130
120
110
100
90
80
70
60
0.0
0.5
1.0
1.5
2.0
2.5
3.0
3.5
4.0
4.5
X_Scale of the motor

Calibration of orifice of combustion air

(type: 6–4 FOM)

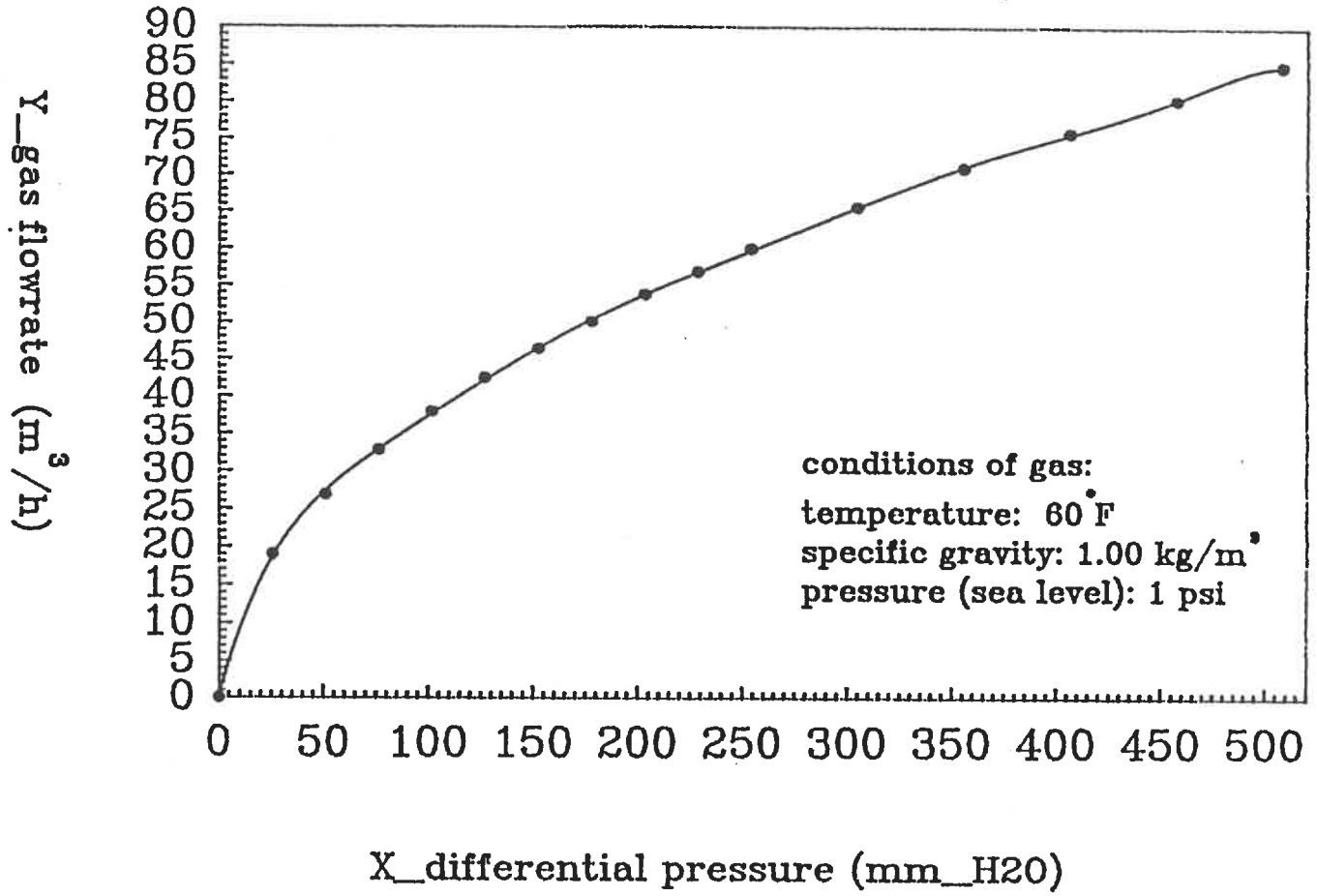

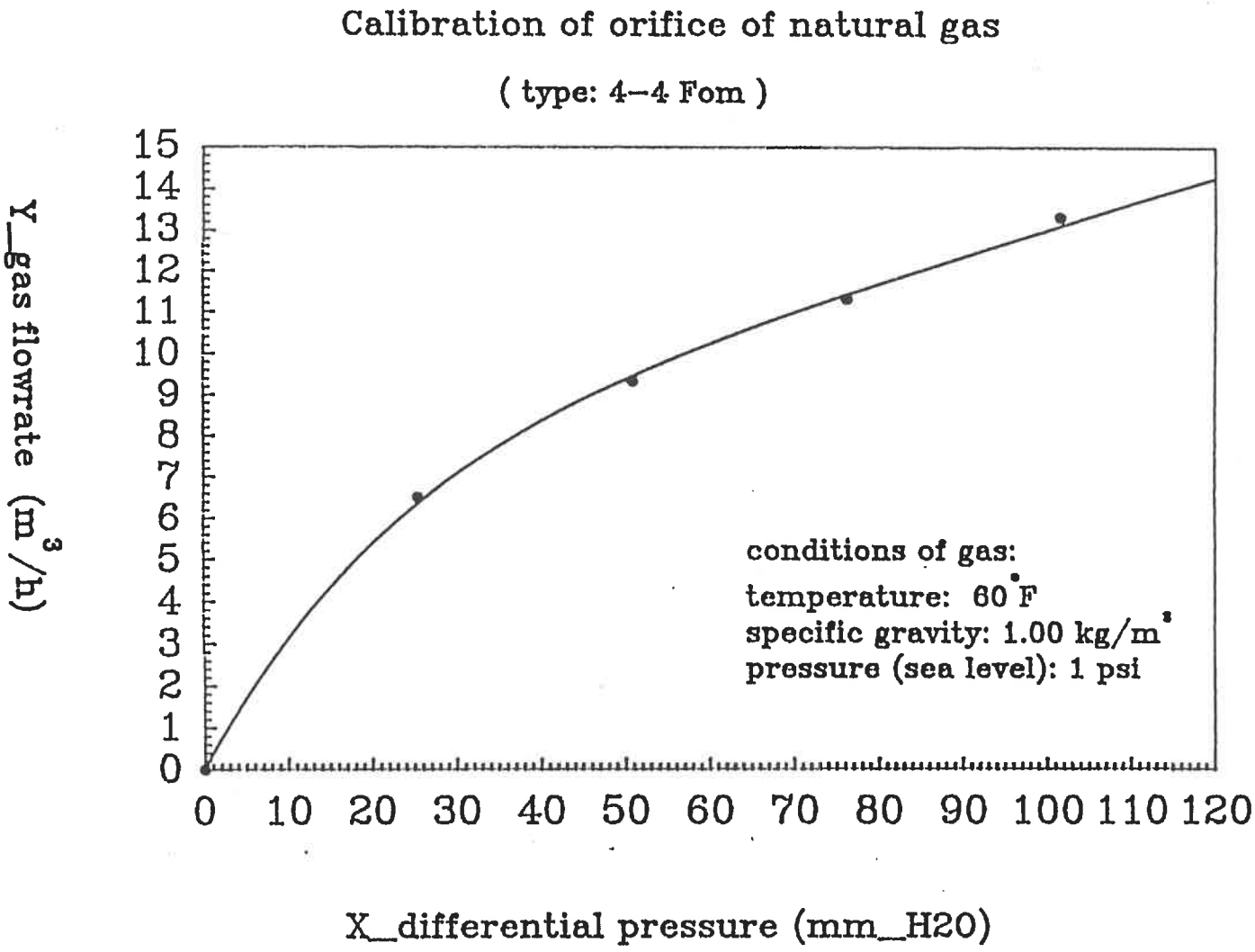
Calibration of orifice of natural gas
(type: 4–4 Fom)
Y_gas flowrate (m3/h)
15
14
13
12
11
10
9
8
7
6
5
4
3
2
1
0
0 10 20 30 40 50 60 70 80 90 100 110 120
X_differential pressure (mm_H20)
conditions of gas:
temperature: 60°F
specific gravity: 1.00 kg/m3
pressure (sea level): 1 psi

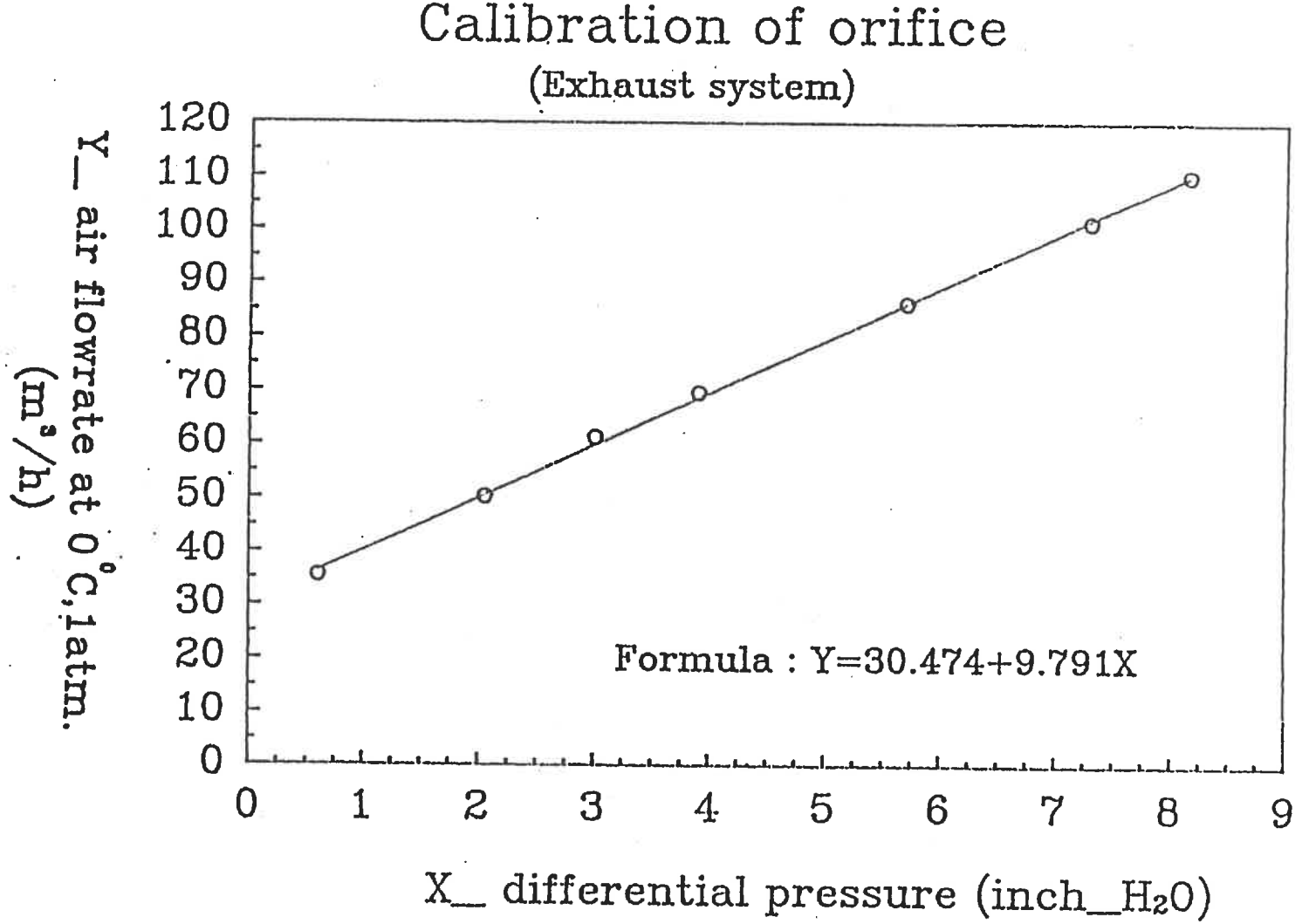
Calibration of orifice
(Exhaust system)
Y_ air flowrate at 0°C,1atm. (m³/h)
120
110
100
90
80
70
60
50
40
30
20
10
0
0
1
2
3
4
5
6
7
8
9
Formula : Y=30.474+9.791X
X_ differential pressure (inch_H₂0)

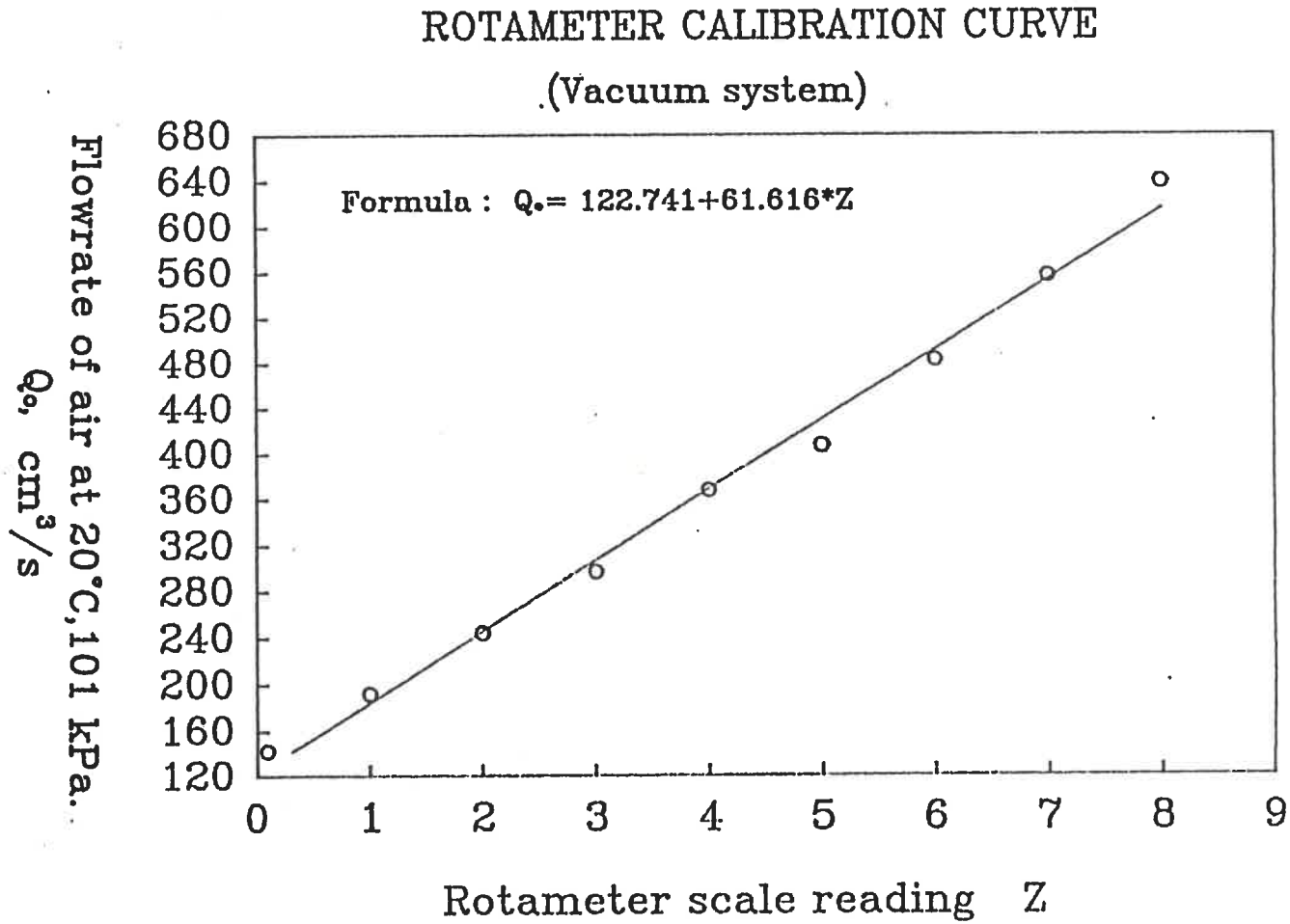
ROTAMETER CALIBRATION CURVE
(Vacuum system)
Formula : Q.= 122.741+61.616*Z
Flowrate of air at 20°C,101 kPa.
Q., cm³/s
680
640
600
560
520
480
440
400
360
320
280
240
200
160
120
0
1
2
3
4
5
6
7
8
9
Rotameter scale reading Z

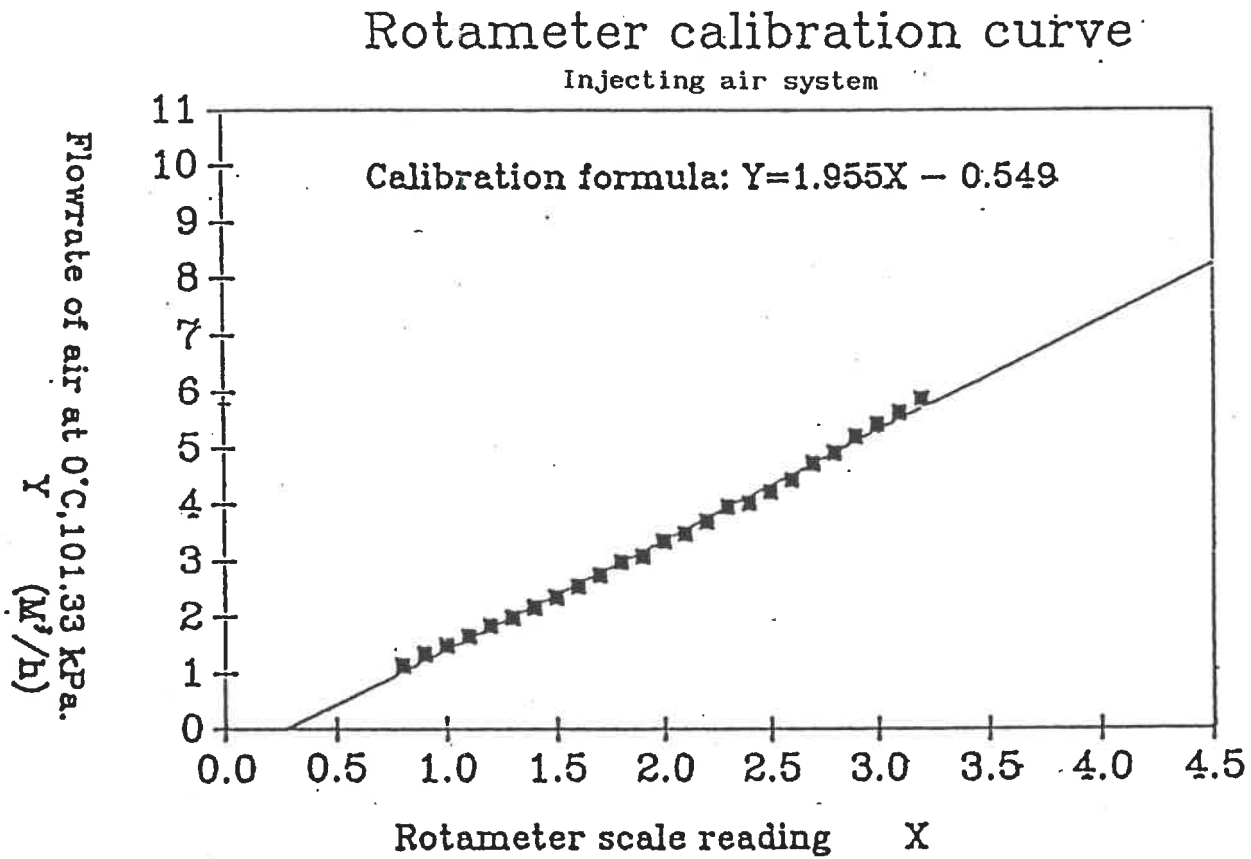
Rotameter calibration curve
Injecting air system
Calibration formula: Y=1.955X – 0.549
Flowrate of air at 0°C,101.33 kPa. Y (M³/h)
Rotameter scale reading X
0
1
2
3
4
5
6
7
8
9
10
11
0.0
0.5
1.0
1.5
2.0
2.5
3.0
3.5
4.0
4.5

APPENDIX III. ERROR ANALYSIS FOR TEMPERATURE MEASUREMENT

III.1 GAS TEMPERATURE MEASUREMENT

Thermocouples are used to measure the gas temperature in the furnace. The probe of the thermocouple is fixed in the centre of the cross section of the furnace (Figure (III-1)). There are two errors in this measurement. First is the systematic error of the thermocouple. The precision of the thermocouple used in this project is 0.5%. Second is the error due to the radiative heat transfer between the probe and the wall of the furnace, because the wall temperature is lower than the gas temperature.

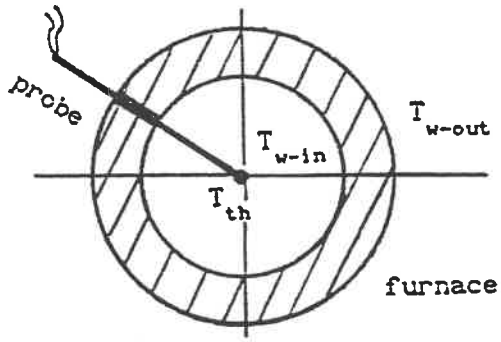

Figure (III-1) Gas temperature measurement

For calculating the second error, the inside surface temperature of the wall need to be estimated. From previous chapters, the average temperature of the outside surface of the wall is known, and the equation (4-30) is used for heat loss calculation. The heat flux between the gas and the inside surface of the wall is equal to the heat flux passing the wall under the steaty state system condition. Thus the temperature of the inside surface of the wall is given by:

$$T_{w\text{-}in} = \frac{h_{in}\, T_g + 2\,\lambda_w\, T_{w\text{-}out}\,/(D_{f,out} - D_f)}{h_{in} + 2\,\lambda_w\,/(D_{f,out} - D_f)} \qquad \text{(III-1)}$$

where h_{in}, λ_w, T_W, D_f have the same definition as in equation (4-30).

h_{in} is given by equation (4-31), its value is around $2*10^3$ W/m^{2}K for a gas temperature equal to 900 °C. When taking the average value of $T_{w\text{-}out}$ as 180 °C, λ_w is 18.6 W/m K, and the temperature of the inside surface of the wall is equal to 830 °C.

When the system is in steady state, the heat transfer rate between the gas and the probe is equal to the radiative heat transfer rate between the probe and the wall. If we just consider the forced convection heat transfer between the gas and the probe, and taking the assumptions that $A_{th} << A_w$ and that the probe and the wall are gray bodies, the energy conservation equation is shown as:

$$h\,(T_g - T_{th})\,\pi\, d_{th}^2 = \frac{\sigma\, T_{th}^4 - \sigma\, T_{w\text{-}in}^4}{(1-\varepsilon_{th})/(A_{th}\varepsilon_{th}) + 1/A_{th} + (1-\varepsilon_w)/(A_W\varepsilon_w)} \qquad \text{(III-2)}$$

where h is the forced convection coefficient between the probe and the gas, it has been given in equation (4-11). Subscript "th" is the characteristics of the thermocouple probe.

In equation (III-2), the value of h is about $2.5*10^3$ W/m^2K when the gas temperature is 900 °C. The diameter of the probe is about 0.002 m. $T_{w\text{-}in}$ has been given in last paragraph. Thus the value of T_{th} is 885 °C.

The difference between the T_g and T_{th} is the second error, it is about -15 °C (1.7%). Combining the two errors, the error of the gas temperature measurement is -10 °C to -20 °C.

III.2 SOLID TEMPERATURE MEASUREMENT

The energy conservation equation of the calorimetric sensor system has been given in equation (5-4). Thus the error of the solid temperature measurement based on this equation is shown as:

$$|\Delta T_p| = \frac{\partial T_p}{\partial T_{H2O}} |\Delta T_{H2O}| + \frac{\partial T_p}{\partial W_{H2O}} |\Delta W_{H2O}| + \frac{\partial T_p}{\partial \dot{m}_g} |\Delta \dot{m}_g| + \frac{\partial T_p}{\partial t} |\Delta t| + \frac{\partial T_p}{\partial W_p} |\Delta W_p| \qquad \text{(III-3)}$$

in which:

$\partial T_p / \partial T_{H2O} = 1;$

$\partial T_p / \partial W_{H2O} = C_{pH2O}(T_{H2O} - T_{H2O\text{-}init});$

$$\partial T_p / \partial \dot{m}_g = C_{pg}(T_{g-in} - T_{g-out})\, t / (W_p C_{pp});$$

$$\partial T_p / \partial t = \dot{m}_g C_{pg}(T_{g-in} - T_{g-out}) / (W_p C_{pp});$$

$$\partial T_p / \partial W_p = \dot{m}_g C_{pg}(T_{g-in} - T_{g-out})\, t / (-W_p^2 C_{pp});$$

where $|\Delta T_{H2O}|$ is the precision of the thermocouple; the value is 0.5%. When the water temperature is 60°C, ΔT_{H2O} is equal to ± 0.3°C.

$|\Delta W_{H2O}|$ is the precision of the balance; the value is $\pm 10^{-3}$g.

$|\Delta \dot{m}_g|$ is the precision of the rotameter and observational error; the value is about 2%. The average flow rate of the gas in this system is about $1.94*10^{-4}$ m^3/s, so Δm_g is equal to $\pm 3.88*10^{-6}$ m^{-3}/s.

$|\Delta W_p|$ is the precision of the balance, the value is $\pm 10^{-3}$g. The quantity of the sand sample is about 12 g.

$|\Delta T_g|$ is the error on the gas temperature measurement, the value is given in last paragraph. T_{g-out} is about 80 °C.

$|\Delta t|$ is the observational error, the value is one second.

Then taking these values into equation (III-3), the error on the solid temperature measurement is 0.5°C for a water temperature of about 60°C.